

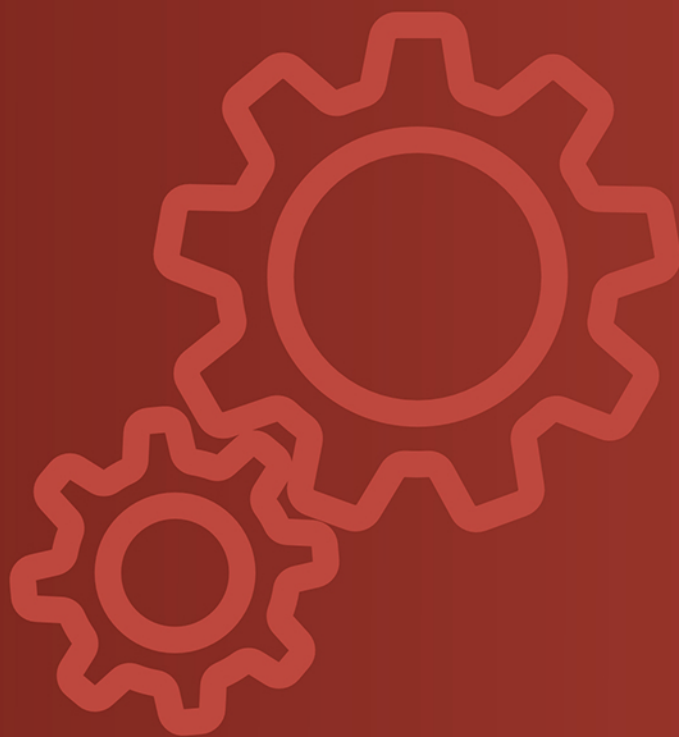
ISSN 2310-5607



Austrian Journal of Technical and Natural Sciences

Premier Publishing s.r.o.

2024
9-10



Austrian Journal of Technical and Natural Sciences

2024, No 9 – 10

Austrian Journal of Technical and Natural Sciences

Scientific journal

№ 9 – 10 2024

ISSN 2310-5607

Editor-in-chief

Hong Han, China, Doctor of Engineering Sciences

International editorial board

Atayev Zagir, Russia, Ph.D. of Geographical Sciences, Dagestan State Pedagogical University
Boselin S.R. Prabhu, India, Associate Professor, Surya Engineering College
Buronova Gulnora, Uzbekistan, PhD in Pedagogical science (Computer Science), Bukhara State University
Giorgi (Gia) Kvinikadze, Georgia, Doctor of Geographical Sciences, Tbilisi State University named after Ivane Javakhsishvili
Inoyatova Flora Ilyasovna, Uzbekistan, Doctor of Medicine, Republican Specialized Scientific and Practical Medical Center of Pediatrics (RSNPMC Pediatrics)
Kurdzeka Aliaksandr, Kazakhstan, Doctor of Veterinary Medicine, Kazakh National Agrarian University
Kushaliyev Kaissar Zhalitovich, Kazakhstan, Doctor of Veterinary Medicine, Zhangir Khan Agrarian Technical University
Mambetullaeva Svetlana Mirzamuratovna, Uzbekistan, Doctor of Biological Sciences, Karakalpak Research Institute of Natural Sciences
Manasaryan Grigoriy Genrihovich, Armenia, Doctor of Technical Sciences, Armenian National Polytechnic University
Martirosyan Vilena Akopovna, Armenia, Doctor of Engineering Sciences, National Polytechnic University of Armenia
Nagiyev Polad Yusif, Azerbaijan, Candidate of Agricultural Sciences, Sciences Institute for Space Research of Natural Resources, National Aerospace Agency

Nenko Nataliya Ivanovna, Russia, Doctor of Agricultural Sciences, State Scientific Institution North Caucasus Zonal Research Institute of Horticulture and Viticulture of the Russian Agricultural Academy
Rayiha Amenzade, Azerbaijan, Dr. Sc. (Architecture), professor, Institute of Architecture and Art of ANAS (Azerbaijan)
Sharipov Muzafar, Uzbekistan, PhD in technical science, Associate professor, Bukhara State university
Skopin Pavel Igorevich, Russia, Doctor of Medicine, Mordovian State University
Suleymanov Suleyman Fayzullaevich, Uzbekistan, Ph.D. of Medicine, Bukhara State Medical Institute (BukhGosMI)
Tegza Alexandra Alexeevna, Kazakhstan, Doctor of Veterinary Medicine, Kostanay State University
Yarashev Kuvondik Safarovich, Uzbekistan, Doctor of Geographical Sciences (DSc), Director, Urgut branch of Samarkand State University named after. Sharaf Rashidov
Zagir V. Atayev, Russia, PhD of Geographical Sciences, Dagestan State Pedagogical University

Proofreading

Kristin Theissen

Cover design

Andreas Vogel

Additional design

Stephan Friedman

Editorial office

Premier Publishing s.r.o.

Praha 8 – Karlín, Lyčkovo nám. 508/7, PSČ 18600

E-mail:

pub@ppublishing.org

Homepage:

ppublishing.org

Austrian Journal of Technical and Natural Sciences is an international, English language, peer-reviewed journal. The journal is published in electronic form.

The decisive criterion for accepting a manuscript for publication is scientific quality. All research articles published in this journal have undergone a rigorous peer review. Based on initial screening by the editors, each paper is anonymized and reviewed by at least two anonymous referees. Recommending the articles for publishing, the reviewers confirm that in their opinion the submitted article contains important or new scientific results.

Premier Publishing is not responsible for the stylistic content of the article. The responsibility for the stylistic content lies on an author of an article.

Instructions for authors

Full instructions for manuscript preparation and submission can be found through the Premier Publishing home page at: <http://ppublishing.org>.

Material disclaimer

The opinions expressed in the conference proceedings do not necessarily reflect those of the Premier Publishing, the editor, the editorial board, or the organization to which the authors are affiliated.

Premier Publishing is not responsible for the stylistic content of the article. The responsibility for the stylistic content lies on an author of an article.

Included to the open access repositories:



TOGETHER WE REACH THE GOAL

SJIF 2024 = 6.62 (Scientific Journal Impact Factor Value for 2024).



Crossref

OAK.UZ

eLIBRARY.RU

Included to the Uzbekistan OAK journals bulletin.

© Premier Publishing

All rights reserved; no part of this publication may be reproduced, stored in a retrieval system, or transmitted in any form or by any means, electronic, mechanical, photocopying, recording, or otherwise, without prior written permission of the Publisher.



Section 1. Chemistry

DOI:10.29013/AJT-24-9.10-3-7



INFLUENCE OF A NANOSTRUCTURAL CATALYST IN THE ALLYLATION REACTIONS OF ANISOLE AND NEROLIN

*Gulmira Azimova*¹, *Mukhabbat Yuldasheva*¹, *Khabibullo Tadjimuhamedov*¹

¹National University of Uzbekistan

Cite: Azimova G., Yuldasheva M., Tadjimuhamedov Kh. (2024). Influence of a Nanostructural Catalyst in the Allylation Reactions of Anisole and Nerolin. Austrian Journal of Technical and Natural Sciences 2024, No 9–10. <https://doi.org/10.29013/AJT-24-9.10-3-7>

Abstract

The allylation reactions of anisole and nerolin with allyl alcohol were studied in nanostructured $\text{FeCl}_3/\text{TiO}_2 \cdot \text{SiO}_2$ catalyst systems and the optimal conditions for obtaining the product with a yield of 70, 75% were determined. The influence of the solvent, the amount of catalyst and the duration of the reaction on the yield of the reaction was studied.

Keywords: *Methoxybenzene (anisole), methoxynaphthalene (nerolin), allylation, nanostructured $\text{FeCl}_3/\text{TiO}_2 \cdot \text{SiO}_2$ catalyst, thin layer chromatography, heterogen catalyst*

Introduction

Allylphenols and allylnaphthols are prepared by the allylation of phenols and naphthols with allylating agents. Friedel–Crafts alkylation is among the most fundamental and convenient processes for construction of fine chemicals, pharmaceuticals, and agrochemicals containing functionalized arenes and heteroaromatic substructures. Allylation of aromatic compounds and their products are notable for its physiological activity and usefulness (Masanari Kimura, a Miki Fukasaka, a Yoshinao Tamaru, 2006. 3611–3612). Various sources contain data on the allylation of substituted phenols and naphthols with allyl alcohols (Masanari Kimura, a Miki Fukasaka, a Yoshinao Tamaru, 2006. 3611–3612; Jimmy A. van Rijn, Martin Lutz, Lars S. von Chr-

zanowski, Anthony L. Spek, Elisabeth Bouwman and Eite Drenta, 2009. 1637–1647; Jimmy A. van Rijn, Angela den Dunnen, Elisabeth Bouwman, Eite Drent, 2010. 96–102; Das B., Veeranjanyulu B., Krishnaiah M., Balasubramanyam P., 2009. 1929–1935), allyl halides (Zadmard R., Aghapoor K., Bolorutchian M. & Saidi M. R., 2013. 4495–4498; Thierry Ollevier, Topwe M. Mwene-Mbeja, 2006. 4051–4055), allyl acesates (Halligudi S. B., Sajjanikumari C. S., Kala Raj N. K., Deshpande S. S., Degaonkar M. P., 2001. 161–167; Amit Saha, John Leazer, Rajender S. Varma, 2012. 67–71, allyl tosylates (Naofumi Tsukada, Yasushige Yagura, Tetsuo Sato, Yoshio Inoue. 2003. 1431–1434), and allyl ethers (Christopher A. D., Graves Alexander G., Deardorf Donald R., 2016. 1–34) in

the presence of various catalysts. As a catalyst for the allylation of phenol and naphthol with various allylating agents, $[\text{Rh}(\text{nbd})(\text{CH}_3\text{CN})_2]\text{PF}_6$, $[\text{Rh}(\text{nbd})\text{Cl}]_2$; $[\text{Rh}(\text{nbd})_2]\text{BF}_4$, $\text{RhCl}(\text{PPh}_3)_3$, $[\text{Ir}(\text{cod})\text{CH}_3\text{CN}_2]\text{PF}_6$, $\text{Pd}(\text{OAc})_2/\text{MS } 4\text{\AA}$, $[\text{Fe}_3\text{O}_4\text{-Dopamine-P}_d]$, $\text{P}_d \cdot \text{Et}_3\text{B}$, $\text{H}\beta$ zeolite.

The fact that each allylating agent reacts differently with phenols and naphthols, depending on the reaction conditions, the influence of solvent and catalyst, is reflected in modern scientific work. Allylation of naphthol-1 and naphthol-2 with allyl alcohol were carried out in the $\text{P}_d \cdot \text{Et}_3\text{B}$ catalyst system and selective methods for the synthesis of C-allyl product were developed (Masanari Kimura, a Miki Fukasaka, a Yoshinao Tamaru. 2006. 3611–3612).

In order to synthesize biologically active allyl derivatives of naphthols, Indian scientists used the widely used catalyst Amberlyst-15 (Das B., Veeranjanyulu B., Krishnaiah M., Balasubramanyam P., 2009. 1929–1935). When using the Amberlyst-15, only C-allylation products-2-allyl-naphthol-1 and 1-allyl-naphthol-2- are mainly formed, the formation of O-allyl products under these conditions was not observed.

The allylation of phenol with allyl acetate catalyzed by $\text{H}\beta$ -30 gave mainly C-allylated phenols (o-allyl phenol and p-allyl phenol), allyl phenyl ether, 1,3-bis-(2-hydroxy phenyl)-propane and an unidentified polymeric product (Halligudi S. B., Sajani-kumari C. S., Kala Raj N. K., Deshpande S. S., Degaonkar M. P., 2001. 161–167).

As part of alternative, sustainable technologies of green chemistry, in the method of allylation of phenols using magnetically extractable catalysts. Allylic ethers were synthesized in water using magnetically recoverable heterogeneous $[\text{Fe}_3\text{O}_4\text{-Dopamine-P}_d]$ catalyst via O-allylation of phenols with allylic acetates under ambient conditions. The aqueous reaction medium, easy recovery of the catalyst using an external magnet, efficient recycling, and the high stability of the catalyst renders the protocol economic and sustainable (Amit Saha, John Leazer, Rajender S. Varma, 2012. 67–71).

Chemists of Japanese conducted an allylation reaction of electron-donating arenes with allyl tosylate at 0°C in the pres-

ence of $[\text{Rh}(\text{nbd})(\text{CH}_3\text{CN})_2]\text{PF}_6$, $[\text{Rh}(\text{nbd})\text{Cl}]_2$; $[\text{Rh}(\text{nbd})_2]\text{BF}_4$, $\text{RhCl}(\text{PPh}_3)_3$, $[\text{Ir}(\text{cod})\text{CH}_3\text{CN}_2]\text{PF}_6$. Various methoxybenzene were allylated with high couple-selectivity in almost all cases. In the allylation of naphthols using the following catalysts $[\text{Rh}(\text{nbd})(\text{CH}_3\text{CN})_2]\text{PF}_6$, $[\text{Rh}(\text{nbd})\text{Cl}]_2$; $[\text{Rh}(\text{nbd})_2]\text{BF}_4$, $\text{RhCl}(\text{PPh}_3)_3$, $[\text{Ir}(\text{cod})\text{CH}_3\text{CN}_2]\text{PF}_6$, the disadvantage is the low reaction yields (up to 33%). In the reaction of allylation of β -naphthol with allyl tosylate in the presence of the catalyst $[\text{Rh}(\text{nbd})(\text{CH}_3\text{CN})_2]\text{PF}_6$, produces 1-allyl-2-naphthol and methyldihydronaphthofuran in 38% and 32% yield (Naofumi Tsukada, Yasushige Yagura, Tetsuo Sato, Yoshio Inoue, 2003. 1431–1434).

Experimental part

A thin layer chromatography plate (TLC) DC-Fertigfolien ALUGRAM ® Xtra SIL G/UV254 (Germany) was used, the appearance of spots was determined under the influence of a UV lamp on the plate. The reaction products were identified by IR analysis (Perkin Elmer Spectrum IR, Version 10.06.1) and NMR H^1 and C^{13} (Unity 400 plus ICPSASR Uz).

Preparation of catalysts from nanoporous metal oxides and iron (III) chloride $\text{FeCl}_3/\text{TiO}_2\text{-SiO}_2$

The catalytic system $\text{FeCl}_3/\text{TiO}_2 \cdot \text{SiO}_2$ was prepared as follows $\text{FeCl}_3 \cdot 6\text{H}_2\text{O}$ and $\text{TiO}_2 \cdot \text{SiO}_2$ (Khusniddin Musaev, Dilorom Mirkhamitova, Abdurasul Yarbekov, Khamdam Akbarov, Suvonkul Nurmanov, Olim Ruzimuradov, 2019) were weighed on an analytical balance in an amount of $2 \cdot 10^{-4}$ –4 grams. In powder form, both substances were melted and mixed in a mortar. It was dried in the oven at $50\text{--}60^\circ\text{C}$ for 1 hour, then at $100\text{--}120^\circ\text{C}$ also for 1 hour.

Synthesis of 2-allylanisole. Anisole (0.05 mol, 5.42 ml), allyl alcohol (0.05 mol, 3.4 ml) and $\text{FeCl}_3/\text{TiO}_2 \cdot \text{SiO}_2$ catalyst ($2.4 \cdot 10^{-4}$ mol, 0.084 g), hydroquinone (0.0005 mol, 0.55 g) are poured into a three-necked round bottom flask connected to a stirrer, thermometer, a reflux condenser and, with a working stirrer. The reaction mixture is heated six hours at a temperature of $100\text{--}120^\circ\text{C}$. After cooling the reaction mixture, distillation was carried out by fractional distillation under vacuum. The 1-fraction

15–80 °C (20mm, remaining allyl alcohol and anisole), 2-fraction 70–90 °C (22 mm.) 3-fraction 98 °C (22 mm, 2-allylanisole). Yield 70%. **IR (KBr, cm^{-1})** 751, 1172 1496, 1587, 2945, 1599. **NMR H^1** (Unity 400 plus ICPS AS RUz, referce HMDSO, Solvent CD3OD, chemical shift of protons, δ , ppm) 3.24 m (2H, CH_2), 3.81 s (3H, OCH_3), 4.838, 5.00–5.20 d (2H, $-\text{CH} = \text{CH}_2$), 5.884 m (1H, $-\text{CH} = \text{CH}_2$), 6.803, 6.82, 7.14, 7.17 t (4H, ArH). **C^{13} spectrum** 100 MHz, CDCl_3 d = 49, 55.442, 63.913, 114.795, 121.511, 129.271, 130.352, 138.827, 161.004

Synthesis of 1-allyl-2-naphthylmethylether. 2-naphthylmethylether (0.01mol, 1.58g), allyl alcohol (0.01mol, 1.45ml) and $\text{FeCl}_3/\text{TiO}_2 \cdot \text{SiO}_2$ catalyst ($2.4 \cdot 10^{-4}$ mol, 0.098g), hydroquinone (0.0005 mol, 0.55g) are poured into a three-necked round bottom flask connected to a stirrer, thermometer, a reflux condenser and, with a working stirrer. The reaction mixture is heated 5 hours at a temperature of 100–120 °C. After cooling the reaction mixture, the precipitate was filtered. Unreacted 2-naphthylmethyl ether and the obtained product-1-allyl-2-naphthylmethyl ether are washed and separated in hexane. Yield 75% (1.485g). Melting point 31–33 °C. **NMR H^1** (Unity 400 plus ICPS AS RUz, referce HMDSO, Solvent CD3OD, chemical shift of protons, δ , ppm) 3.55 m (2H, CH_2), 3.81 s (3H, OCH_3), 4.838 d (2H, $-\text{CH} = \text{CH}_2$), 5.884 m (1H, $-\text{CH} = \text{CH}_2$), 6.803, 6.82, 7.24, 7.81t (6H, ArH). **C^{13} spectrum** 100 MHz, CDCl_3 d = 31.4, 56.1, 109.0, 115.9, 118.4, 123.4, 124.3, 126.3, 128.0, 128.3, 129.2, 133.6, 153.2.

Results and discussion

The formation of mainly para-allyl phenols in the allylation of phenols and naph-

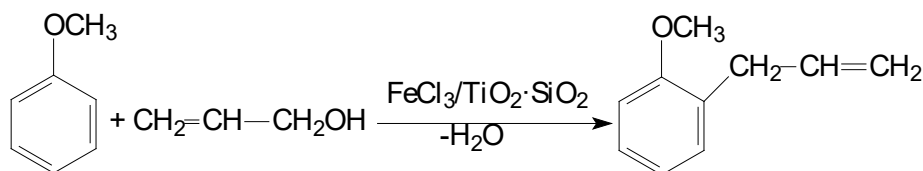
thols in the presence of $\text{FeCl}_3 \cdot 6\text{H}_2\text{O}$ by the Friedel-Crafts method was proved by gas-liquid chromatography (Azimova G. Z., Tajimuhamedov H. S., Yuldasheva M. R., 2019. 39–42). The formation of mainly ortho-allylphenols in the isomerization reactions of allylphenyl ethers using a new type nanostructured catalyst $\text{FeCl}_3/\text{TiO}_2 \cdot \text{SiO}_2$ was confirmed by chromatography-mass spectrometry (Khusniddin Musaev, Azimova Gulmira, Yuldasheva Mukhabbat, Tadjimuhamedov Khabibullo, Khamdam Akbarov, Olim Ruzimuradov, 2019. 40–45). Allylation reaction of 2-naphthol under catalytic conditions $\text{FeCl}_3/\text{TiO}_2 \cdot \text{SiO}_2$ with allyl alcohol and allyl acetate have also been studied. It was observed that iron (III) chloride with a nanostructured catalyst has a higher selectivity for the production of mono- and ortho- products, according to the ratio of iron (III) chloride itself is used as a catalyst. This can be explained by the fact that iron (III) chloride is adsorbed on the surface of the nanocatalyst and forms unstable complexes with allylating agent and this reduce the polyallylating ability of the reagent (Azimova Gulmira, Yuldasheva Mukhabbat, Tadjimuhamedov Khabibullo, 2020).

In this study, the allylation of electron-rich arenes, namely methoxybenzene (anisole) and methoxynaphthalene (2-naphthylmethyl ether, nerolin) in the presence of a catalyst containing $\text{FeCl}_3/\text{TiO}_2 \cdot \text{SiO}_2$ impregnated with nanostructured metal oxides, was studied.

The allylation of anisole with allyl alcohol in the presence of $\text{FeCl}_3/\text{TiO}_2 \cdot \text{SiO}_2$ was carried out under solvent-free conditions in a magnetic stirrer at 100–120 °C. The reaction showed that 2-allylanisole was formed.

Table 1. Reaction conditions of anisole with allyl alcohol and the results obtained

The molar ratio of anisole: allyl alcohol: catalyst	Conditions of reaction, °C	Reaction duration, hours	Products	Yield, %	R_t , system= hexane: ethylacetate = 5 : 1
1:1:10 ⁻⁴	100–120	3		10%	0.45
1:1:10 ⁻⁴	100–120	6	2-allyl-	22%	0.45
1:1:2,4*10 ⁻⁴	100–120	3	anisole	62%	0.45
1:1:2,4*10 ⁻⁴	100–120	6		70%	0.45



Allylation reactions anisole: allyl alcohol: catalyst = 1: 1: $2.4 \cdot 10^{-4}$ in a benzene solvent at 76–80 °C for 6 hours, the reaction yield was low (53%), the reaction time was increased to 8 hours profitability (55%) has not changed significantly.

The reaction of 2-naphthylmethyl ether with allyl alcohol on a $\text{FeCl}_3/\text{TiO}_2 \cdot \text{SiO}_2$ catalyst was carried out in a reagent ratio of 1: 1: $2.4 \cdot 10^{-4}$, when it was carried out in a benzene solvent in a magnetic stirrer for 5 hours with a yield of 75%.

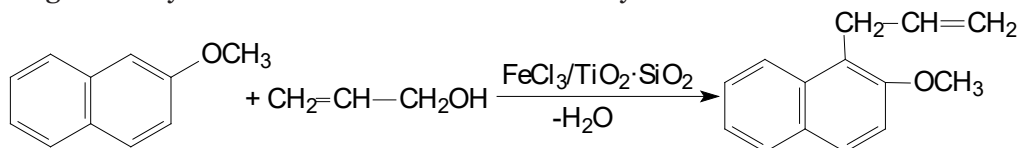


Table 2. Reaction conditions of 2-naphthylmethyl ether with allyl alcohol and the results obtained

The molar ratio of 2-naphthylmethyl ether: allyl alcohol: catalyst	Conditions of reaction, °C	Reaction duration	Products	Yield, %	R_f system= hexane: ethylacetate = 5 : 1
1:1:10 ⁻⁴	76–80	3		45%	0.93
1:1:10 ⁻⁴	76–80	4	1-allyl-2-naphthyl-	63%	0.93
1:1:2,4*10 ⁻⁴	76–80	5	methyl ether	75%	0.93
1:1:2,4*10 ⁻⁴	76–80	6		75%	0.93

The resin was observed when the allylation reactions of naphthyl methyl ether were carried out in the absence of a solvent.

Conclusions

Based on the results obtained, it can be concluded that allylation of anisole with allyl alcohol leads to a selective reaction with a high yield when carried out in a solvent-free state and 2-naphthylmethyl ether in good yield for 1-allyl-2-naphthylmethyl ether in good yield at using a benzene solvent achieved. The use of a nanostructured catalytic system – $\text{FeCl}_3/\text{TiO}_2 \cdot \text{SiO}_2$ at allylation reactions made it possible to carry out them selectively with respect to ortho-allylation and with increased product yield than at using Lewis acids, and

the reaction of 2-naphthylmethyl ether with allyl alcohol proceeds with the participation of the C1 carbon atom at using nanostructured catalyst $\text{FeCl}_3/\text{TiO}_2 \cdot \text{SiO}_2$. In the anisole allylation reactions, it was found that anisole also acts as a solvent in the reaction process and that 2-naphthylmethylether is a crystalline substance that can complicate the reaction without a solvent.

Thanks

We thank to O.Ruzimuradov who is professor of the Turin Polytechnic Institute in Tashkent and H. Musayev who is senior teacher of National University of Uzbekistan for the synthesis of nanostructured $\text{TiO}_2 \cdot \text{SiO}_2$, $\text{FeCl}_3 \cdot 6\text{H}_2\text{O}$ is belong to Aldrich company.

References

- Masanari Kimura, a Miki Fukasaka, a Yoshinao Tamaru. (2006). Palladium-Catalyzed, Triethylborane-Promoted C-Allylation of Naphthols and Benzene Polyols by Direct Use of Allyl Alcohols. SYNTHESIS DOI: 10.1055/s-2006-950220;

- Jimmy A. van Rijn, Martin Lutz, Lars S. von Chrzanowski, Anthony L. Spek, Elisabeth Bouwman and Eite Drenta. (2009) Cationic Ruthenium-Cyclopentadienyl-Diphosphine Complexes as Catalysts for the Allylation of Phenols with Allyl Alcohol; Relation between Structure and Catalytic Performance in *O*- vs. *C*-Allylation. *Adv. Synth. Catal.*, – 351. – P. 1637–1647. URL: <http://dx.doi.org/10.1002/adsc.200900085>.
- Jimmy A. van Rijn, Angela den Dunnen, Elisabeth Bouwman, Eite Drent. (2010) Palladium–diphosphine complexes as catalysts for allylations with allyl alcohol. *Journal of Molecular Catalysis A: Chemical* – 329. – P. 96–102. Doi: 10.1016/j.molcata.2010.06.023.
- Das B., Veeranjanyulu B., Krishnaiah M., Balasubramanyam P. (2009). Benzoylation and Allylation of Naphthols Using Amberlyst-15. *Synthetic Communications: An International Journal for Rapid Communication of Synthetic Organic Chemistry*. P. 1929–1935
- Zadmard R., Aghapoor K., Bolourchian M. & Saidi M. R. (2013). Solid Composite Copper-Copper Chloride Assisted Alkylation of Naphthols Promoted by Microwave Irradiation, *Synthetic Communications: An International Journal for Rapid Communication of Synthetic Organic Chemistry*. – 28/24. – P. 4495–4499. DOI: 10.1080/00397919808004511
- Thierry Ollevier, Topwe M. Mwene-Mbeja. (2006). Bismuth triflate catalyzed Claisen rearrangement of allyl naphthyl ethers. *Tetrahedron Letters* – 47. – P. 4051–4055. Doi: 10.1016/j.tetlet.2006.03.193
- Halligudi S. B., Sajanikumari C. S., Kala Raj N. K., Deshpande S. S., Degaonkar M. P. (2001). Liquid phase allylation of phenol using H β zeolite. *Journal of Molecular Catalysis A: Chemical* – 175. – P. 161–167.
- Amit Saha, John Leazer, Rajender S. Varma. (2012). *O*-Allylation of phenols with allylic acetates in aqueous medium using a magnetically separable catalytic system. *Green Chem.* – 14. – P. 67–71. DOI: 10.1039/c1gc16174a
- Naofumi Tsukada, Yasushige Yagura, Tetsuo Sato, Yoshio Inoue. (2003). Rhodium- and Iridium-Catalyzed Allylation of Electron-Rich Arenes with Allyl Tosylate. *Synlett No.* – 10. – P. 1431–1434.
- Christopher A. D., Graves Alexandr G., Deardorf Donald R. (2016). Regio and stereospecific *C*- and *O*-allylation of phenols via π -allyl Pd complexes derived from allylic estercarbonates. *The Journal of Organic chemistry*. P. 1–34. DOI:10.1021/acs.joc.6b02608
- Khusniddin Musaev, Dilorom Mirkhamitova, Abdurasul Yarbekov, Khamdam Akbarov, Suvonkul Nurmanov, Olim Ruzimuradov. (2019). Facile synthesis of PEG-templated SiO₂-TiO₂ nanocomposite photocatalyst for degradation of phenolic water pollutants. *SN Applied Sciences*, Springer, – 1: 1164. – P. 1–10.
- Azimova G. Z., Tajimuhamedov H. S., Yuldasheva M. R. (2019). Allylation of phenol and naphthol with allyl acetate in the presence of small amounts of aqueous ferric chloride. *Universum: Chemistry and Biology* – No. 1 (55). – P. 39–42
- Khusniddin Musaev, Azimova Gulmira, Yuldasheva Mukhabbat, Tadjimuhamedov Khabibullo, Khamdam Akbarov, Olim Ruzimuradov. (2019). Influence of nanostructural catalyst in the synthesis of allylphenyl ether and of its isomerization products. *Journal of Chemistry and chemical technology* – No. 4. – P. 40–45
- Azimova Gulmira, Yuldasheva Mukhabbat, Tadjimuhamedov Khabibullo (2020). Influence of a nanostructural catalyst in the synthesis of allylnaphthols. “Austrian Journal of Technical and Natural Sciences”. No. 5–6.

submitted 15.09.2024;

accepted for publication 29.09.2024;

published 28.11.2024

© Azimova G., Yuldasheva M., Tadjimuhamedov Kh.

Contact: gulmira.azimova.84@mail.ru

DOI:10.29013/AJT-24-9.10-8-13



STUDY OF THE STRUCTURE OF COMPLEX COMPOUNDS BASED ON 2-AMINO-1,3,4-THIADIZOLE AND ADIPIC ACID OF SALTS OF CO(LL), NI(LL), CU(LL), ZN(LL) USING PHYSICAL MEANS

Alieva Mushtari Zaylobidin qizi ¹, Nuraliyeva Guzal Abdulhamidovna ¹

¹National University of Uzbekistan, Department of
Inorganic Chemistry, Faculty of Chemistry

Cite: Alieva M.Z., Nuraliyeva G.A. (2024). Study of the structure of complex compounds based on 2-amino-1,3,4-thiadiazole and adipic acid of salts of Co(II), Ni(II), Cu(II), Zn(II) using physical means. *Austrian Journal of Technical and Natural Sciences* 2024, No 9–10. <https://doi.org/10.29013/AJT-24-9.10-8-13>

Abstract

Complex compounds with heteroligands were synthesized based on 2-amino-1,3,4-thiadiazole, adipic acid and salts of Co(II), Ni(II), Cu(II), Zn(II). The physicochemical properties of the synthesized complex compounds were studied using IR-spectrum, SEM-EDA and thermal analysis. The results are presented in tables. The chemical structure of complex compounds was determined based on the above results.

Keywords: Coordination compounds, ligands, metal-complex formers, IR-spectrum, thermal analysis, endothermic and exothermic effects

Introduction

Five-membered heterocyclic compounds have high biological properties, of which 2-amino-1,3,4-thiadiazole is significant for its biological activity. Therefore, thiadiazol and its derivatives are used as anti-parasitic, anti-coagulant, anti-microbial, anti-cancer, anti-inflammatory and anti-tuberculosis agents (Atmaram, U. A., Roopan, S. M. 2022). According to the results of various studies, 2-amino-1,3,4-thiadiazole has excellent pharmacological value as an anti-fungal, diuretic, and anthelmintic activity, and several methods of synthesis of this substance have been created. Recently, the synthesis of heteroligand metal complexes based on 2-amino-1,3,4-thiadiazole and its derivatives has

attracted interest because these substances are widely used in medicine and material science. The 2-amino-5-methyl-1,3,4-thiadiazole (amtz) ligand containing one S and three N coordination sites has been recognized as a potential multidentate ligand to form some interesting compounds. In this literature, the following complex compound $\text{CoCl}_2(\text{C}_3\text{H}_5\text{N}_3\text{S})_2$ was synthesized with CoCl_2 salt and 2-amino-5-methyl-1,3,4-thiadiazole. In this complex, Co(II) is tetracoordinated from two monodentate 2-amino-5-methyl-1,3,4-thiadiazole ligands by two chlorine anions and two nitrogen atoms and forms a monoclinic syngonia (Ye Song, Yu-Fei Ji, Min-Yan Kang and Zhi-Liang Liu, 2012). The authors presented the synthesis

and crystal structure of the tetramis (I) complex connected with the 2-amino-1,3,4-thiadiazole ligand. Another structural feature is that two different hydrogen bonds are formed between the ClO_4^- anions and the NH_2 group of the 2-amino-1,3,4-thiadiazole ligand. Two new tetracopper(I) and tetrasilver(I) complexes $\text{Cu}_4(\text{atdz})_6(\text{ClO}_4)_4 \cdot 2\text{CH}_3\text{OH}$ (1) and $[\text{Ag}_4(\text{atdz})_6](\text{ClO}_4)_4$ (2) formed a tetranuclear structure (Masahiko Maekawa, Megumu Munakata, Takayoshi Kuroda-Sowa, Yusaku Suenaga, Kunihiisa Sugimoto, 1999).

Two new mixed ligand complexes $[\text{M}(\text{atdz})(\text{DCA})(\text{H}_2\text{O})_2] \cdot \text{H}_2\text{O}$, ($\text{M} = \text{Co(II)}, \text{Zn(II)}$; $\text{atdz} = 2\text{-amino-1,3,4-thiadiazole}$, $\text{C}_2\text{H}_3\text{N}_3\text{S}$; $\text{DCA} = \text{demethylcanthate}$, 7-oxabicyclo[2,2,1]heptane-2,3-dicarboxylate, $\text{C}_8\text{H}_8\text{O}_5$) was prepared and characterized by elemental analysis. The structure of the complexes was determined by X-ray diffraction. The crystals have the empirical formulas $\text{CoC}_{10}\text{H}_{19}\text{N}_3\text{O}_9\text{S}$ (1) and $\text{ZnC}_{10}\text{H}_{19}\text{N}_3\text{O}_9\text{S}$ (2) respectively. Syngonia of complexes 1 and 2 showed a monoclinic structure (Na Wang, Qiu-Yue Lin, Jie Feng, Yu-Ling Zhao, Yan-Jun Wang, Shi-Kun Li, 2010).

The literature analysis shows that much scientific research has been carried out on the synthesis, structure, and properties of complexes of dicarboxylic acids, including adipic acid with intermediate metals. This shows the need to carry out tasks such as synthesizing complex compounds with the same and mixed ligands with heterocyclic compounds of intermediate metals, analyzing their composition and structure, determining relevant laws from the analysis of the obtained results, and defining the fields of application of complex compounds according to the identified properties.

Research methodology

Salts of metals in crystalline hydrate form: zinc(II), nickel(II), cobalt(II) and copper(II) chloride, acetate, sulfate and nitrate salts were used to synthesize complex compounds.

Carbon, sulfur and metals in complex compounds were determined using elemental analysis in an atomic absorption “Bruker” (Germany) spectrophotometer.

Absorption IR-spectra of the compounds in the range of $400\text{--}4000\text{ cm}^{-1}$ were recorded on Avatar System 360 FT-IR and Rrotege

460 Magna-IR technology spectrophotometers from “Bruker” (Germany) using a KBr tablet sample with a diameter of 7 mm and an accuracy of 4 cm^{-1} . was studied.

Thermal analysis was carried out with a thermodynamic apparatus — DTG-60 SMIL-TANEOUS DTA-TG APPARATUS (Japan), K-type (Shimadzu) thermo steam and porcelain crucible. All measurements were carried out in an inert argon atmosphere with an argon flow rate of 80 ml/min. The temperature range of the analysis was $20\text{ }^\circ\text{C}$, the heating rate was 5 K/min. The amount of sample in one measurement is 6–10 mg. The measuring system vibrates using a set of standard substances KNO_3 , In, Bi, Sn, Zn, CsCl.

Experiment

Complex compounds were synthesized according to a specific methodology (Wu Q. et al., 2015). According to it (0.001 mol) 0.101 g 2-amino-1,3,4-thiadiazole (LT), (0.001 mol) 0.146 g adipic acid (LA), (0.001 mol) 0.04 g sodium hydroxide, (0.001 mol) 0.295 g of Co(II) nitrate crystal hydrate was obtained. Initially, adipic acid, Co(II) nitrate and sodium hydroxide were dissolved in 5 ml of distilled water. Subsequently, 2-amino-1,3,4-thiadiazole was dissolved in methanol. To neutralize adipic acid, sodium hydroxide solution was poured over it and heated at $65\text{ }^\circ\text{C}$ for 30 minutes. Sodium adipinate was added to the dissolved salt with stirring. A solution of 2-amino-1,3,4-thiadiazole in methanol was poured onto the resulting mixture and heated at $60\text{ }^\circ\text{C}$ for 2 hours. As a result, the color of the solution turned pink. The mixture was removed for crystallization. After 10 days, pink crystals began to fall. They were filtered and washed several times in ethanol. Yield 81%.

Result and discussion

Complex compounds of Co(II), Ni(II), Cu(II), Zn(II) chloride, nitrate and acetate salts with 2-amino-1,3,4-thiadiazole and adipic acid were synthesized in the same way.

Co(II), Cu(II), Ni(II) and Zn(II) chloride, nitrate, acetate and sulfate salts of complex compounds synthesized in the presence of adipic acid and 2-amino-1,3,4-thiadiazole IR-spectroscopic were analyzed based on the analysis (Table 1) and compared with the IR-spectra of the original ligands (Fig. 1).

Table 1 shows the results of the IR spectra of the synthesized mixed-ligand complexes. Symmetric and asymmetric valence vibrations of the = N-N= bond in the 2-amino-1,3,4-thiadiazole ring are manifested in the low-frequency region in the area of 1011–1040 cm⁻¹. The valence vibrations of the amino group give vibrations in the ν(NH₂) 3277 cm⁻¹ region and the deformation vibrations in the δ(NH₂)1524 cm⁻¹ region. Absorption lines of characteristic valence vibrations of C-S-C bonds of medium intensity were recorded in the region of C=N bond 1614 cm⁻¹, 664–783 cm⁻¹ (Nuralieva G.A., Xayrullayev G.U., Kadirova Sh.A., 2020). Also, the characteristic valence vibrations of the CH bond in the heteroring were manifested in the high-frequency region at 3099–3162 cm⁻¹ (Tarasevich B. N., 2012).

- In the IR-spectra of adipic acid, the absorption spectra of the valence vibrations of the ν(C=O) bond are in the 1694 cm⁻¹ region, δ(OH) is in the

1280 cm⁻¹ region, and δ(CH) is in the 737 cm⁻¹ region (Kazitsyna L. A., Kupletskaya N. B., 1971);

- When the IR spectra of complex compounds were analyzed, new wavelengths were observed, unlike the ligands;
- Valence vibrations of C=N bonds in complex compounds gave an intense signal in the range of 1654–1686 cm⁻¹. Valence vibrations of -N-N- bonds appeared in the range of 1020–1098 cm⁻¹, with absorption lines of the NH₂ group around 3090–3107 cm⁻¹.

In the IR spectra of coordination compounds, absorption areas appear in the region of 1620–1525 cm⁻¹, which is characteristic of asymmetric stretching vibrations of the carboxylate anion. In the spectra of the synthesized compounds, symmetric stretching vibrations of the anion appear in the region of 1440–1340 cm⁻¹.

Table 1. The main vibrational frequencies of IR-spectra

Compound	ν _s (C=N)	δ (NH ₂)	ν(COO ⁻)	ν (-N-N)	ν (C-S)	ν (M-N)	ν (M-O)
[Zn(L)(Adp)(H ₂ O)] ₂	1691	3279	1505	1044	613	554	491
[Cu(L)(Adp)(H ₂ O)] ₂	1686	3277	1507	1086	611	557	511
[Co(L) ₂ (Adp) ₂ (H ₂ O) ₂]	1654	3291	1508	1098	616	506	455
[Ni(L) ₂ (Adp) ₂ (H ₂ O) ₂]	1684	3281	1552	1060	637	511	458

The difference in the wavelengths of the asymmetric and symmetric stretching vibrations of the carboxylate anion ranges from 86 cm⁻¹ to 255 cm⁻¹. Such values of ν indicate that in coordination compounds, both monodentate and bidentate, as well as bidentate-bridge methods of coordination of the carboxylate anion are implemented. It should be noted that for polymeric carboxylates, a combination of different modes of ligand coordination is often observed. In the IR spectrum, it was confirmed that the valence vibrations of M ← N, and M ← O bonds appeared at frequencies of 407–491 and 511–554 cm⁻¹.

The thermal decomposition process is a complex multi-step process with the release of intermediate products. Thermal decomposition of complexes is significantly affected

by the presence of metal and components of complex compounds (Nakanishi K., 2013; Wendlandt W. 1978).

The results of thermal analysis, the nature of thermal effects, observation of thermal decomposition of compounds, temperature intervals of effects and their nature, as well as mass loss in percentages in the same effect interval are presented in Table 2.

Analysis of the dynamic thermogravimetric curve (DTGA) of [Ni(L)₂(adi)₂(H₂O)₂] shows that the DTGA curve mainly takes place in the 2 intense decomposition temperature ranges, and one mass loss process that goes with absorption occurs. Decomposition range 1 corresponds to the temperature of 186–222 °C, decomposition range 2 corresponds to the temperature of 222–353 °C, and the mass absorption

range corresponds to the temperature of 353–800 °C.

The analysis shows that an intensive decay process took place during the 2nd decay

interval. In this interval, 32% of the decomposition has taken place. A detailed analysis of dynamic thermogravimetric analysis curve and DSK curve is shown in Table 2–3.

Table 2. DTGA and DSK curve results of $[Ni(L)_2(Adp)_2(H_2O)_2]$

No.	Temperature, °C	Mas Loss mg	Mass Loss, %	The amount of energy consumed, J	Time, min.
1	100	0.271	4.77	1.23	7.33
2	200	0.726	12.79	7.76	16.97
3	300	3.434	60.48	16.22	27.35
4	400	3.701	65.18	13.66	37.52
5	500	3.771	66.41	3.56	47.77
6	600	3.914	68.93	15.57	58.07
7	700	4.340	76.43	54.83	68.38
8	800	4.633	81.60	118.06	78.83

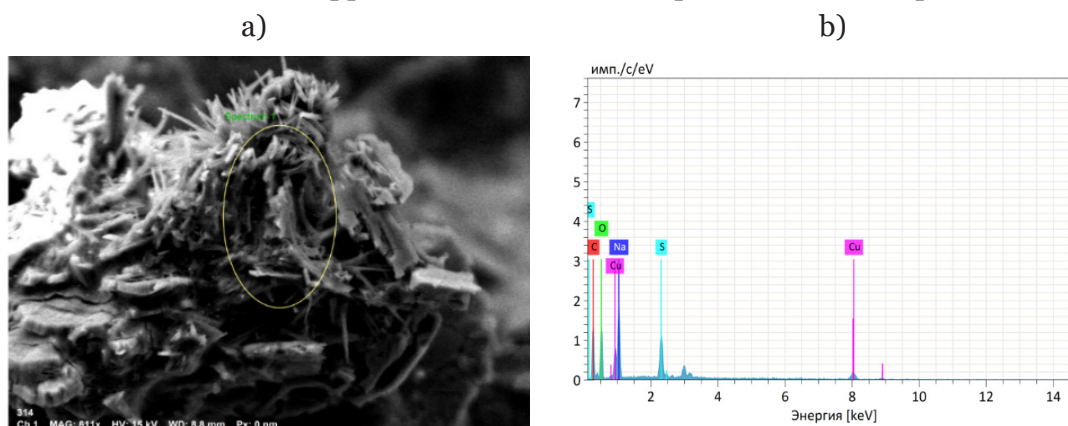
Table 3. DTGA and DSK curve results of $[Cu(L)(Adp)(H_2O)]_2$

No.	Temperature °C	Mass Loss, mg	Mass Loss, %	The amount of energy consumed, J	Time, min.
1	100	0.067	1.56	2.39	7.70
2	200	0.349	8.10	6.81	17.77
3	300	1.332	30.95	12.28	27.83
4	400	1.698	39.45	11.09	38.02
5	500	2.297	53.37	3.65	42.27
6	600	2.342	54.41	18.19	58.57
7	700	2.475	57.50	41.85	68.9
8	800	2.946	68.45	81.57	79.35

Element analysis SEM-EDA – With the help of electron beams (in electron microscopes) or X-rays (in X-ray fluorescence analyzers), the atoms of the studied sample are stimulated and emit X-ray radiation characteristic of each

chemical element. By studying the energy spectrum of such radiation, it is possible to draw a conclusion about the qualitative and quantitative composition of the sample (Nuralieva G. A., Aliyeva M., 2023; Marshall J. L. 1991).

Figure 1. a) microstructure and b) EDA diagrams of $[Cu(L)(Adp)(H_2O)]_2$
From the SEM-EDA data of complex compounds formed with ligands, it was determined that copper and nickel ions were present in the complex

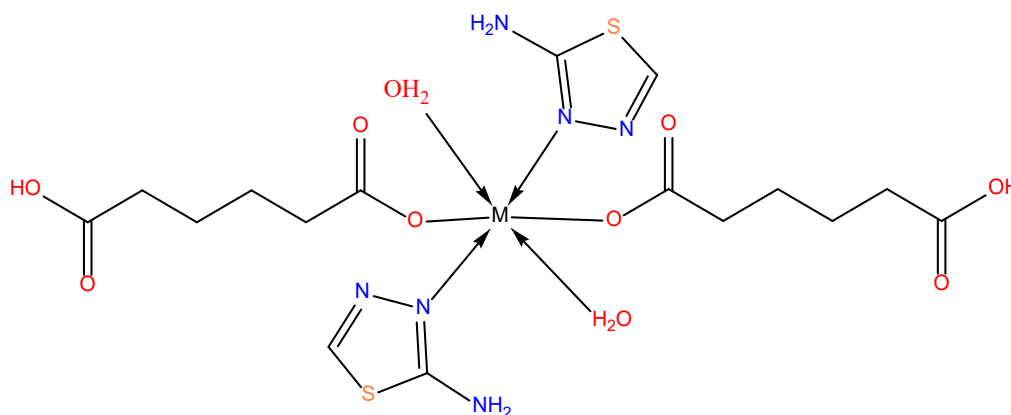


The amounts of elements (carbon, nitrogen, sulfur, oxygen, metal elements) in the synthesized mixed ligand complexes were analyzed using the SEM-EDA method. The microstructure and EDA diagrams of the obtained complexes are presented in (Fig. 1). The amount of nitrogen, sulfur and metal in the obtained complex compounds was determined using energy-dispersive analysis (SEM-EDA) by scanning energy microscopy. Based on the SEM and EDA data, it can be concluded that the complex formation of metal ions with organic ligands leads to changes in the microstructure of the ligands, in particular, many metal peaks are recorded, which is confirmed by EDA analysis.

Conclusion

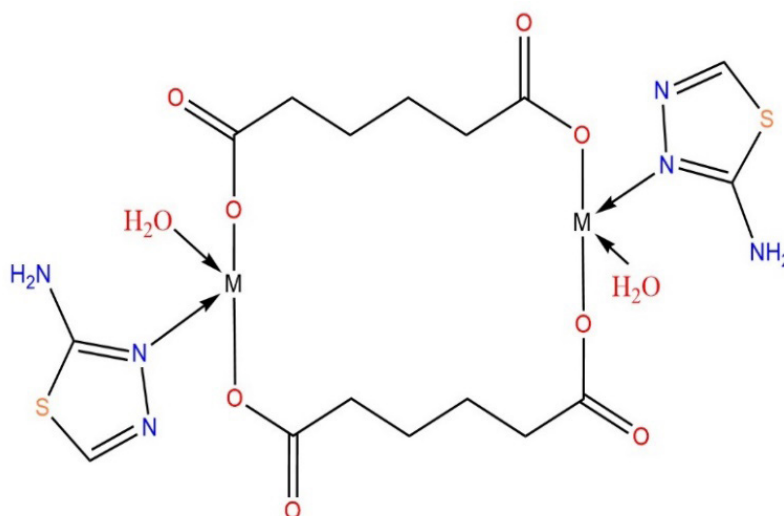
The composition, structure and properties of the synthesized complex compounds were analyzed using physico-chemical methods: elemental analysis, IR-spectroscopy, thermal analysis and SEM-EDA methods. It was found that in complex compounds with synthesized Co(II) and Ni(II) metal salts, the nitrogen atom in the 2-amino-1,3,4-thiadiazole molecule is coordinated to the central atom, and adipic acid is coordinated to the oxygen atoms of the carboxyl group.

Based on physical and chemical studies, it was concluded that the structure of the complex compound is composed of 2-amino-1,3,4-thiadiazole – metal-adipine in a ratio of 2:1:2, and the structure of the complex compounds synthesized with Ni(II), Co(II) metal salts recommended as follows:



It was found that with Cu(II) and Zn(II) salts, the nitrogen atom in the 2-amino-1,3,4-thiadiazole molecule was coordinated to the central atom through the atom, and adipic acid was coordinated to the oxy-

gen atoms of the carboxyl group in the bridge position, forming a binuclear complex compound. The structure of complex compounds synthesized with Cu(II), Zn(II) metal salts was suggested as follows.



References

- Atmaram, U. A., Roopan, S. M. (2022). Biological activity of oxadiazole and thiadiazole derivatives // *Appl. Microbiol. Biotechnol.* – 106. – P. 3489–3505. [CrossRef] [PubMed]
- Ye Song, Yu-Fei Ji, Min-Yan Kang and Zhi-Liang Liu. (2012). Acta Crystallographica Section E Structure Reports ISSN 1600-536 Bis(2-amino-5-methyl-1,3,4-thiadiazole-3) dichloridocobalt(II) // Acta Crystallographica Section E Structure Reports. Doi:10.1107/S1600536812020995
- Masahiko Maekawa, Megumu Munakata, Takayoshi Kuroda-Sowa, Yusaku Suenaga, Kunihi Sugimoto. (1999). Synthesis and crystal structure of tetranuclear copper(I) and silver(I) complexes bridged by 2-amino-1,3,4-thiadiazole(atdz): $[\text{Cu}_4(\text{atdz})_6](\text{ClO}_4)_4 \cdot 2\text{CH}_3\text{OH}$ and $[\text{Ag}_4(\text{atdz})_6](\text{ClO}_4)_4$ // P. 153–158.
- Na Wang, Qiu-Yue Lin, Jie Feng, Yu-Ling Zhao, Yan-Jun Wang, Shi-Kun Li. (2010). Crystal structures, DNA interaction and antiproliferative activities of the cobalt (II) and zinc (II) complexes of 2-amino-1,3,4-thiadiazole with demethylcantharate // *Inorganica Chimica Acta* – № 363. – P. 3399–3406.
- Wu Q. et al. (2015). Two novel Cu (II) complexes: Synthesis, structure and application in C–H bond activation // *Polyhedron.* – T. 87. – P. 390–397.
- Nuralieva G. A., Xayrullayev G. U., Kadirova Sh.A. (2020). Challenges of heterocyclical mixed ligand unions with d-metals of acetamid and thiosemikarbazid // *Solid state technology* – 63. – No. 6. – P. 360–369.
- Tarasevich B. N. (2012). IR spectra of the main classes of organic compounds // Reference materials.
- Kazitsyna L. A., Kupletskaya N. B. (1971). Application of UV, IR, and NMR spectroscopy in organic chemistry // *Vyshshaya Shkola, Moscow.* – P. 23–60.
- Наканиси К. (2013). Инфракрасные спектры и строение органических соединений. – Рипол Классик,
- Уэндландт У. Термические методы анализа // *Thermal Methods of Analysis*// Пер. с англ. под ред. Степанова В.А. и Берштейна В. А. – М.: Мир, 1978. – 526 с.
- Nuralieva G. A., Aliyeva M. (2023). Complex compounds of 2-amino 1,3,4- thiadiazole with 3d-metals and glutar acid // *Universum: химия и биология: электрон. научн. журн.* 11(113). URL: <https://7universum.com/ru/nature/archive/item/16087>
- Marshall J. L. (1991). Scanning electron microscopy and energy dispersive X-ray (SEM/EDX) characterization of solder solderability and reliability // *Solder joint reliability: theory and applications.* – Boston, MA: Springer US, – P. 173–224.

submitted 09.10.2024;

accepted for publication 24.10.2024;

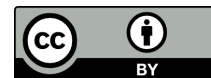
published 28.11.2024

© Alieva M. Z., Nuraliyeva G. A.

Contact: mushtariy3975@gmail.com; nuralieva.guzal@mail.ru



DOI:10.29013/AJT-24-9.10-14-19



POLYSACCHARIDE-BASED CROSSLINKED GEL MATERIALS AND THEIR PROPERTIES

*Boydedaev Azizbek Anvarjon ugli*¹, *Mukhitdinov Bakhtiyor Ikromovich*¹,
*Amonova Dilnoza Mukhtarovna*¹, *Normakhamatov Nodiralii*
*Sakhobataliyevich*², *Turaev Abbaskhan Sabirkhanovich*¹

¹ Academy of sciences of the Republic of Uzbekistan Institute of
Bioorganic chemistry named after academician A. S. Sadykov

² Tashkent Pharmaceutical Institute

Cite: Boydedaev A.A., Mukhitdinov B.I., Amonova D.M., Normakhamatov N.S., Turaev A.S. (2024). Polysaccharide-Based Crosslinked Gel Materials and Their Properties. Austrian Journal of Technical and Natural Sciences 2024, No 9–10. <https://doi.org/10.29013/AJT-24-9.10-14-19>

Abstract

The article presents research on obtaining gel-based delivery systems from hyaluronic acid and low molecular weight chitosan in H₂O and DMF environments, utilizing activators CIMPI/HOBt. It was determined that the obtained gel-based delivery systems form saturation curves at the highest percentage in aqueous solution. Additionally, studies on the acute toxicity of the gel-based delivery systems revealed that these samples belong to class VI-non-toxic compounds, and it was found during the experiments that the hemostatic properties of the obtained gel-based delivery systems are 3.0 times higher compared to the control group.

Keywords: Hyaluronic acid, chitosan, low molecular weight chitosan, hydrogel, swelling degree, hemostatic pharmacotoxicology

Introduction

Depending on their location and functions in the body, hyaluronic acid can exist in various molecular weights (5–20000 kDa) (Chistyakov et al., 2019; Xue et al., 2020). High molecular weight, low molecular weight, and (Gao et al., 2019) forms of hyaluronic acid participate in various biochemical and physiological processes as signaling molecules. In addition to its signaling function, high molecular weight hyaluronic acid also plays a role in the structure of cells

and tissues. Hyaluronic acid is particularly important for obtaining therapeutic delivery systems in various forms, such as conjugates with biologically active compounds, nanomaterials, and hydrogel materials (Bencherif et al., 2008; Guo et al., 2021; Nikjoo et al., 2021). Gel-based delivery systems derived from hyaluronic acid can be prepared by conjugating with biomolecules, including chito-oligosaccharides, which have the ability to enhance anti-cancer immunity by activating macrophages in the body through

polysaccharide chains (Chokradjaroen et al., 2018; Lee et al., 2002). In our recent research, an efficient and glycosidic bond-specific method for preparing functional oligosaccharides has been developed (Toole et al., 2008). Preliminary research results on applying these findings to other biopolymers indicate that this method can be used to obtain low molecular weight chitosans (LMW-CS) with any desired degree of polymerization. However, it remains crucial to deeply analyze the optimal reaction conditions for producing LMW-CS's and the changes that may occur in the polysaccharide chain during the reaction. Recently, there has been an increasing interest in developing biomaterials with the ability to form injectable hydrogels, therapeutic implants, and drug delivery systems (Drury & Mooney, 2003; Hoffman, 2002). Traditional hydrogel materials do not allow for direct administration into the body, requiring surgical procedures. To address these shortcomings, it is crucial to develop injectable hydrogel matrices based on biocompatible, biodegradable polysaccharides that have minimal adverse effects on the body. These types of hydrogel matrices can be administered into the body using a syringe. Therefore, obtaining hydrogel materials based on hyaluronic acid and LMW-CS that can be directly injected into the body and investigating the optimal reaction conditions is one of the urgent tasks.

The purpose of this scientific work is to prepare hydrogel samples through covalent bonding of hyaluronic acid and LMW-CS under the influence of activating reagents, as well as to study their physicochemical properties and biological activity.

Research Objectives:

- to synthesize covalently bonded hydrogel samples based on LMW-CS using sodium salt of high molecular weight hyaluronic acid at various molar ratios under the influence of activating reagents;
- to purify the obtained hydrogel samples from additives. to study the physicochemical properties of prepared hydrogel samples;
- to study the swelling ratio, pharmacotoxicology, and hemostatic activity of the hydrogel samples.

Materials and methods:

Obtaining Hydrogels Based on hyaluronic acid and LMW-CS

A 40.0 mg/ml concentration solution of hyaluronic acid (Mw = 1480 kDa, DP = 3691, DPI = 4.11) was prepared. After hyaluronic acid formed a clear viscous solution in the solvent, a 15.0 mg/ml concentration solution of LMW-CS (Mw = 12.2 kDa, DP = 75.3, DPI = 1.25) was added at a ratio of 0.5 mol/mol of hyaluronic acid unit (HAU) and stirred for 30–60 minutes. Subsequently, 2-chloro-1-methylpyridinium iodide (ClMPI)/1-hydroxybenzotriazole (HOBt) was added to the reaction mixture at a ratio of 0.6/1.0 mol/mol of HAU and the reactions continued until hydrogel samples were formed. The resulting hyaluronan/chitosan-based (H-LMW-CS) hydrogel matrices were purified by dialysis for 48 hours in a phosphate buffer solution (pH = 7.4) and for 24 hours in deionized water to remove additives.

Study of the Structures of Samples

The IR spectra of the samples were obtained using the Thermo Nicolet AVATAR 370 FTIR spectrometer by the KBr pellet method or directly using the Shimadzu IRTracer-100 spectrometer in the absorption range of 400–4000 cm⁻¹.

Determining the Swelling Degree of H-LMW-CS

The swelling ratio of the prepared hydrogel samples was observed in three types of solutions: deionized water, phosphate buffer solution (pH = 7.4), and 0.9% NaCl solution. The initial weights of the hydrogels were 15 ± 3 g. To determine the swelling ratios of each gel system, 400 ml of the above solutions were placed in 500 ml beakers, and the prepared gel samples were immersed in the solutions. At specific time intervals, the gel samples were removed from the solutions, excess water was blotted with filter paper, and they were immediately weighed. This process was repeated three times, and the average value was adjusted for measuring the swelling ratio (%). The swelling degree was calculated using the following equation.

$$A = \frac{W_0 - W_1}{W_1} \cdot 100\% \quad (2.1)$$

In the formula: W_0 is the mass of the swollen gel in water, and W_1 is the initial mass of the gel.

Determining the Pharmacotoxicological Properties of H-LMW-CS

The acute toxicity of H-LMW-CS was studied in male and female mice (weight 20 ± 2.0 g, $n = 6$) according to the Litchfield and Wilcoxon method. In the experiments, H-LMW-CS gel samples were administered subcutaneously via syringe at doses of 5000–10000 mg/kg. Changes in the overall condition, tremors, and mortality were recorded hourly on the first day of the experiment after the gel samples were administered to the mice. In the subsequent phase, changes in the functional status of the animals were observed over a period of 14 days under experimental conditions, including indicators such as general condition, activity, behavior, respiration, changes in the skin, body weight variation, survival, convulsions, and mortality. All mice in the experiment were kept under uniform conditions and fed a common diet. At the end of the experiment, the average lethal dose (LD50) and toxicity class were determined.

Hemostatic Properties of H-LMW-CS

The hemostatic properties of H-LMW-CS samples were studied in male white rats weighing 180 ± 20 g, which were anesthetized by administering 1% sodium thiopental (50 mg/kg). The experiment involved opening

the abdominal cavity of the anesthetized rats using a surgical instrument (scalpel). For hepatic hemostasis, an incision was made longitudinally along the midline of the abdominal cavity, and a wide incision was created in the thoracic cavity using special clamps. The anterior part of the liver was exposed and delineated with a special gauze or filter paper. The liver was resected with a scalpel. The segment cut in the vertical projection resembled a circle or an ellipse, maintaining a constant size. A wound with soft edges and uniform curvature was created, with an approximate area of 1–1.5 cm in depth and about 0.3 cm in diameter. Free bleeding was allowed for 20 seconds, after which 0.3 ml of H-LMW-CS was immediately applied to the defect. At the end of the experiment, the hemostatic properties of the sample were analyzed.

Results and discussion

This study explored the possibilities of obtaining gel-based delivery systems from hyaluronic acid and LMW-CS. Additionally, during the research, the effects of reaction conditions on the molecular sizes of the obtained products were examined to determine optimal reaction conditions, and gel systems necessary for investigating biological activity were prepared. The research on obtaining H-LMW-CS gel samples was conducted in H_2O and DMF environments with the activators ClMPI/HOBt.

Figure 1. Reaction for obtaining hydrogel under the influence of activating reagents based on sodium hyaluronate and low molecular weight chitosan



The studies indicated that to obtain gel samples with suitable molecular sizes, a ratio of 0.5 mol/mol of chitosan to HAU, along with 0.6 and 1.0 mol/mol of ClMPI and HOBt respectively, and a hyaluronic acid concentration of 40 mg/ml at 20 °C were optimal. The reaction for the formation of hydrogel samples proceeded through the formation of direct amide bonds ($-\text{CO}-\text{N}(\text{H}, \text{R})-$) between the carboxyl groups in hyaluronic acid and the amino groups in LMW-CS. The reaction scheme for the gel-based delivery system involving high molecular weight hyaluron-

ic acid and LMW-CS with ClMPI/HOBt is shown in Figure 1.

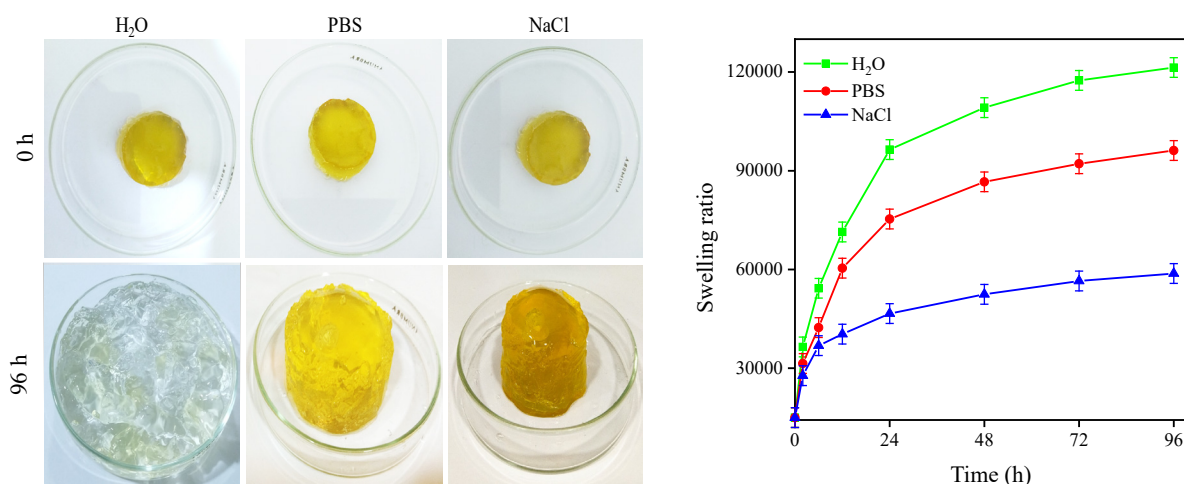
The FTIR spectra of the obtained gel samples based on high molecular weight hyaluronic acid and LMW-CS were analyzed, revealing characteristic signals corresponding to the O–H, N–H, C6–H, amide II, C–O–C, and C–C bonds in hyaluronic acid and LMW-CS samples. These signals were observed in the spectral regions of 3200–3600, 2900, 1556, 1060, and 600–894 cm^{-1} , respectively.

The swelling ratio of H-LMW-CS was determined in three different solutions: distilled

water, phosphate buffer solution (pH=7.4), and 0.9% NaCl solution. The swelling of gel materials in these solutions is of great importance, as even a small change in the swelling value leads to changes in the free volumes of water molecules passing through the polysaccharide matrix. Thus, this significantly affects the swelling properties of the gel materials. In the study, the equilibrium swell-

ing behavior of H-LMW-CS was examined at 4–8 °C over a period of 0–96 hours. The swelling ratios of H-LMW-CS in H₂O, PBS, and NaCl solutions are presented in Figure 2(a). The results of the swelling study (Figure 2(b)) showed that the swelling ratios reached a maximum of 120±3% in the aqueous solution, indicating the gel materials' insolubility and their high water retention properties.

Figure 2. Swelling degree of H-LMW-CS. In the figures: (a) Swelling state of H-LMW-CS in H₂O, PBS, and NaCl solutions; (b) Swelling dynamics of H-LMW-CS over different time intervals



According to the swelling dynamics of H-LMW-CS, the gel materials exhibited high water absorption during the initial 0–24 hours, with maximum water absorption observed at 96 hours. In PBS (pH = 7.4), H-LMW-CS showed an initial maximum swelling coefficient of $15 \pm 3 - 75 \pm 3\%$ over 0–24 hours, reaching $96 \pm 3\%$ saturation after 96 hours. This indicates that the swelling characteristics of H-LMW-CS depend on the solution environment and nature. In experiments, the presence of a small amount of 0.9% NaCl in the dialysis solution was observed to slightly reduce the swelling degree of the gel materials. It was found that increasing the concentration of the saline solution significantly affects the swelling characteristics of the gel materials. In 0.9% NaCl solution, H-LMW-CS initially exhibited a swelling of $15 \pm 3 - 46 \pm 3\%$ over 0–24 hours, with minor changes in the following hours and demonstrating a saturation of $58 \pm 3\%$ after 96 hours.

The studies investigated the overall effect and acute toxicity of H-LMW-CS on animal organisms. The experiments were conduct-

ed on male, non-purebred white laboratory mice with a body weight of 20 ± 2.0 g. All pharmacological tests were carried out on healthy, sexually mature mice that were kept under quarantine for 10–14 days. H-LMW-CS was administered subcutaneously to the mice at doses of 5000, 7000, 9000, and 10000 mg/kg. The control group received an equal volume of physiological solution.

During the first day of the experiments in laboratory conditions, the general condition of the animals in both the experimental and control groups was monitored hourly, along with any signs of tremors and mortality as indicators of their functional status. Over the next two weeks, daily assessments were made of the general condition, activity, coat condition, skin status, respiratory rate and depth, urination, body weight changes, and other parameters of all groups of animals under vivarium conditions. All experimental animals were maintained on a uniform feeding regimen, with unrestricted access to water and food.

At the end of the experiment, the average lethal dose (LD_{50}) and toxicity class of the tested samples were determined. No acute toxicity effects were observed in the aforementioned parameters at any of the doses of H-LMW-CS. Throughout the entire experiment, no deaths among the animals were recorded at these doses. Based on the results, it was determined that the average

lethal dose (LD_{50}) for the preparation when administered subcutaneously is greater than 10000 mg/kg. The results are presented in the following Table 1. The findings indicate that the acute toxicity properties of H-LMW-CS classify these samples in the VI – non-toxic compounds category, with an average lethal dose (LD_{50}) greater than 10000 mg/kg.

Table 1. Acute toxicity indicators of H-LMW-CS material when administered subcutaneously to mice in a single dose

Samples	Animal Type / Administration Method	Dose (mg/kg)	Number of Dead/Surviving Animals	$LD_{50} - m + m$ (mg/kg)
H-LMW-CS	Mouse / Subcutaneous	5000	5/0	>10000 mg/kg
		7000	5/0	
		9000	5/0	
		10000	5/0	
Control		0.5	5/0	

The hemostatic properties of H-LMW-CS were studied. Groups treated with medical gauze were used as controls. In the experiments, bleeding time (in seconds) and blood loss were recorded immediately. The results showed that when medical gauze was applied to the control group, the bleeding time from the liver's parenchyma was 125 ± 5 seconds, while in the groups treated with H-LMW-CS, bleeding was stopped within intervals of 40 ± 5 seconds. It was determined that the hemostatic properties of H-LMW-CS were 3.0 times higher compared to the control group.

Conclusion

The gels were obtained based on hyaluronic acid ($M_w = 1480$ kDa, $DP = 3691$, $DPI = 4.11$) and LMW-CS ($M_w = 12.2$ kDa, $DP = 75.3$, $DPI = 1.25$). The study of the degree of saturation of the obtained samples showed that they formed saturation curves with a maximum of $120 \pm 3\%$ in an aqueous solution. The results of the study of the acute toxicity characteristics of H-LMW-CS indicated that these samples belong to the class of VI-non-toxic compounds, and when administered subcutaneously, the average lethal dose (LD_{50}) was found to be > 10000 mg/kg.

References

- Bencherif, S.A., Srinivasan, A., Horkay, F., Hollinger, J.O., Matyjaszewski, K., & Washburn, N.R. (2008). Influence of the degree of methacrylation on hyaluronic acid hydrogels properties. *Biomaterials*, – 29(12). – P. 1739–1749. URL: <https://doi.org/10.1016/j.biomaterials.2007.11.047>
- Chistyakov, D.V., Astakhova, A.A., Azbukina, N.V., Goriainov, S.V., Chistyakov, V.V., & Sergeeva, M.G. (2019). High and low molecular weight hyaluronic acid differentially influences oxylipins synthesis in course of neuroinflammation. *International Journal of Molecular Sciences*, (2016). URL: <https://doi.org/10.3390/ijms20163894>
- Chokradjaroen, C., Theeramunkong, S., Yui, H., Saito, N., & Rujiravanit, R. (2018). Cytotoxicity against cancer cells of chitosan oligosaccharides prepared from chitosan powder degraded by electrical discharge plasma. *Carbohydrate Polymers*, – 201. – P. 20–30. URL: <https://doi.org/10.1016/J.CARBPOL.2018.08.037>

- Drury, J. L., & Mooney, D. J. (2003). *Hydrogels for tissue engineering: scaffold design variables and applications*. — 24. — P. 4337–4351. URL: [https://doi.org/10.1016/S0142-9612\(03\)00340-5](https://doi.org/10.1016/S0142-9612(03)00340-5)
- Gao, Y., Sun, Y., Yang, H., Qiu, P., Cong, Z., Zou, Y., Song, L., Guo, J., & Anastassiades, T. P. (2019). A Low Molecular Weight Hyaluronic Acid Derivative Accelerates Excisional Wound Healing by Modulating Pro-Inflammation, Promoting Epithelialization and Neovascularization, and Remodeling Collagen. *International Journal of Molecular Sciences*, — 20(15). — 3722(1–19). URL: <https://doi.org/10.3390/ijms20153722>
- Guo, L., Chai, Y., Zhou, F., & Wang, P. (2021). Preparation and Properties of Hyaluronic Acid Hydrogel Modified by L-cysteine Hydrochloride. *IOP Conference Series: Earth and Environmental Science*, — 651(4). URL: <https://doi.org/10.1088/1755-1315/651/4/042022>
- Hoffman, A. S. (2002). *Hydrogels for biomedical applications*. — 43. — P. 3–12.
- Lee, H.-W., Park, Y.-S., Jung, J.-S., & Shin, W.-S. (2002). Chitosan oligosaccharides, dp 2–8, have prebiotic effect on the Bifidobacterium bifidum and Lactobacillus sp. *Anaerobe*, — 8(6). — P. 319–324. URL: [https://doi.org/10.1016/S1075-9964\(03\)00030-1](https://doi.org/10.1016/S1075-9964(03)00030-1)
- Nikjoo, D., van der Zwaan, I., Brülls, M., Tehler, U., & Frenning, G. (2021). Hyaluronic acid hydrogels for controlled pulmonary drug delivery — a particle engineering approach. *Pharmaceutics*, — 13(11). URL: <https://doi.org/10.3390/pharmaceutics13111878>
- Toole, B., Ghatak, S., & Misra, S. (2008). Hyaluronan Oligosaccharides as a Potential Anti-cancer Therapeutic. *Current Pharmaceutical Biotechnology*, — 9(4). — P. 249–252. URL: <https://doi.org/10.2174/138920108785161569>
- Xue, Y., Chen, H., Xu, C., Yu, D., Xu, H., & Hu, Y. (2020). Synthesis of hyaluronic acid hydrogels by crosslinking the mixture of high-molecular-weight hyaluronic acid and low-molecular-weight hyaluronic acid with 1,4-butanediol diglycidyl ether. *RSC Advances*, — 10(12). — P. 7206–7213. URL: <https://doi.org/10.1039/C9RA09271D>

submitted 10.09.2024;

accepted for publication 25.09.2024;

published 28.11.2024

© Boydedaev A. A., Mukhitdinov B. I., Amonova D. M., Normakhamatov N. S., Turaev A. S.
Contact: azizbek.boydedaev@gmail.com

DOI:10.29013/AJT-24-9.10-20-26



TARGETED MODIFICATIONS OF 5,6-DISUBSTITUTED-4-CHLOROTHIENO[2,3-d]PYRIMIDINES WITH BENZYLAMINE

*Guzal Khamraeva*¹, *Yunusjon Valiev*¹, *Abdugani Berdiev*¹,
*Foziljon Saitkulov*¹, *Burkhon Elmuradov*²

¹ Organic Synthesis Department, Institute of the Chemistry of Plant
Substances, Academy of Sciences of the Republic of Uzbekistan

² Tashkent state agrarian university, Uzbekistan

Cite: Khamraeva G., Valiev Y., Berdiev A., Saitkulov F., Elmuradov B. (2024). Targeted modifications of 5,6-Disubstituted-4-Chlorothieno[2,3-d]Pyrimidines with benzylamine. *Austrian Journal of Technical and Natural Sciences* 2024, No 9–10. <https://doi.org/10.29013/AJT-24-9.10-20-26>

Abstract

Formed from two different components and covalently linked, hybrid blocks make it possible to achieve more effective results due to the fact that each molecule has specific properties that differ from those expected. This concept has been successfully used in the creation and production of hybrid drugs. The combination of chemically distinct pharmacophores in the form of a single molecule results in at least two or multiple manifestations of the hybrid molecule potential. Therefore, this article highlights the processes of joining two fragments with high biological activity – thienopyrimidine and benzylamine – as well as the synthesis of new hybrid molecules and the study of their structure using modern methods of physical and chemical analysis. The structures of the obtained compounds were elucidated using IR, ¹H and ¹³C NMR spectroscopy. X-ray crystal structure analyses of the synthesized compounds were performed. **Keywords:** 4-chlorothieno[2,3-d]pyrimidines; nucleophilic substitution products; thienopyrimidine derivatives; benzylamine; targeted syntheses

1. Introduction

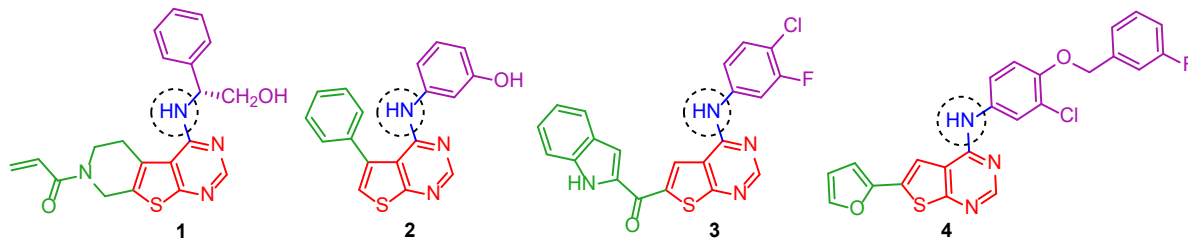
Thieno[2,3-d]pyrimidines most of them are potential biologically active compounds that exhibit activity against microbes (Bozorov Kh., Zhao J. Yu., Elmuradov B., Pataer A., Aisa H. A. 2015; Elmahdy K. M., Elkazak A. M., Megid A. M., Seada M., Mohamed O. F., 2013), viruses (Rashad A. E. Ali M. A., 2006), inflammation (El-Gazzar A. B., Hussein H. A., Hafez H. N., 2007), and diabetes (Deng J. F.,

Peng L., Zhang G. C., Lan X. B., Li C. F., Chen F. X., Zhou Y. Y., Lin Z. X., Chen L., Dai R. K., Xu H. J., Yang L., Zhang X. Q., Hu W. H. Eur. J., 2011). Several TP derivatives are antidepressants, antihypertensive agents (Nagaraju K., Harikrishna N., Vasu K., Rao C. V., 2015), and antioxidants (Guo Y., Li J., Ma J., Yu L. Z., Wang H., Zhu W., Liao X., Zhao Y., 2015). Those with an NH bridge in the 4-position have therapeutic activity against malig-

nant tumors (Bozorov Kh., Zhao J. Yu., Elmuradov B., Pataer A., Aisa H. A., 2015; Zhu W., Chen C., Sun C., Xu S., Wu C., Lei F., Xia H., Tu Q., Zheng P., 2015); Kim Y., Kim M., Park M., Tae J., Baek D., Park K. D., Choo H., 2015) and are especially interesting for synthesizing hybrid nucleophile–thienopyrimidine molecules. In most of the data presented in the literature, as a result of chemical changes in the 4th position of the thieno[2,3-d]pyrimidine ring, in particular, aromatic or heterocyclic fragments connected to the 4th position through -NH-, -NR- bridges and containing various substituents are used in increases the synthetic and biological potential for molecules (Berdiev A. U., Ortikov I. S., Turgunov K. K., Elmuradov B. Zh., Abdullaev N. D., Tashkhodzhaev B., 2024). Especially, compounds with this structure show high activity against cancer cells. It is noteworthy that currently used drugs with high cytotoxic activity (*erlotinib*, *gefitinib*, *lapatinib*, *afatinib*, *canertinib*, etc.) and the active substances of the drugs are also formed by means of such

imino bridges (Berdiev A. U., Mirsodikov M. M., Ortikov I. S., Elmuradov B. Zh., 2023). This is the reason for the synthesis of new types of active thienopyrimidine analogues of these compounds (Berdiev A. U., Ortikov I. S., Elmuradov B. Zh., 2022). Thieno[2,3-d]pyrimidines are one of the most widely used and studied important sections of synthetic organic chemistry, demonstrating activity against various types of cancer tumors by inhibiting protein kinases (Berdiev A. U., Ortikov I. S., Elmuradov B. Zh., 2022). Biological studies of these compounds have shown that the property of inhibiting protein kinases occurs due to the introduction and replacement of various functional groups in the structure of the thienopyrimidine fragment (Berdiev A. U., Mirsodikov M. M., Ortikov I. S., Elmuradov B. Zh., 2022). This leads to the emergence of anticancer activity. Below is the structure of various protein kinase inhibitors, which are obtained on the basis of studies and contain the thieno[2,3-d]pyrimidine base with high inhibition property.

Figure 1. Structure of protein kinase inhibitors with some strong effects



Based on this, among the interesting chemical changes of 4-chlorothieno[2,3-d]pyrimidines, we performed their nucleophilic exchange reactions with benzylamine.

2. Materials and Methods

IR spectra were taken from KBr pellets on a System 2000 FTIR spectrometer (PerkinElmer, USA). ¹H and ¹³C NMR spectra were recorded in CDCl₃, DMSO-d₆, and Py-D₅ solutions with TMS internal standard (0 ppm) on a JNM-ECZ400R instrument (JEOL, Japan) at 400 MHz for ¹H and 100 MHz for ¹³C. TLC used TLC Silicagel 60 F254 L/W 20cm × 20cm (Merck, Germany) and Whatman® UV-254 plates (Sigma-Aldrich, Germany) with elution by C₆H₆ –

– MeOH (5:1, **I**) and hexane – ethyl acetate (5:1, **II**). Melting points of synthesized compounds were determined on Biobase BMP-M70 (China) and Mel-Temp apparatuses (USA).

2-Amino-5,6-disubstituted thio-*phene-3-ethylcarboxylates* (5-9) were prepared by the literature method (Berdiev A.U., Ortikov I.S., Elmuradov B.Zh. (2022)). Cyclopentanone (3.55 mL, 3.36 g, ρ = 0.95 g/mL, 0.04 mol), cyanoacetic ester (4.52 g, ρ = 1.06 g/mL, 0.04 mol), S₈ (1.408 g, 0.044 mol), anhydrous EtOH (12 mL), and morpholine (4.0 mL, 4.05 g, 0.046 mol) gave **5** (7.10 g, 85%), mp 88-90°C (cyclohexane), R_f 0.70 (system II).

5,6-Disubstituted thieno[2,3-d]pyrimidin-4-ones (10-14) were prepared by the literature method (Berdiev A.U., Ortikov I.S., Elmuradov B.Zh. (2022)). *2-Amino-4,5,6-trihydrocyclopenta [b] thiophene-3-ethylcarboxylate (5)*, 4.22 g, 0.002 mol) and formamide (10 mL, 11.3 g, $\rho = 1.13$ g/mL, 0.24 mol) gave **10** (3.27 g, 85%, mp 216-218°C (EtOH), Rf 0.36 (system I)).

4-Chloro-5,6-disubstituted thieno[2,3-d]pyrimidines (15-19) (General Method). A mixture of *3,5,6,7-tetrahydro-4H-cyclopenta (El-Gazzar A.B., Hussein H.A., Hafez H.N. (2007); Deng J.F., Peng L., Zhang G.C., Lan X.B., Li C.F., Chen F.X., Zhou Y.Y., Lin Z.X., Chen L., Dai R.K., Xu H.J., Yang L., Zhang X.Q., Hu W.H. Eur. J. (2011)) thieno[2,3-d]pyrimidin-4-one (10)*, 0.96 g, 0.005 mol), POCl₃ (2.0 mL), CCl₄ (5.0 mL), and Et₃N (1.0 mL) was refluxed at 77°C for 4 h and cooled to room temperature. The mixture was diluted with CHCl₃ (15 mL), neutralized with NaHCO₃ solution (15%, 50 mL), and washed several times with distilled H₂O. The CHCl₃ part was dried over anhydrous Na₂SO₄ (4 h). The Na₂SO₄ was filtered off. The CHCl₃ was distilled in a rotary evaporator. The solid was recrystallized from EtOH to afford **15** (1.0 g, 96%) as a white crystalline product, mp 103-104°C, Rf 0.89 (system II). ¹H NMR (400 MHz, CDCl₃, δ , ppm): 2.53 (2H, m, H-6), 3.06 (2H, m, H-5), 3.16 (2H, m, H-7), 8.70 (1H, s, H-2).

Synthesis of N-benzyl-5,6-disubstituted thieno[2,3-d]pyrimidin-4-amines (20-24) (General Method)

In a 50 ml round-bottomed flask were poured 0.002 mol of *4-Chloro-5,6-disubstituted thieno[2,3-d]pyrimidines (15-19)*, 0.50 ml (0.490 g, $\rho = 0.981$ g/ml, 0.004 mol) of benzylamine, 0.55 ml (0.40 g, $\rho = 0.726$ g/ml, 0.004 mol) of triethylamine, 15.0 ml of ethanol, a reflux condenser was connected and the mixture was boiled in a water bath for 6 hours. The mixture was left overnight at room temperature and the resulting precipitate was filtered off. The precipitate was washed with 5% NaOH solution, then several times with water, dried at room temperature and the product was obtained. The resulting technical mass was purified by recrystallization from ethanol. As a result, white crystalline products (**20-24**) were obtained.

N-Benzyl-6,7-dihydro-5H-cyclopenta thieno[2,3-d]pyrimidin-4-amine (20) was prepared analogously to the method above from **15** (0.421 g) to afford **20** (0.522 g, 93%) mp 152-154°C (ethanol), Rf 0.73 (system I). Table 2 presents the ¹H NMR spectral data. ¹³C NMR (100 MHz, CDCl₃, δ , ppm): 28.07, 29.33, 29.61, 44.76, 113.38, 127.65, 127.70, 128.94, 134.38, 138.67, 138.94, 153.25, 156.73, 171.00.

N-Benzyl-5,6,7,8-tetrahydrobenzo thieno[2,3-d]pyrimidin-4-amine (21) was prepared by the above method from **16** (0.449 g) to afford **21** (0.578 g, 98%) mp 112-114°C (ethanol), Rf 0.78 (system I). Table 2 presents the ¹H NMR spectral data. ¹³C NMR (100 MHz, CDCl₃, δ , ppm): 22.57, 22.62, 25.54, 26.52, 44.99, 116.16, 125.45, 127.69, 127.73, 128.96, 133.50, 138.72, 153.19, 157.31, 165.58.

N-Benzyl-6,7,8,9-tetrahydro-5H-cyclohepta thieno[2,3-d] pyrimidine-4-amine (22) was prepared analogously to the method above from **17** (0.477 g) to afford **22** (0.587 g, 95%) mp 95–97 °C (ethanol), Rf 0.77 (system I). Table 2 presents the ¹H NMR spectral data. ¹³C NMR (100 MHz, CDCl₃, δ , ppm): 26.35, 27.12, 28.97, 30.40, 30.42, 45.15, 117.28, 127.67, 127.76, 128.94, 130.26, 137.27, 138.78, 152.74, 157.23, 164.43.

N-Benzyl-5,6-dimethylthieno [2,3-d] pyrimidin-4-amine (23) was prepared by the above method from **18** (0.397 g) to afford **23** (0.505 g, 94%) mp 164–166 °C (ethanol), Rf 0.69 (system I). Table 2 presents the ¹H NMR spectral data. ¹³C NMR (100 MHz, CDCl₃, δ , ppm): 13.48, 14.56, 45.02, 117.06, 123.05, 127.69, 128.94, 130.09, 138.68, 153.10, 157.26, 164.84.

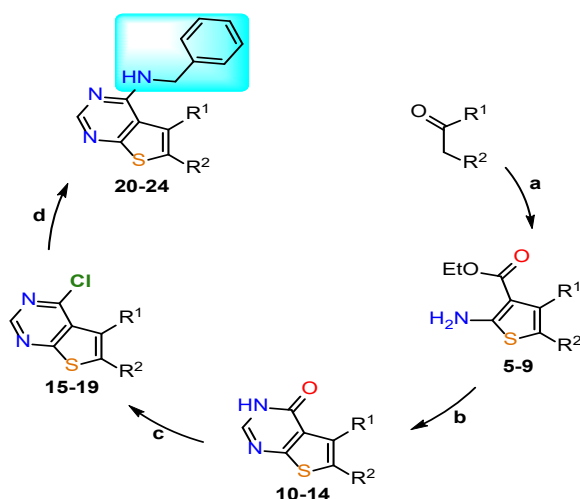
N-Benzyl-5-methyl-6-ethoxycarbonylthieno[2,3-d]pyrimidin-4-amine (24) was prepared analogously to the method above from **19** (0.513 g) to afford **24** (0.621 g, 95%) mp 129-131 °C (ethanol), Rf 0.81 (system I). Table 2 presents the ¹H NMR spectral data. ¹³C NMR (100 MHz, CDCl₃, δ , ppm): 14.41, 15.95, 45.26, 61.55, 117.17, 122.94, 127.81, 127.96, 129.09, 137.89, 138.04, 156.04, 159.00, 163.00, 167.35.

3. Results and Discussion

For this, substituted thieno[2,3-d]pyrimidine-4-ones (**10–14**) were synthesized in two steps via formation of 2-aminothiophene esters (**5–9**) according to the published method (Berdiev A.U., Ortikov I.S., Elmuradov B.Zh. (2022)). Compounds **10–14** reacted with POCl_3 in CCl_4 solution to form 4-chlorothieno[2,3-d]pyrimidines (**15–19**) with a 4-Cl atom in high yields. These compounds were intermediates for the synthesis of antitumor agents and played important roles as necessary synthons in targeted organic syntheses. The imidoyl Cl atom on the pyrimidine ring was highly reactive although the molecules (**15–19**) were stable, so they could be used in reactions with various nucleophilic reagents.

Reactions were carried out by boiling a 1:2 equiv mixture of substrate and reagent in ethanol medium (80 °C) in the presence of TEA (2 equiv) for 6 h. As a result, corresponding substances **20–24** were synthesized with high yields (93–98%).

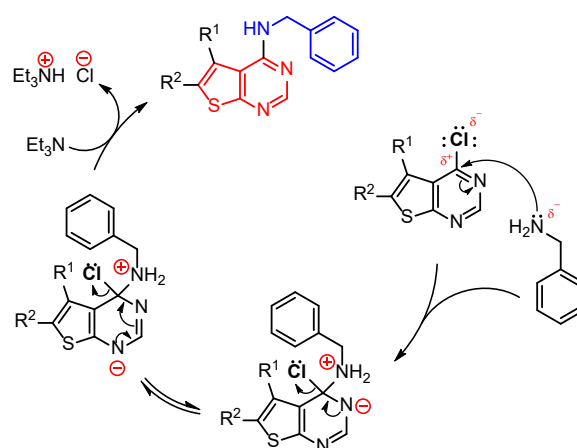
Figure 2. Reagents and reaction conditions: (a) Ethyl cyanoacetate, S_8 , morpholine, anhydr. EtOH, 40–45 °C, 24 h; (b) formamide, 150 °C, 8 h; (c) POCl_3 , CCl_4 , TEA, 77 °C, 4 h; (d) benzylamine, TEA, anhydr. EtOH, 80 °C, 6 h



Accordingly, the electron density of the carbon bound to chlorine and nitrogen atoms in the pyrimidine ring is reduced due to the effect of atoms with high electronegativity, so the nucleophilic attack of ben-

zylamine nitrogen takes place. At the next stage, the energetic instability of the sp^3 hybridized C atom in the 4th state decreases as a result of redistribution of electrons in the pyrimidine ring, hydrogen and chlorine ions are released, and a new C-N bond is formed. TEA participating in the reaction, in turn, acts as an acceptor for the formed HCl. Below is an approximate mechanism of the process:

Figure 3. The structure of all obtained compounds was fully proved based on the results of modern physicochemical methods, including IR, ^1H , ^{13}C NMR spectroscopy and X-ray structure analysis (XRD) of some of them



In the IR spectra of the compounds, there are absorption lines belonging to the NH group bridging thienopyrimidine-benzyl fragments, and this absorption appears at 3367 cm^{-1} in compound **20**, **21** at 3370 cm^{-1} , **22** at 3351 cm^{-1} , **23** at 3430 cm^{-1} and for compound **24** is 3446 cm^{-1} . Also, the absorption frequencies of the C-H aryl bond in the aromatic ring are at $3028\text{--}3032\text{ cm}^{-1}$, at $2919\text{--}2945\text{ cm}^{-1}$ for the C-H bonds of the aliphatic groups in the molecule, at $2840\text{--}2860\text{ cm}^{-1}$ at the aliphatic C-H bonds of the benzyl fragment, $2\text{C}=\text{N}$ and Intense absorption max. characteristic of $^4\text{C}=\text{N}$ bond at $1551\text{--}1573\text{ cm}^{-1}$ and valence vibrations of imino group nitrogen at $1493\text{--}1510\text{ cm}^{-1}$ characteristic of both C-N-C bonds were determined.

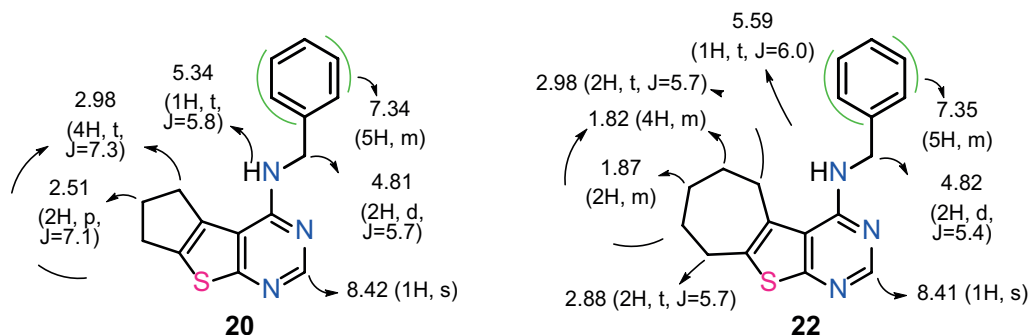
Table 1. Some physicochemical data of the obtained compounds 20–24

Compounds	R ¹	R ²	Brutto formula	Time, h	Yields, %
20	-(CH ₂) ₃ -		C ₁₆ H ₁₅ N ₃ S		93
21	-(CH ₂) ₄ -		C ₁₇ H ₁₇ N ₃ S		98
22	-(CH ₂) ₅ -		C ₁₈ H ₁₉ N ₃ S	6	95
23	-CH ₃	-CH ₃	C ₁₅ H ₁₅ N ₃ S		94
24	-CH ₃	-CO ₂ Et	C ₁₇ H ₁₇ N ₃ O ₂ S		95

In their NMR spectra (**20–24**) CDCl₃ ¹H, the most characteristic chemical shifts are the presence of the aromatic proton (H-2) at position 2 of the pyrimidine ring as a one-proton singlet in the range of 8.41–8.53 ppm, which is slightly stronger than that of the starting products (**15–19**), showing that it has shifted upfield. In addition, we can see that the signal corresponding to the ⁴C-NH hydrogen is in the form of a single proton triplet present in the 5.34–5.98 ppm regions.

Also, chemical shifts in the form of a two-proton doublet in the 4.81–4.85 ppm area belonging to the hydrogens of the benzyl group of methylene (CH₂) and in the form of a five-proton multiplet characteristic of hydrogens of the aromatic phenyl group in the area of 7.34–7.37 ppm (C₆H₅) characterize the structure of all compounds in general.

Also, as an example of the specific signals of some of these compounds, the hydrogen atoms belonging to the methylene groups at positions C-5 and C-7 of substance **20** represent a four-proton (4H, t, J = 7.3) triplet in the region of 2.98 ppm; the methylene group at position 6 at 2.51 ppm can give signals of hydrogens in the form of a two-proton pentet (2H, p, J = 7.1). Moreover, in the 2.98 and 2.88 ppm fields corresponding to the hydrogens of the C-5 and C-9 methylene groups of substance **22**, they appear as triplets with two protons (2H, t, J=5.7) each. The chemical shift values of the hydrogens of the -CH₂- group in position C-7 in the two-proton (2H, m) multiplet at 1.87 ppm and the four-proton (4H, m) multiplet in the region of 1.82 ppm methylene hydrogens in positions C-6 and C-8 indicate the structure of the compounds.

Figure 4. ¹H NMR spectrum analysis of compounds **20** and **22**

It should be noted that the results of the ¹³C NMR (CDCl₃) spectrum prove that all carbon atoms in the synthesized compounds (**20–24**) are compatible (in the experimental part) and, in turn, confirm their molecular structures.

The synthesized compounds include N-benzyl-6,7-dihydro-5H-cyclopenta (El-Gazzar A.B., Hussein H.A., Hafez H.N. (2007); Deng J.F., Peng L., Zhang G.C., Lan X.B., Li C.F., Chen F.X., Zhou Y.Y., Lin Z.X., Chen L., Dai R.K., Xu H.J., Yang L., Zhang X.Q., Hu W.H. Eur. J. (2011)) thieno

(Elmahdy K. M., Elkazak A. M., Megid A. M., Seada M., Mohamed O. F. (2013); Rashad A. E. Ali M. A. (2006)) pyrimidin-4-amine (**20**) and N-benzyl-6,7,8,9-tetrahydro-5H-cyclohepta thieno (Elmahdy K. M.,

Elkazak A. M., Megid A. M., Seada M., Mohamed O. F. (2013); Rashad A. E. Ali M. A. (2006)) pyrimidin-4-amines (**22**) which were also fully confirmed by X-ray diffraction (XRD) analysis.

Table 2. Multiplets of the corresponding protons in the ^1H NMR spectra of the obtained compounds (20–24) (δ , ppm, J, Hz)

No	N=CH	C ₆ H ₅	NH	C ₆ H ₅ CH ₂	Protons of substituents in positions 5 and 6
20	8.42 (1H, s)	7.34 (5H, m)	5.34 (1H, t, J=5.8)	4.81 (2H, d, J=5.7)	C-5 and C-7, $-(\text{CH}_2)_2-$, 2.98 (4H, t, J=7.3), C-6, $-\text{CH}_2-$, 2.51 (2H, p, J=7.1)
21	8.42 (1H, s)	7.35 (5H, m)	5.55 (1H, t, J=5.6)	4.81 (2H, d, J=5.4)	C-5, $-\text{CH}_2-$, 2.87 (2H, t, J=5.1), C-8, $-\text{CH}_2-$, 2.81 (2H, t, J=4.7), C-6 and C-7, $-(\text{CH}_2)_2-$, 1.89 (4H, m)
22	8.41 (1H, s)	7.35 (5H, m)	5.59 (1H, t, J=6.0)	4.82 (2H, d, J=5.4)	C-5, $-\text{CH}_2-$, 2.98 (2H, t, J=5.7), C-9, $-\text{CH}_2-$, 2.88 (2H, t, J=5.7), C-7, $-\text{CH}_2-$, 1.87 (2H, m), C-6 and C-8, $-(\text{CH}_2)_2-$, 1.82 (4H, m)
23	8.42 (1H, s)	7.35 (5H, m)	5.71 (1H, t, J=5.5)	4.82 (2H, d, J=5.4)	C-5, $-\text{CH}_3$, 2.41 (3H, s), C-6, $-\text{CH}_3$, 2.42 (3H, s),
24	8.53 (1H, s)	7.37 (5H, m)	5.98 (1H, t, J=5.6)	4.85 (2H, d, J=5.4)	C-5, $-\text{CH}_3$, 2.94 (3H, s), C-6, $-\text{CO}_2\text{CH}_2\text{CH}_3$, 1.40 (3H, t, J=7.1), C-6, $-\text{CO}_2\text{CH}_2\text{CH}_3$, 4.36 (2H, q, J=7.1)

4. Conclusion

Thus, nucleophilic exchange reactions of benzylamine with various substituted-4-chlorothieno[2,3-d]pyrimidine series compounds were carried out, and as a result, the corresponding new products were synthesized with high yields. Due to the high nucleophilicity of benzylamine and the high reactivity of compounds of the imidoyl chloride type, it was found that the nature of the substituents in the 5th and 6th positions of 4-chlorothieno (Elmahdy K. M., Elkazak

A. M., Megid A. M., Seada M., Mohamed O. F. (2013); Rashad A. E. Ali M. A. (2006)) pyrimidines (electron-donating or electron-withdrawing), and the size of the polymethylene rings do not significantly affect the yields of the target compounds.

Acknowledgments

The research was financially supported by the Ministry of Higher Education, Science, and Innovation of the Republic of Uzbekistan (Grant F-FA-2021-408).

References

- Bozorov Kh., Zhao J. Yu., Elmuradov B., Pataer A., Aisa H.A. (2015). *Eur. J. Med. Chem.*, – 102. – 552 p.
- Elmahdy K. M., Elkazak A. M., Megid A. M., Seada M., Mohamed O. F. (2013). *Adv. Chem.*, – 5, – 581 p.
- Rashad A. E. Ali M. A. (2006). *Nucleosides, Nucleotides Nucleic Acids*, – 25. – 17 p.
- El-Gazzar A. B., Hussein H. A., Hafez H. N. (2007). *Acta Pharm.*, – 57 (4). – 395 p.

- Deng J.F., Peng L., Zhang G.C., Lan X.B., Li C.F., Chen F.X., Zhou Y.Y., Lin Z.X., Chen L., Dai R.K., Xu H.J., Yang L., Zhang X.Q., Hu W.H. Eur. J. (2011). Med. Chem., – 46 (1). – 71 p.
- Nagaraju K., Harikrishna N., Vasu K., Rao C. V. (2015). Indo Am. J. Pharm. Res., – 5 (4). – 1604 p.
- Guo Y., Li J., Ma J., Yu L.Z., Wang H., Zhu W., Liao X., Zhao Y. (2015). Chin. Chem. Lett., – 26. – 755 p.
- Zhu W., Chen C., Sun C., Xu S., Wu C., Lei F., Xia H., Tu Q., Zheng P. (2015). Eur. J. Med. Chem., – 93. – 64 p.
- Kim Y., Kim M., Park M., Tae J., Baek D., Park K. D., Choo H. (2015). Molecules, – 20 (3). – 5074 p.
- Berdiev A. U., Ortikov I. S., Turgunov K. K., Elmuradov B. Zh., Abdullaev N. D., Tashkhodzhaev B. (2024). Chem. Nat. Compd., – 60 (1). – P. 127–132.
- Berdiev A. U., Mirsodikov M. M., Ortikov I. S., Elmuradov B. Zh. (2023). Uzbek chemical journal, – 3. – P. 76–84.
- Berdiev A. U., Ortikov I. S., Elmuradov B. Zh. (2022). Proceedings of the Republican scientific-practical conference, Abstarcts, – Tashkent, – P. 110–111.
- Berdiev A. U., Ortikov I. S., Elmuradov B. Zh. (2022). Actual problems of the chemistry of natural compounds, Abstarcts, – Tashkent, – 22.
- Berdiev A. U., Mirsodikov M. M., Ortikov I. S., Elmuradov B. Zh. (2022). Proceedings of the 10th Republican Conference of Young Chemists, Part II, Namangan, – P. 46–48.
- Berdiev A. U., Ortikov I. S., Elmuradov B. Zh. (2022). Uzbek chemical journal, – 4. – P. 59-65.

submitted 23.09.2024;

accepted for publication 08.10.2024;

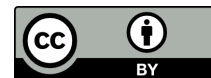
published 28.11.2024

© Khamraeva G., Valiev Y., Berdiev A., Saitkulov F., Elmuradov B.

Contact: saitulovfoziljon@gmail.com



DOI:10.29013/AJT-24-9.10-27-33



ISOTHERMAL SOLUBILITY DIAGRAM OF THE SODIUM HYDROXIDE – HUMIC ACID – WATER SYSTEM AT 25 °C

*Yunusova Maftuna Valijon qizi*¹, *Babasadikov Shukrullo Sayfulloyevich*²,
*Erkaev Aktam Ulashevich*², *Kucharov Bakhrom Khayrievich*¹,
*Yulbarsova Mashkhura Vakhobovna*¹, *Zakirov Bakhtiyor Sabirjanovich*¹

¹ Institute of General and Inorganic Chemistry, Academy of
Sciences of the Republic of Uzbekistan, Tashkent

² Tashkent Institute of Chemical Technology, Tashkent

Cite: Yunusova M. V., Babasadikov Sh. S., Erkaev A. U., Kucharov B. Kh., Yulbarsova M. V., Zakirov B. S. (2024). Isothermal Solubility Diagram of the Sodium Hydroxide – Humic Acid – Water System at 25 °C. *Austrian Journal of Technical and Natural Sciences* 2024, No 9–10. <https://doi.org/10.29013/AJT-24-9.10-27-33>

Abstract

The article presents data from a study of solubility in the sodium hydroxide – humic acid – water system at 25°C isothermal method and data from a study of the rheological properties of solutions formed by adding humic acid to 0.5 and 1.0% aqueous solutions of sodium hydroxide. The formation of a new compounds based on the initial components, for which the concentration limits of existence at 25 °C have been determined. By studying the rheological properties of solutions formed by adding humic acid to 0.5 and 1.0% aqueous solutions of sodium hydroxide, we have established that when sodium hydroxide interacts with humic acid in aqueous solutions, a complex compound of the composition NaOH•HA (1:1) is formed. These characteristic inflection points are less clearly manifested in the pH values of the solutions.

Keywords: *sodium hydroxide, humic acid, sodium humate, ternary system, complex salt, growth stimulator, isothermal diagram, synthesis*

Introduction

The authors (Fakerov G. M., Erkaev A. U., Sharipova H. T., Mirzoev B., 2022; Fakerov G. M., Erkaev A. U., Sharipova H. T., Mirzoev B., 2023; Fakerov G. M., Erkaev A. U., Sharipova H. T., Mirzoev B., 2022) obtained the following data based on the results of physicochemical and technological studies of the oxidation stages and extraction of alkali metal humates. The optimal oxidation mode

of brown coal from the Shurabskoye deposit with nitric acid was found: nitric acid concentration of 50%, oxidation temperature of 45 °C, process duration of 1 hour, and the ratio of the organic part of coal to nitric acid monohydrate of 0.81:1. As a result of oxidation of Shurabskoye brown coal with nitric acid, the content of active functional groups in the latter increases, both in the coal itself and in humic acids.

Optimal conditions for humic acid extraction from oxidized brown coal of the Shurab deposit have been determined. It has been established that the greatest amount of humic acids, more than 80%, is extracted from coal with a 10% sodium hydroxide solution at 80 °C and 30-minute extraction. Increasing the L: S ratio from 5 to 20 leads to an increase in the yield of humic acids. The yield of humic acids in the case of using 10% sodium hydroxide at 80 °C, L: S = 15 and 30 min is 84.43; 70.75%, respectively, when using sodium and potassium hydroxides.

Along with sodium humate, included in the “List of preparations permitted for use in agriculture,” plant growth stimulants such as ammonium and potassium humates, obtained by treating oxidized coals with ammonium and potassium hydroxides, have undergone extensive production testing.

The positive influence of ammonium humate on the cultivation of wheat, sugar beets, corn, potatoes, cabbage, and cotton was already discussed in the analysis of works (Gizatullin Slicks of adenumates on the yield of agricultural crops, 1963; Petrik G. K., 1971; Imakova S. T., Mukhanova V. L., Sultanov A. S., 1968; Abolina G. I., Tashkhodjaev A. T. 1968; Abolina G. I., Tashkhodjaev A. T., 1965; Imakova S. T., Mukhanova V. L., 1965).

When comparing the methods of applying ammonium humate to grain crops, the best results were obtained with a combination of seed soaking and sprout irrigation in the concentration range of 10–5–10–6%. On cucumber (Vyaznikovsky variety), the best results were obtained when using the preparation in a concentration of 10–4–10–5% for seed soaking and 10–5–10–6% for sprout irrigation (Bulli V. A., Antonova, Oleynik N. A., 1994). Spraying wheat in the tillering phase with ammonium humate solutions of 0.5; 0.05 and 0.005% concentration increased the yield by 2.5–3.5 c/ha (Larina V. A., Astrakhantseva G., Vasilyeva N., Galaganova A., Zhuravleva N., Markadanova E., Pokul T. V., Sokolova N., Starovoi-tova E.). In addition to increasing the wheat yield, its quality significantly improves. An increase in protein in wheat grain by 0.69–0.85% is noted, which increases the protein harvest from 1 ha from 461.3 kg to 529.9 kg, i.e. by 14.8%. Good results were also obtained when

spraying corn, potatoes and other vegetables. Quite positive results were shown by testing the stimulating effect of ammonium humates in closed ground when growing cucumbers and tomatoes. The best concentration of ammonium humates in this case is 0.05%. This solution was used for soaking seeds, spraying plants during vegetation and watering plants under the root. The increase in cucumber yield was 23.6% when soaking, 15.0% when spraying and 15.7% when watering under the root. The quality of cucumbers also increased. The content of vitamin C in them increased from 11.64 to 14.06 mg.

Materials and methods

The study of phase equilibria in physicochemical systems was carried out using the isothermal solubility method (Van't Hoff J. G., 1936).

The solubility of salts was studied by the isothermal method by mixing the solutions of the studied compounds at a constant temperature while maintaining a sufficient amount of solid phases in the mixture. The study was conducted in a therabolic flask with a stirrer placed in a thermostat, the temperature in which was maintained by a thermostat and a contact thermometer with an accuracy of ± 0.1 °C. After equilibrium was established, samples were taken from the liquid and solid phases for analysis and the location of the figurative point of the system was determined. The composition of the liquid and solid phases was established by chemical analysis.

The composition of solid phases was determined according to Skreinemakers. The essence of the method is that in the equilibrium system under study, the liquid phase is separated from the sediment and their composition is determined. Then, they are found along the lines corresponding to the compositions of their wet residues. The true composition of the desired solid phase is established at the intersection point of these lines (Dukelsky M., 1911).

The specific gravity of the samples of the studied compounds and solutions was determined by the pycnometric method (Zdanovsky A. B. Hallurgy, 1972) using a capillary pycnometer with a volume of 10 sm³. To determine the volume, the pyc-

nometer was filled with bidistilled water, thermostatted at 25 °C and weighed. Knowing the weight of the dry pycnometer, the density of water at 25 °C and the weight of the pycnometer filled with water, its volume was calculated. Weighing was carried out with an accuracy of ± 0.00005 mg. The results are presented with an accuracy of ± 0.1 kg/m³.

Measuring the pH value of solutions in a laboratory ion meter I-130M with an electrode system of ESL 63–07, EVL-1M3.1 and TKA-7 electrodes with an accuracy of up to 0.05 pH units (GOST 24596. 5–81).

The kinematic viscosity of the solutions was determined using a VPZh capillary viscometer (Florov Yu.G., 1982) with a capillary diameter of 1.16–2.75 mm. The accuracy of the results was ± 0.0001 10–1 mm²/s.

The phase characteristics of the samples under study were measured using a Panalytical Empyrean powder X-ray diffractometer. The equipment operation was controlled by a computer using the Data Collector program, and the X-ray diffraction pattern was analyzed using the High Score program with the PDF 2013 database. The X-ray phase analysis of the powders under study was performed using a Panalytical Empyrean X-ray diffractometer equipped with a Cu tube ($K\alpha_1 = 1.5406\text{\AA}$). The measurements were performed at room temperature in the 2θ angle range from 5 ° to 90 ° in the step-by-step scanning mode with a step of 0.013 degrees and a signal accumulation time at a point of 5 s.

Results and discussion

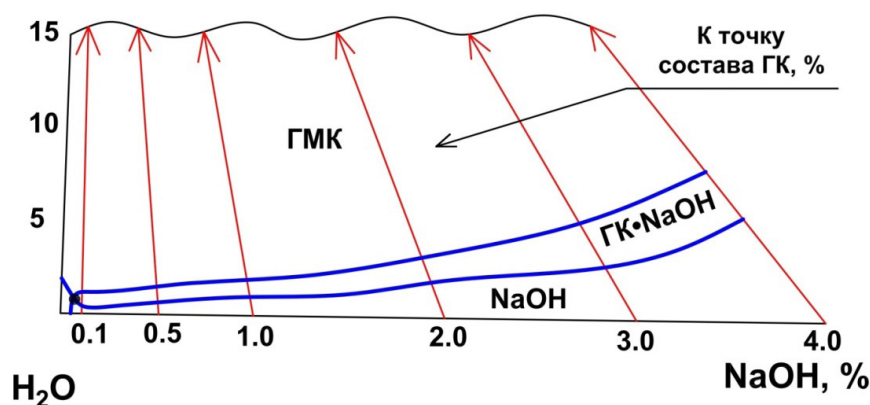
The extraction process was carried out at a ratio of OC: NaOH (10% solution) equal to 1:15; a temperature of 20–25 °C and stirring for 60 min. To obtain the first batch of fractions of HA (humic acids) samples, settling was carried out for 24 hours, then after separation of the liquid part, the system was thickened. The liquid part was acidified with 40% nitric acid to pH 0.80–0.85.

The resulting sediment was separated using a centrifuge at 2000 rpm for 15 minutes. The wet sediment was dried in a drying apparatus at a temperature of no more than 90 °C. The yield of HA was calculated based on the dry mass obtained.

1500 ml of distilled water were added to the remaining thick mass, and the process was continued for 12 hours, thus obtaining humic acid fractions and calculating the yield of the fractions. The first fraction was obtained by settling for 3 hours (Yunusova M. V., Erkaev A. U., Kucharov B. X., Yo'lbarsova M. V., Zakirov B. S., Reymov A. M., 2024).

Further, in order to obtain stimulants, we studied the mutual solubility of salts in the sodium hydroxide – humic acid (HA) – H₂O system using the isothermal method at a temperature of 250 °C. Equilibrium in the system was established within three days. Based on the chemical analysis of the compositions of the liquid and solid phases, an isothermal diagram of the solubility of this system was constructed (Figure 1).

Figure 1. Isothermal diagram of solubility of the NaOH-HA-H₂O system at 25 °C



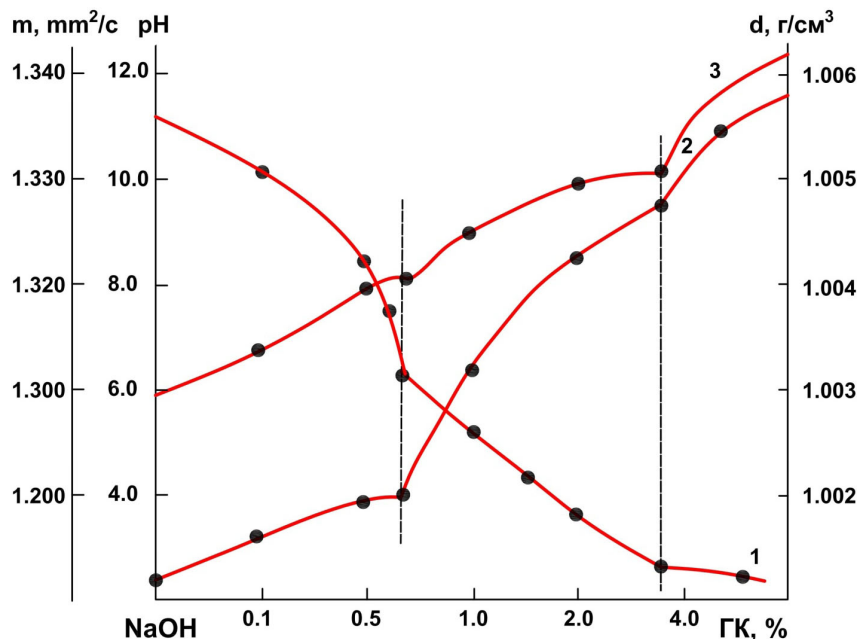
Data on solubility in the ternary system sodium hydroxide – humic acid (HA) – H₂O are presented in Figure 1, from which it follows that the components of the system have a salt-

ing-out effect on each other, therefore, with an increase in the concentration of the initial components, the crystallization region of the formed compound expands. This is obviously

associated with complex formation in the system. Indeed, the liquidus curve of the solubility diagram breaks down into three branches corresponding to the crystallization of two initial components – sodium hydroxide and humic acid and the compound $\text{NaOH} \cdot \text{HA}$.

Next, with the aim of synthesizing sodium humate, we studied the rheological properties of solutions formed by adding humic acid to 0.5 and 1.0% aqueous solutions of sodium hydroxide (Figures 2 and 3).

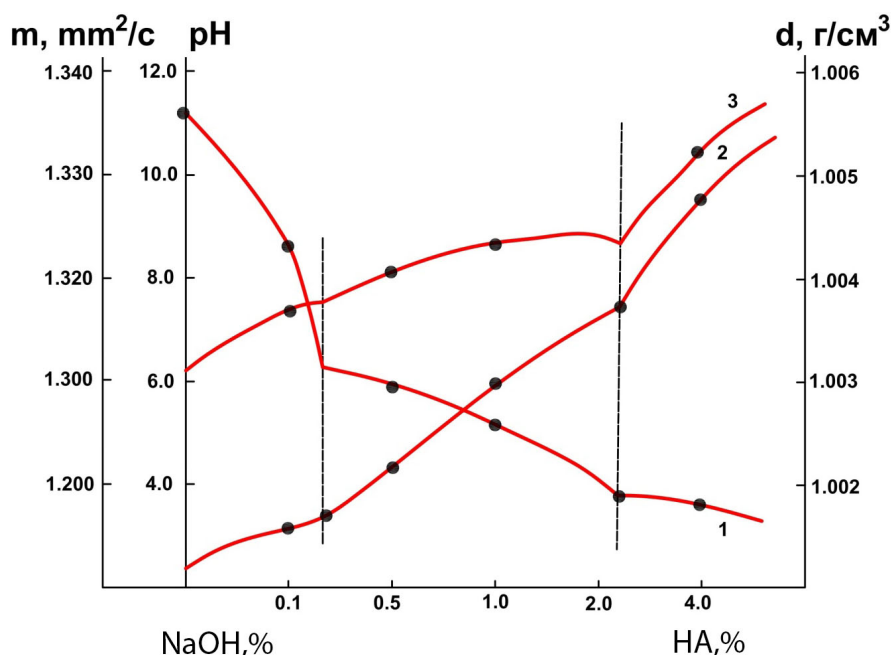
Figure 2. Dependence of pH of the medium (1), density (2) and viscosity (3) on the concentration of humic acid in a 0.5% sodium hydroxide solution



The pH, density and viscosity of solutions of these systems were determined depending on the content of components at a tempera-

ture of 25 °C. Based on the data obtained, diagrams of the “composition-properties” of the above components were constructed.

Figure 3. Dependence of pH of the medium (1), density (2) and viscosity (3) on the concentration of humic acid in a 1.0% sodium hydroxide solution



From the diagram of the dependence of the pH of the solution medium on the concentration of humic acid in a 0.5% sodium hydroxide solution, it is evident that with an increase in the concentration of humic acid in the solution, a sharp decrease in the pH of the solutions is observed, and an increase in the density and viscosity of the system is observed in the density and viscosity of the solutions.

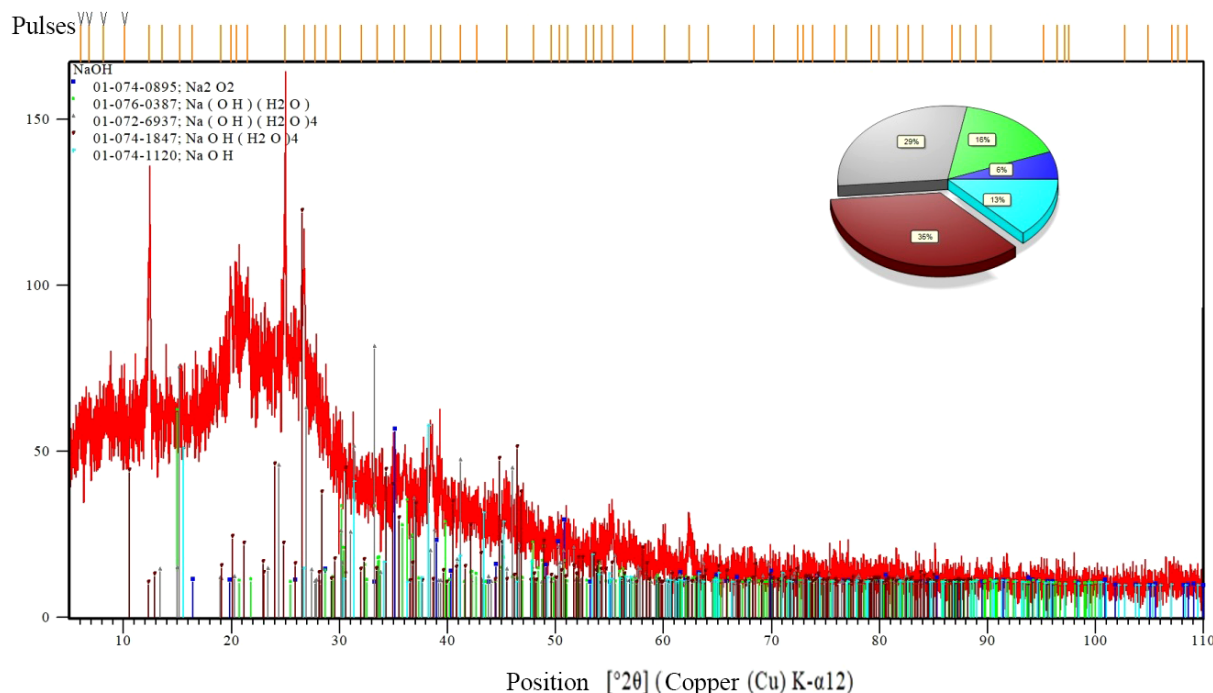
A study of the sodium hydroxide – humic acid – water system of viscosity, density and pH of the medium showed that the constructed “composition – properties” diagram has two breaks corresponding to a change in the crystallizing phases of the system at the double cryohydrate point, which indicate the formation of a double compound of the composition: NaOH • HA.

The diagram of the dependence of pH, density and viscosity of solutions on the con-

centration of humic acid in a 1.0% sodium hydroxide solution is of a similar nature. It is evident from the diagram that in a 1.0% sodium hydroxide solution in the humic acid concentration range of 0.27–2.12%, a decrease in the pH of solutions is observed in the curves of the dependences and a sharp increase in the values of density and viscosity of solutions is observed (Figure 3). Thus, it can be assumed that when sodium hydroxide interacts with humic acid in aqueous solutions, a complex compound of the composition NaOH • HA (1:1) is formed. These characteristic inflection points are less clearly manifested in the pH values of solutions.

The complex salt NaOH • HA was synthesized on the basis of solutions of sodium hydroxide and crystalline humic acid in a molar ratio resulting from the results of the study of the “Composition-properties” diagram.

Figure 4. X-ray diffraction pattern of formed NaOH • HA



The data of X-ray phase analysis of the compound of sodium hydroxide with humic acid show that all reflections on the diffraction patterns are, as a rule, characterized by their own reflection angles, a set of interplanar distances and diffraction line intensities (Fig. 4). This indicates the individuality of the crystal lattices of the obtained compounds.

Conclusion

Thus, the mutual solubility of salts was studied by the isothermal method at a temperature of 25 °C in the sodium hydroxide – humic acid – water system, and an isothermal diagram of this system was constructed based on the analysis of the compositions of the liquid and solid phases. It was studied that due to complexation in the system, with an

increase in the concentrations of the original components, the crystallization region of the formed compound expands. It was investigated that the liquidus curve of the solubility diagram breaks down into three branches corresponding to the crystallization of two original components – sodium hydroxide, humic acid and the compound NaOH · HA. Then, the rheological properties of the solutions formed by adding humic acid to 0.5 and 1.0% aqueous solutions of sodium hydroxide were studied. pH, density and viscosity of solutions of

these systems were determined depending on the content of components at a temperature of 25 °C, and composition-property diagrams were constructed. It has been investigated that the constructed diagram «composition-properties» has a break corresponding to the change in crystallizing phases at the double cryohydrate point, which indicate the formation of a double compound of the composition: NaOH · GC. A complex salt of NaOH · HA based on solutions of sodium hydroxide and crystalline humic acid has been synthesized.

References

- Fakerov G. M., Erkaev A. U., Sharipova H. T., Mirzoev B. Influence of technological parameters on the process of extraction of humic acids from oxidized coals of the Shurabskoye deposit // *Composite materials*. 2022. – No. 3. – P. 150–155.
- Fakerov G. M., Erkaev A. U., Sharipova H. T., Mirzoev B. Study of the process of obtaining organomineral fertilizers by nitric acid oxidation of coals of the Shurab deposit // *Fan va tekhnologiyalar tarakqiyoti*. 2023. – No. 1. – P. 53–58.
- Fakerov G. M., Erkaev A. U., Sharipova H. T., Mirzoev B. Kinetics of humic acid extraction from coal of the Shurab deposit // *Republican scientific and practical conference with the participation of foreign scientists “Innovative technologies for the production of single, complex and organomineral fertilizers”*, dedicated to the 80th anniversary of Academician of the Academy of Sciences of the Republic of Uzbekistan, Doctor of Technical Sciences, Professor, Honored Inventor and Innovator of the Republic of Uzbekistan Namazov Shafolat Sattarovich, December 13–14, 2022. – P. 262–264.
- Gizatullin Slicks of adenumates on the yield of agricultural crops // *Chemicalization of agriculture in Bashkiria*. – Ufa, 1963, issue. 4–5. – P. 373–378.
- Petrik G. K. Experience in the production of ammonium humate solution and its use as a plant growth stimulator in the conditions of the Irkutsk region // *Proceedings of the Frunze Polytechnic Institute*, 1971. – P. 317–326.
- Imakova S. T., Mukhanova V. L., Sultanov A. S. Results of the study of the effect of humic fertilizers from coal on cotton and corn // *Humic fertilizers. Theory and practice of their application*, Part III. – Kyiv: Urozhai, 1968. – P. 363–367.
- Abolina G. I., Tashkhodjaev A. T. Effect of humic fertilizers obtained from coal on the activity of physiological processes in plants and potato yield in Uzbekistan // *Humic fertilizers. Theory and practice of their application*. Part III. – Kyiv: Urozhai, 1968. – P. 356–362.
- Abolina G. I., Tashkhodjaev A. T. Effect of humic fertilizers, humophos and ammonium humate obtained from coal on potato yield and its quality in the conditions of Uzbekistan // *Fertilizers and growth stimulants from brown coal and their effectiveness: Abstract of the report at the interuniversity scientific conference*. April 12–15, 1965. – Ufa, 1965. – P. 46–47.
- Imakova S. T., Mukhanova V. L. Effect of humic fertilizers on cotton and corn // *Fertilizers and growth stimulants from brown coals and their effectiveness: Abstract of the report at the interuniversity scientific conference*. April 12–15, 1965. – Ufa, 1965. – 45 p.
- Bulli V. A., Antonova, Oleynik N. A. Study of biological activity of humates on agricultural crops // *Chemistry in agriculture*. 1994. – No. 5. – P. 10–19.
- Larina V. A., Astrakhantseva G., Vasilyeva N., Galaganova A., Zhuravleva N., Markadanova E., Pokul T. V., Sokolova N., Starovoitova E. Humic fertilizers from coals of Eastern Siberia and their effectiveness in soil and climatic conditions of the Irkutsk region // *Theoretical foundations of the action of physiologically active substances and the effectiveness of fertilizers containing them*. – Dnepr.

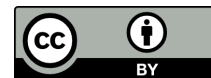
- Van't Hoff J. G. Oceanic salt deposits. – L.: ONTI Khimteoret.6 1936. – 344 p.
- Dukelsky M. The method of Skreinemakers residues in application to the study of chemical systems of three components. – Kyiv. 1911. – 80 p.
- Zdanovsky A. B. Hallurgy. -L.: Chemistry, 1972. – 572 p.
- GOST 24596.5–81. Method for determination of pH of a solution or suspension. – M.: IPK Publishing House of Standards, 2004.
- Florov Yu. G. Course of Colloid Chemistry. Surface Phenomenon and Disperse Systems. – M.: Chemistry, 1982. – P. 117–124.
- Yunusova M. V., Erkayev A. U., Kucharov B. X., Yo'lbarsova M.V., Zakirov B. S., Reymov A. M. Study of rheological properties of solutions when producing sodium humates // ISSN 2181-9203 Qoraqalpog'istonda fan va ta'lim 3/2 son Nukus 2024. 87–91 b.

submitted 10.10.2024;
accepted for publication 25.10.2024;
published 28.11.2024

© Yunusova M. V., Babasadikov Sh.S., Erkaev A. U., Kucharov B. Kh., Yulbarsova M. V., Zakirov B. S.

Contact: mashhura_1909@mail.ru

DOI:10.29013/AJT-24-9.10-34-38



AMIDE REACTIONS OF IZONICOTINE ACID WITH SOME AROMATIC AMINES

*Nurmatov Doston Urolovich*¹, *Abdushukurov Anvar Kabirovich*¹,
*Xoliqov Tursunali Suyunovich*¹, *Yusufov Muxriddin Saidovich*¹,
*Yodgorov Chinmurot G'ulomovich*¹

¹ Faculty of Chemistry, National university of Uzbekistan

Cite: Nurmatov D. U., Abdushukurov A. K., Xoliqov T. S., Yusufov M. S., Yodgorov Ch. G. (2024). Amide Reactions of Isonicotinic Acid With Some Aromatic Amines. *Austrian Journal of Technical and Natural Sciences* 2024, No 9–10. <https://doi.org/10.29013/AJT-24-9.10-34-38>

Abstract

Corresponding amides were synthesized from the reactions of isonicotinic acid with o-toluidine, m-toluidine, p-toluidine 2,4-xylidine 2,5-xylidines. The influence of the nature of the solvent on the course of reactions was studied and the results obtained were compared. It was found that isonicotinic acid reacts with some aromatic amines to form amides when heated in non-polar solvents. The physical constants of the synthesized amides were determined. The structure of the reaction products was analyzed using IR- and ¹H and ¹³C NMR spectroscopy methods.

Keywords: *Isonicotinic acid, o-toluidine m-toluidine, p-toluidine 2,4-xylidine, 2,5-xylidine, amide, organic solvent*

Introduction

It can be seen from the analysis of literature data that it is possible to obtain acid amides with high yields from N-acylation (benzoylation) reactions of amines, especially aromatic amines with anhydrides and halogen anhydrides of carboxylic acids. However, finding ways to synthesize any organic substance through low-level reactions using ready-made reagents is one of the important tasks for chemists. It should be noted that special attention is paid to these aspects in the synthesis of acid amides. As a result, effective methods of product synthesis with high yield are being developed by direct use of carboxylic acids as acylating agents in the

synthesis of amides. Below is an analysis of relevant literature data.

The results of research related to the study of the reactions of carboxylic acids with amines show that the reactions proceed with the formation of intermediate protonated quaternary ammonium salts, as a result of condensation when heated under certain conditions, acid amides are formed.

The ligand N, N'-(2,5-dimethyl-1,4-phenylene)diisonicotinamide was synthesized by reacting 2,5-dimethyl-1,4-phenylenediamine with isonicotinyl chloride hydrochloride in pyridine for 5 days at 25 °C (Pingwah Tang, 2012).

The acid amide was synthesized in high yield in 40 min by reacting heteroaromatic isonicotinic acid with aniline, 2,4-dimethylaniline and n-propylamine under ultrasonic bath using rGO-SO₃H (sulfonated reduced graphene oxide) catalyst (Baevsky A. M., Tskalov V. V., Baevsky M. Yu., Sheludko A. B., 2011).

Nicotinic acid was first reacted with oxalyl chloride to form nicotinic anhydride, then nicotinic anhydride was reacted with amines to synthesize acid amides in high yield (Yoshikawa M. et al. 2008).

In other literature, the formylation of aliphatic, aromatic, heterocyclic, primary and secondary amines with DMF in the presence of nickel (II) quinazolone was brought out with high efficiency, and the mechanism of the reaction was shown with a catalytic cycle (Sonawane R. B., Rasal N. K., Jagtap S. V., 2017).

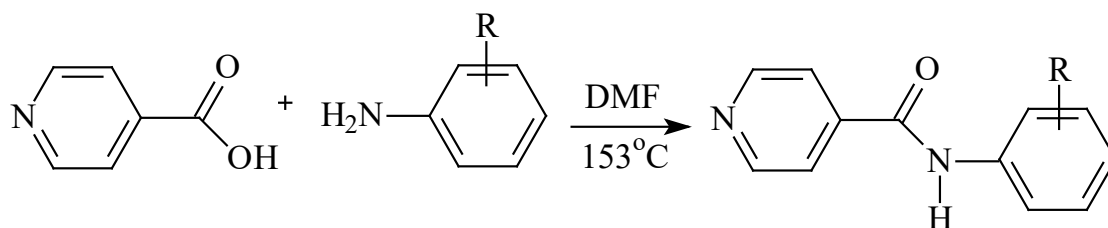
In recent years, research has been developing on the use of nitrogen heterocyclic compounds in acid-amine condensation reactions. For example, 4-(4,6-dimethoxy-1,3,5-triazin-2-yl)-4-methylmorpholine chloride (Kunishima M., Kawachi C., Hioki K., Terao K., Tani S., 2001), 2,4,6-trichloro-1,3,5-triazine (Gholap S., Gunjal N. 2017), and nitrogen heteropolyanions (Jaita S., Phakhodee W.,

Chairungsi N., Pattarawarapan M., 2018) are used as active condensation catalysts. Also, N, N-diisopropylcarbodiimide showed catalytic activity in the reaction of carboxylic acids with amines in an aqueous medium at room temperature. This method is important because it ensures environmental safety and, in particular, reveals new aspects of organic synthesis in water (Fattahi N., Ayubi M., Ramazani A. 2018). When the reaction of substituted phenylacetic acids with benzylamine derivatives was carried out in the presence of various nickel compounds, the following series of catalytic activity was determined: NiCl₂ > (CH₃COO)₂Ni > NiCl₂(PPh₃)₂ > NiCl₂·H₂O > without catalyst. Solvents – diethyl ether, TGF, toluene, fluorobenzene, acetonitrile, DMF and DMSO were used in this process, and the highest yield (80% in 10 hours, 99.2% in 20 hours) was achieved in toluene (Cheng L., Ge X., Huang L., 2018).

Research methods

Initially devoted to studying the reaction of isonicotinic acid with o-toluidine. The reaction of isonicotinic acid with o-toluidine was carried out in a flask equipped with a reflux condenser at the boiling temperature of DMF on a magnetic stirrer for 7 hours.

The reaction equation is:



R = o-Toluidin, R = m-Toluidin, R = p-Taluidin, R = 2,4-xylidine, R = 2,5-xylidine

The obtained product was recrystallized from a 40% ethanol-water mixture and dried in a desiccator with calcium chloride. The melting temperature was determined, the IR and NMR spectra were taken, and the purity was checked using the TLC method.

Experimental part

IR spectra were recorded on a FT-IR/NIR Spectrum 3 spectrometer (Perkin Elmer, Switzerland) using an ATR system. ¹H and ¹³C NMR spectra were recorded on a JNM-ECZ400R spectrometer (JEOL, Japan) at an

operating frequency of 400 MHz for ¹H in CD₃OD solutions. TMS (0 ppm) was used as an internal standard in ¹H NMR spectra. In ¹³C NMR spectra, the chemical shift of the solvent (CD₃OD, 49.00 ppm relative to TMS) was used as an internal standard.

N-(o-tolylphenyl)isonicotinamide is a white crystalline substance, yield 45%, *T*_{melt-ing} = 158 °C, *R*_f = 0.61 (benzene-acetone system 3: 1). IR spectrum *sm*⁻¹ 3198 (NH), 2917 (–CH₂–), 1680 (C=O), 1281 (C–N), 1586 (C=C aromatic ring). NMR¹H-spectr (400 MHz, METHANOL-*D*₄) δ 9.12–9.07 (m, 1H), 8.71

(dd, $J = 5.0$, 1.6 Hz, 1H), 8.35 (dt, $J = 8.1$, 2.0 Hz, 1H), 7.57 (dd, $J = 8.1$, 5.0 Hz, 1H), 7.37–7.12 (m, 4H), 2.28 (s, 3H), 1.36–1.24 (m, 1H). ^{13}C NMR (101 MHz, METHANOL- D_4) δ 166.03, 162.13, 150.96, 136.10, 132.08, 131.83, 131.55, 128.03, 127.38, 126.84, 125.09, 124.74, 123.57, 18.00, 17.81.

N-(m-tolylphenyl)isonicotinamide is a white crystalline substance, yield 43%, $T_{\text{melting}} = 122$ °C, Rf = 0.58 (benzene-acetone system 3: 1). IR spectrum cm^{-1} 3138 (NH), 1674 (C=O), 1306 (C-N), 1612 (C=C aromatic ring). ^1H NMR (600 MHz, METHANOL- D_4) δ 9.05 (dd, $J = 2.7$, 1.5 Hz, 1H), 8.71–8.66 (m, 1H), 8.34–8.28 (m, 1H), 7.59–7.53 (m, 1H), 7.50 (s, 1H), 7.49–7.44 (m, 1H), 7.22 (td, $J = 8.5$, 3.5 Hz, 1H), 7.00–6.95 (m, 1H), 2.33 (dd, $J = 5.5$, 2.7 Hz, 3H). ^{13}C NMR (101 MHz, METHANOL- D_4) δ 164.88, 161.59, 150.96, 136.36, 135.82, 135.34, 131.10, 130.38, 124.77, 121.10, 119.87, 20.80.

N-(p-tolylphenyl)isonicotinamide is a pink crystalline substance, 55%, $T_{\text{melting}} = 130$ °C, Rf = 0.56 (benzene-acetone system 3: 1). IR spectrum cm^{-1} 3308 (NH), 2921 (–CH₂–), 1673 (C=O), 1290 (C-N), 1592 (C=C aromatic ring). ^1H NMR (600 MHz, METHANOL- D_4) δ 9.04 (d, $J = 2.3$ Hz, 1H), 8.69 (dd, $J = 4.3$, 2.3 Hz, 1H), 8.34–8.29 (m, 1H), 7.59–7.54 (m, 1H), 7.55 (s, 1H), 7.53 (s, 1H), 7.19–7.14 (m, 2H), 5.00–4.92 (m, 1H), 4.60 (s, 1H), 2.31 (d, $J = 1.8$ Hz, 3H). ^{13}C NMR (151 MHz, METHANOL- D_4) δ 164.98, 151.36, 147.99, 135.99, 135.56, 134.51, 131.45, 129.03, 129.00, 128.98, 123.87, 121.13, 121.02, 48.23, 48.10, 47.96, 47.81, 47.77, 47.75, 47.67, 47.63, 47.60, 47.53, 47.48, 47.44, 47.39, 47.34, 47.32, 47.29, 47.25, 19.65, 0.64.

N-(2,4-dimethylphenyl)isonicotinamide is a white powdery substance, 42%, $T_{\text{melting}} = 102$ °C, Rf = 0.52 (benzene-acetone

system 3: 1). IR spectrum cm^{-1} 3272 (NH), 2920 (–CH₂–), 1653 (C=O), 1230 (C-N), 1591 (C=C aromatic ring). ^1H NMR (400 MHz, METHANOL- D_4) δ 9.08 (dd, $J = 2.3$, 0.9 Hz, 1H), 8.70 (dd, $J = 4.9$, 1.6 Hz, 1H), 8.39–8.30 (m, 1H), 7.57 (ddd, $J = 7.9$, 4.9, 0.9 Hz, 1H), 7.18 (d, $J = 7.9$ Hz, 1H), 7.12–7.06 (m, 1H), 7.02 (dd, $J = 8.1$, 2.1 Hz, 1H), 2.30 (s, 3H), 2.23 (s, 3H). ^{13}C NMR (101 MHz, METHANOL- D_4) δ 165.21, 162.07, 134.43, 131.07, 130.17, 129.49, 128.69, 126.08, 125.27, 124.54.

N-(2,5-dimethylphenyl)isonicotinamide is a white crystalline substance, 46%, $T_{\text{melting}} = 108$ °C, Rf = 0.56 (benzene-acetone system 3: 1). IR spectrum cm^{-1} (KBr, ν , cm^{-1}): 3243 (NH), 2918 (–CH₂–), 1645 (C=O), 1289 (C-N), 1592 (C=C aromatic ring). ^1H NMR (400 MHz, METHANOL- D_4) δ 8.24 (s, 1H), 7.47–7.41 (m, 1H), 7.08 (t, $J = 8.0$ Hz, 2H), 6.98–6.86 (m, 2H), 2.30–2.09 (m, 9H). ^{13}C NMR (101 MHz, METHANOL- D_4) δ 166.06, 162.16, 137.21, 131.91, 131.44, 128.64, 128.05, 127.58, 125.61, 124.16, 21.05, 20.90, 17.57, 17.37.

Results and discussion

Initially, the reaction with isonicotinic acid and o-toluidine, m-toluidine, p-toluidine, 2,4-xylylidine, 2,5-xylylidine in different molar ratio was carried out in a flask with a reflux condenser in a magnetic stirrer for 7 hours at the boiling point of DMF. As a result of the studies, arylamides were synthesized in high yields using a 1:1 molar ratio reaction, which is the most alternative of the reactions obtained in different molar ratios. Initially, reactions carried out at the boiling point of a non-polar organic solvent in the presence of isonicotinic acid and aromatic amines in equal molar ratios gave unique results.

Table 1.

Primary amine	The proportions of the mol	Time,	Product yield in solvent, %		Reaction product R_f
			DMF (144 °C)	TS, °C	
o-Toluidin	1:1	7	45	158–160	0.60
	1:2	7	38		
	1:3	7	34		
	1:1	7	42		

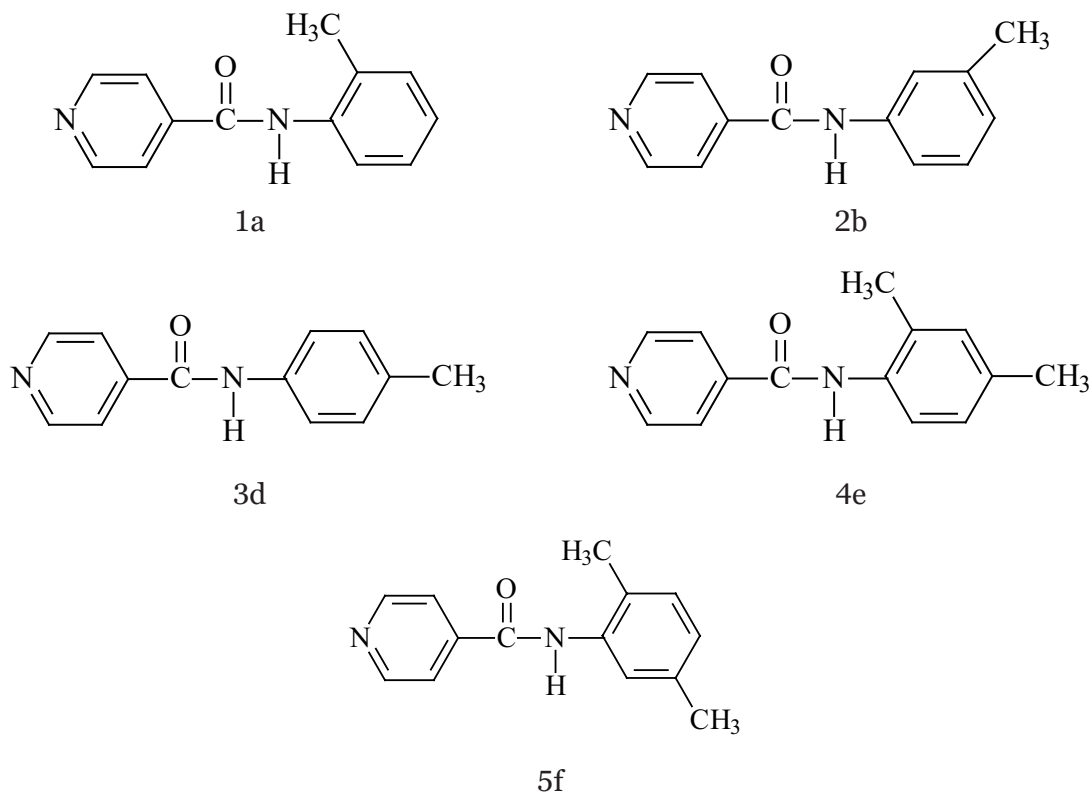
Primary amine	The proportions of the mol	Time,	Product yield in solvent, %		Reaction product R_f
			DMF (144 °C)	TS, °C	
m-Toluidin	1: 2	7	36	152–154	0.5
	1: 3	7	27		
	1: 1	7	52		
p-Toluidin	1: 2	7	44	135–137	0.56
	1: 3	7	40		
	1: 1	7	38		
2,4-xylidine	1: 2	7	33	102–104	0.5
	1: 3	7	31		
	1: 1	7	41		
2,5-xylidine	1: 2	7	36	108–110	0.56
	1: 3	7	32		

The reason is that as a result of experiments m-toluidine, 2,4-xylidines with relatively lower basicity gave amide products with lower yield, on the contrary, basicity in reactions with o-toluidine, p-toluidine, 2,5-xylidines with higher basicity arylamides of isonicotinic acid were synthesized with high yield compared to lower aromatic amines.

The result of the reaction of arylamides with isonicotinic acid and aromatic amines in molar ratios of 1:1, 1:2 and 1:3.

From the values presented in the table, it is evident that arylamides were formed in the presence of the solvent used for the reactions. Moreover, the yield of products increases depending on the basicity of the amines.

Synthesized amides



Conclusion

As a result of the experiments, arylamides of isonicotinic acid were synthesized. The physical constants of the reaction products were determined and their structure was

confirmed by IR spectroscopy and NMR spectra. It was possible to obtain quaternary ammonium salts of isonicotinic acid and aromatic amines in an organic solvent at high temperature.

References

- Pingwah Tang. Boric Acid Catalyzed Amide Formation from Carboxylic Acids and Amines: *n*-Benzyl-4-phenylbutyramide // *Organic Syntheses-2012*, – Vol. 89. – P. 432–437.
- Баевский А. М., Цикалов В. В., Баевский М. Ю., Шелудько А. Б. Борные кислоты в реакциях конденсации карбоновых кислот с ароматическими аминами // *Ученые записки Таврического национального университета им. В. М. Вернадского Серия «Биология, химия»*. Том 24 (63). 2011. – № 2. – С. 339–346.
- Yoshikawa M. et al. Pyridinium cationic-dimer antimalarials, unlike chloroquine, act selectively between the schizont stage and the ring stage of *Plasmodium falciparum* // *Bioorganic & medicinal chemistry*. 2008. – T. 16. – № . 11. – С. 6027–6033.
- Sonawane R. B., Rasal N. K., Jagtap S. V. Nickel-(II)-Catalyzed N-Formylation and N-Acylation of Amines // *American Chemical Society, Organic Letters*. 2017. – 19. – P. 2078–2081.
- Kunishima M., Kawachi C., Hioki K., Terao K., Tani S. Formation of carboxamides by direct condensation of carboxylic acids and amines in alcohols using a new alcohol- and water-soluble condensing agent: DMT-MM // *Tetrahedron*. – 57. 2001. – P. 1551–1558.
- Gholap S., Gunjal N. 2,4,6-Trichloro-1,3,5-triazine (TCT) mediated one pot direct synthesis of N-benzoylthioureas from carboxylic acids // *Arabian Journal of Chemistry*. 2017. – 10. – P. 2750–2753.
- Jaita S., Phakhodee W., Chairungsi N., Pattarawarapan M. Mechanochemical synthesis of primary amides from carboxylic acids using TCT/NH₄SCN // *Tetrahedron Letters*. – 59. 2018. – P. 3571–3573.
- Chen Z., Fu R., Chai W., Zheng H., Sun L., Lu Q., Yuan R. An eco-benign and highly efficient procedure for N-acylation catalyzed by heteropolyanion-based ionic liquids using carboxylic acid under solvent-free conditions // *Tetrahedron*. – 70. 2014. – P. 2237–2245.
- Fattahi N., Ayubi M., Ramazani A. Amidation and esterification of carboxylic acids with amines and phenols by N, N-diisopropylcarbodiimide: A new approach for amide and ester bond formation in water // *Tetrahedron*. – 74. 2018. – P. 4351–4356.
- Cheng L., Ge X., Huang L. Direct amidation of non-activated phenylacetic acid and benzylamine derivatives catalysed by NiCl₂ // *The Royal Society of Chemistry*, 2018. – 5. – 171870 p. URL: <http://dx.doi.org/10.1098/rsos.171870>.

submitted 27.08.2024;

accepted for publication 09.09.2024;

published 28.11.2024

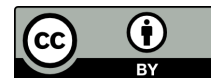
© Nurmatov D. U., Abdushukurov A. K., Xoliqov T. S., Yusufov M. S., Yodgorov Ch. G.

Contact: doston nu@mail.ru; abdushukurov-ximik@mail.ru; xoliqov@mail.ru;

yusufov_ms@mail.ru; Chinmurot-chem@mail.ru



DOI:10.29013/AJT-24-9.10-39-42



SYNTHESIS AND METHYLATION OF SOME DERIVATIVES OF 2,3-TETRAMETHYLENE-3,4- DIHYDROQUINAZOLIN-4-ONE AND -THIONE

*Nasrullaev Azizbek Ozodovich*¹, *Tukhtaev Davlat*¹, *Samiev Rajab Akbarovich*¹,
*Kodirov Khakim Iskandarzoda*², *Karimov Ilyasbek*²,
*Zohidov Kasim Akilovich*¹, *Saitkulov Foziljon Ergashevich*³

¹ Samarkand State University

² Uzbek-Finnish Pedagogical Institute

³ Tashkent State Agrarian University

Cite: *Nasrullaev A.O., Tukhtaev D.B., Samiev R.A., Kodirov Kh.I., Karimov I.M., Zohidov K.A., Saitkulov F.E. (2024). Synthesis and Methylation of Some Derivatives of 2,3-Tetramethylene-3,4-Dihydroquinazolin-4-one and – Thione. Austrian Journal of Technical and Natural Sciences 2024, No 9–10. <https://doi.org/10.29013/AJT-24-9.10-39-42>*

Abstract

Formylation reactions of 2,3-tetramethylene-3,4-dihydroquinazolin-4-one (thione) with Vilsmeier-Haack reagent were carried out. It was found that 2,3-tetramethylene-3,4-dihydroquinazolin-4-one yields α -formyl-2,3-tetramethylene-3,4-dihydroquinazolin-4-one, and 2,3-tetramethylene-3,4-dihydroquinazolin-4-thione yields α -hydroxymethylidene-2,3-tetramethylene-3,4-dihydroquinazolin-4-thione.

Keywords: *Vilsmeier-Haack reagent, 2,3-tetramethylene-2,3-dihydroquinazolin-4-one (thione), α -formyl-2,3-tetramethylene-3,4-dihydroquinazolin-4-one, α -hydroxymethylidene-2,3-tetramethylene-3,4-dihydroquinazolin-4-one (thione)*

Introduction

Currently, one of the urgent tasks in the agricultural, medical and veterinary fields is the development of new high-quality and safe for humans and the environment drugs. One of the important approaches to the creation of these drugs is the synthesis of candidate compounds with bioactive groups in their molecules or the introduction of new pharmacophoric groups using appropriate modification methods among heterocyclic compounds, tricyclic substituted quinazolo-

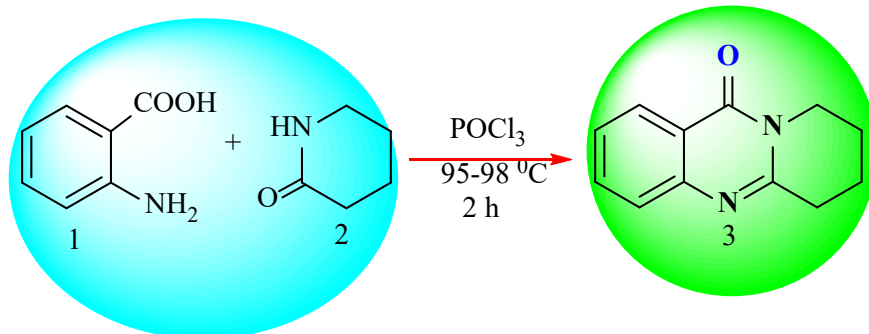
nes and their thioanalogues occupy an important and interesting place. The synthesis of new derivatives of these compounds, the identification of biologically active substances among them will make a significant contribution to the development of chemistry and biology of this class of compounds. In the world, drugs based on tricyclic quinazolones and quinazolinethiones are widely used in agriculture (anthelmintics, stimulants and pesticides) in medicine (against cancer and viruses). Among these compounds, anticho-

linesterase (deoxypeganine) and anticancer drugs (erlotinib, lapatinib, gefitinib, etc.) are especially successfully accepted. Therefore, it is very important to conduct targeted synthesis and chemical transformations of biologically active substances with a pharmacophoric (quinoxaline ring) in the molecule, determine their biological properties, and create promising medicinal and pesticide preparations based on the obtained substances (Gordon A., Ford R., 1976). The aim of this work is to synthesize the reaction of 2,3-tetramethylene-3,4-dihydroquinazolin-4-one and -thione using phosphorus pentasulfide reagent (Nasrullaev A. O., Tillaev S. U., Tukhtaev D. B., Gaibullaev Sh. Sh., Kadyrov Kh. I., Zakhidov K. A., 2023; Elmuradov B. Zh., Yakubov U. M., Zhurayev B. B., Tadjimukhamedov K. S., Zakhidov K. A., 2017; Samarov Z. U., Urazov T. S., Urinov I. O.,

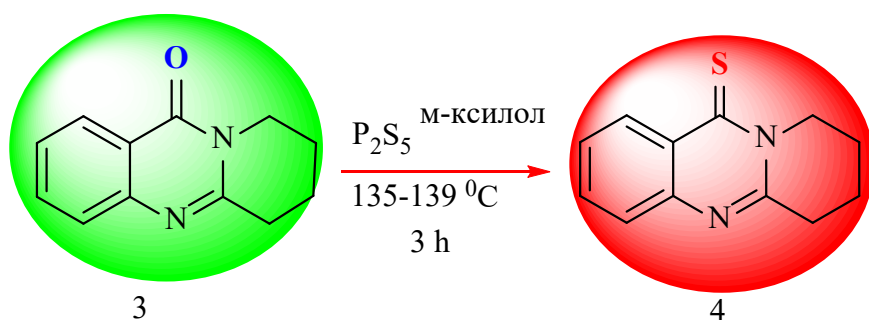
Ravshanov A. S., Zakhidov K. A. 2017; Samarov Z. U., Urinov I. O., Zhavkharov Zh. Zh. 2018; Gaibullaev Sh. Sh., Tukhsanov F. S., Asrorov D. A., Nasrullaev A. O., Tillaev S. U., Zakhidov K. A., 2022; Nasrullaev A. O., Tillaev S. U., Tukhtaev D. B., Gaibullaev Sh. Sh., Zakhidov K. A., 2023).

Methods and results

Continuing the research in this direction, we decided to study the reactions of formylation of 2,3-tetramethylene-3,4-dihydroquinazolin-4-one and its thioanalogue, as well as to study the reactions of nucleophilic substitution of the obtained formylation products. The first synthesized compound 2,3-tetramethylene-3,4-dihydroquinazolin-4-one (3) was obtained by condensation of anthranilic acid (1) with valerolactam (2) in the presence of chloroxyphosphorus.



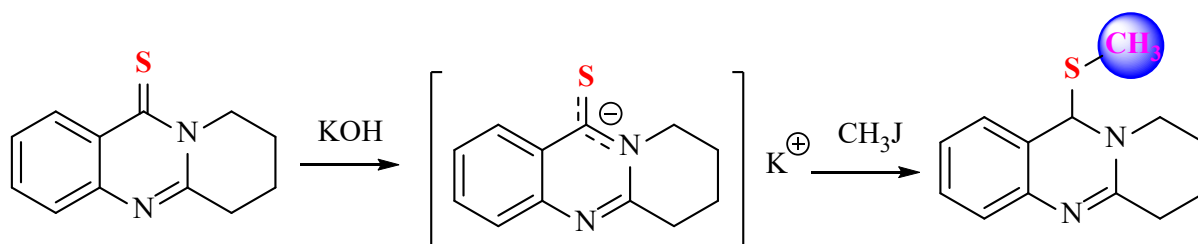
The reaction of 2,3-tetramethylene-3,4-dihydroquinazolin-4-one (3) with phosphorus pentasulfide in *m*-xylene yielded the second compound 2,3-tetramethylene-3,4-dihydroquinazolin-4-thione (4)



It should be said that the methylation reactions in the corresponding 2,3-tetramethylene-3,4-dihydroquinazolin-4-thione (4) in relation to 2,3-tetramethylene-3,4-dihydroquinazolin-4-one (3) take place mainly on the sulfur atom

Methylation reactions of 2,3-tetramethylene-3,4-dihydroquinazolin-4-thione (4) in different organic solvents (absolute alcohol, dioxane-1,4, DMFA, DMSO) with three different methylating agents (methyl iodide,

methyl tosylate, dimethylsulfate) was carried out in the presence of an alkaline catalyst (KOH). Reactions were carried out at room temperature for 24 hours or heated at 70–75 °C (85–90 °C) for 3–4 hours.



Experimental Part

To achieve the set goal, we carried out reactions of formylation of 2,3-tetramethylene-3,4-dihydroquinazolin-4-one and its thioanalogue using the Vilsmeier-Haack reagent.

For this purpose, the following operations were carried out: Solvents and reagents: *m*-xylene, DMF, ether, thionyl chloride, chloroform, benzene were anhydrous by the known method (Gordon A., Ford R., 1976). Identification of substances using thin-layer chromatography (TLC) was carried out on Sorbfil (Russia), Whatman UV-254 (Germany) and G60F-254 (Qingdao Haiyang Chemical) plates. Eluents: benzene: methanol = 5: 1 (system A) and benzene: methanol = 3:1 (system B).

Purification of anthranilic acid. 10 g of technical anthranilic acid were placed in a 500 ml flat-bottomed flask and 250 ml of distilled water were poured in. The suspension was boiled until the starting material was completely dissolved. 2–3 g of activated carbon were added to the resulting brown solution and mixed. The undisclosed precipitate was separated by filtering the hot solution under vacuum. When cooled in a water bath with cold water, pure crystals of anthranilic acid precipitated from the filtrate solution. The precipitate was separated by filtration, washed with water and dried in a drying cabinet. Recrystallization was carried out until the required amount of anthranilic acid was accumulated.

Obtaining phosphorus oxychloride.

A mixture of 61 g of benzoic acid and 105 g of phosphorus pentachloride was prepared in a 0.5 l flask. The reaction mixture was left for 30 minutes and boiled. The resulting phosphorus oxychloride was distilled in the range of 105–120 °C. The yield of the product was 70.5 ml (72 g, 94%).

Synthesis of 2,3-tetramethylene-3,4-dihydroquinazolin-4-one. A mixture of 30 g (0.219 mol) of anthranilic

acid and 32.9 g (0.332 mol) of δ -valerolactam was placed in a 250 ml round-bottomed flask equipped with a reflux condenser, and 122 g (73 ml) ($\rho = 1.675 \text{ g/cm}^3$) (0.794 mol) of phosphorus oxychloride were added from a dropping funnel over 1 hour. The reaction mixture was then heated in a water bath (95–98 °C) for 2 hours. The reaction mixture was cooled and poured onto ice. The temperature of the reaction mixture was maintained at 0–2 °C. After complete decomposition of the reaction mixture, it was neutralized with a 25% ammonia solution to pH = 8–9. The alkaline solution was extracted three times with chloroform (3×100 ml), the extract was washed with water and dried over anhydrous sodium sulfate. The extract was filtered and the chloroform was distilled off in vacuum. The yield of the residue was 41.5 g. Recrystallization from the reaction residue yielded 35 g (80%) of 2,3-tetramethylene-3,4-dihydroquinazolin-4-one (3).

Synthesis of 2,3-tetramethylene-3,4-dihydroquinazolin-4-thione.

In a 100 ml round-bottomed flask equipped with a reflux condenser and stirrer, a solution of 7.2 g (0.036 mol) of 2,3-tetramethylene-3,4-dihydroquinazolin-4-one and 8.3 g (0.037 mol) of phosphorus pentasulfide in 40 ml of *m*-xylene was prepared. The reaction mixture was boiled at a temperature of 135–139 °C for 3 hours. Then the reaction mixture was cooled, 80 ml (10%) sodium hydroxide solution was added and left for 1 hour. The formed precipitate was filtered, washed with water until neutral reaction and dried. Product yield 5.45 g (70%). Mass spectrum: m/z (I, %): 217([M+1]⁺, 52.6), 201 (10.5), 183 (26.3), 176 (100), 169 (23.7), 162 (10.5), 149 (15.8), 143 (21), 129 (24), 102 (5.3).

Methylation of some derivatives of 2,3-tetramethylene-3,4-dihydroquinazolin-4-one and -thione. A solvent (absolute ethanol/1,4-dioxane/DMFA/or DMSO) is poured into a three-necked round-

bottom flask equipped with a reflux condenser, a calcium chloride tube, a thermometer, a separatory funnel, and a mechanical stirrer, and 0.01 mol of 2,3-tetramethylene-3,4-dihydroquinazolin-4-thione and 0.01 mol KOH are added, then a solution of 0.01 mol methylating agent (methyl iodide/methyltosylate/ or dimethylsulfate) in 5 ml solvent is added dropwise. The mixture is heated at room temperature for 24 hours or 4 hours (70–75 °C or 85–90 °C), then decomposed with water, extracted with chloroform, the extract is dried

over dry Na_2SO_4 . After removal of the solvent, the residue is purified by recrystallization or column chromatography.

Conclusion

Thus, the direction of the methylation reaction is significantly affected by the nature of the alkylating agent, solvent and temperature. In the case of methylation with methyl iodide, the reaction is selective for the sulfur atom, regardless of the nature of the solvent and temperature.

References

- Gordon A., Ford R. Chemist's Companion. Physicochemical properties, methods, bibliography. Per. from English – M: Mir, 1976. – 541 p.
- Nasrullaev A. O., Tillaev S. U., Tukhtaev D. B., Gaibullaev Sh.Sh., Kadyrov Kh.I., Zakhidov K. A. Synthesis of some derivatives of 2,3-trimethylene-3,4-dihydroquinazolin-4-thione // *Universum: chemistry and biology*. – No. 10(112). October, 2023. – P. 20–26.
- Elmuradov B. Zh., Yakubov U. M., Zhurayev B. B., Tadjimukhamedov K. S., Zakhidov K. A. Selective Bromination of Tricyclik Quinazolines // *World wide journal of multidisciplinary research and development*. 2017. – 3(10). – P. 1–5.
- Samarov Z. U., Urazov T. S., Urinov I. O., Ravshanov A. S., Zakhidov K. A. Amidomethylation of 2,3-polymethylene-1,2,3,4-tetrahydroquinazolin-4-ones with N-methylolpyrrolidine-2 // *Scientific Bulletin of SSU*. – 5(105). 2017. – P. 140–144.
- Samarov Z. U., Urinov I. O., Zhavkharov Zh. Zh. Interaction of 2,3-polymethylene-1,2,3,4-tetrahydroquinazolin-4-ones with o-, m-chlorophenylisocyanates // *Proceedings of the V international scientific and practical conference "Problems and Prospects of Chemistry of Goods and Traditional Medicine"*. (Andijan, 2018, September 4–5) – P. 104–105.
- Gaibullaev Sh. Sh., Tukhsanov F. S., Asrorov D. A., Nasrullaev A. O., Tillaev S. U., Zakhidov K. A. Synthesis and nitration of 2,3-polymethylene-3,4-dihydroquinazolin-4-thiones // *Scientific Bulletin of SSU*. 3(133). 2022. – P. 61–64.
- Nasrullaev A. O., Tillaev S. U., Tukhtaev D. B., Gaibullaev Sh. Sh., Zakhidov K. A. Synthesis and biological activity of α -arylidene(furfurylidene-2)-2,3-polymethylene-3,4-dihydroquinazolin-4-thiones // *Universum: Chemistry and biology*. – No. 6 (108). June, 2023. – P. 14–20.

submitted 26.09.2024;

accepted for publication 11.10.2024;

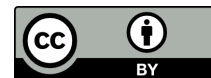
published 28.11.2024

© Nasrullaev A. O., Tukhtaev D. B., Samiev R. A., Kodirov Kh. I., Karimov I. M., Zokhidov K. A., Saitkulov F. E.

Contact: z.qosim2019@g.mail.com



DOI:10.29013/AJT-24-9.10-43-48



SYNTHESIS OF SOME DERIVATIVES OF 2,3-TETRAMETHYLENE-3,4-DIHYDROQUINAZOLIN-4-ONE AND -THIONE

*Nasrullaev Azizbek Ozodovich*¹, *Tukhtaev Davlat*¹, *Samiev Rajab Akbarovich*¹, *Kodirov Khakim Iskandarzoda*², *Karimov Ilyasbek*², *Zohidov Kasim Akilovich*¹, *Saitkulov Foziljon Ergashevich*³

¹ Samarkand State University

² Uzbek-Finnish Pedagogical Institute

³ Tashkent State Agrarian University

Cite: *Nasrullaev A. O., Tukhtaev D. B., Samiev R. A., Kodirov Kh. I., Karimov I. M., Zokhidov K. A., Saitkulov F. E. (2024). Synthesis of Some Derivatives of 2,3-Tetramethylene-3,4-Dihydroquinazolin-4-one and -Thione. Austrian Journal of Technical and Natural Sciences 2024, No 9 – 10. <https://doi.org/10.29013/AJT-24-9.10-43-48>*

Abstract

In the article a new method of reaction formylation of 2,3-tetramethylene-3,4-dihydroquinazolin-4-one (thione) with Vilsmeier-Haack reagent is carried out. It is established that from 2,3-tetramethylene-3,4-dihydroquinazolin-4-one α -formyl-2,3-tetramethylene-3,4-dihydroquinazolin-4-one is formed, and from 2,3-tetramethylene-3,4-dihydroquinazolin-4-thione α -hydroxymethylidene-2,3-tetramethylene-3,4-dihydroquinazolin-4-thione. Reactions of nucleophilic substitution of the obtained products are studied. Representatives of selenium-containing tricyclic quinazolin-4-ones and their thioanalogues with hydrogenated pyridine ring are synthesized for the first time.

Keywords: *Vilsmeier-Haack reagent, 2,3-tetramethylene-2,3-dihydroquinazolin-4-one (thione), α -formyl-2,3-tetramethylene-3,4-dihydroquinazolin-4-one, α -hydroxymethylidene-2,3-tetramethylene-3,4-dihydroquinazolin-4-thione, α -chloromethylidene-2,3-tetramethylene-3,4-dihydroquinazolin-4-one (thione) and their hydrochloride, α -hydroroselenylmethylidene-2,3-tetramethylene-3,4-dihydroquinazolin-4-one (thione)*

Introduction

In the world, drugs based on tricyclic quinazolones and quinazolinethiones are widely used in agriculture (anthelmintics, stimulants and pesticides) in medicine (against cancer and viruses). Among these compounds, anticholinesterase (deoxypeganine) and anticancer drugs (erlotinib, lapatinib gefitinib, etc.)

are especially successfully accepted. Therefore, it is very important to carry out targeted synthesis and chemical transformations of biologically active substances with a pharmacophoric (quinazoline ring) in the molecule, determine their biological properties, create promising medicinal and pesticide preparations based on the obtained substances.

It is known that the formylation reaction is widely used to introduce an aldehyde group in organic chemistry. With the help of the formylation reaction, a highly reactive formyl group ($-\text{CH}=\text{O}$) is introduced into the substrate. The existence of this group in the molecule enables the substrate to react with electrophilic and nucleophilic reagents. Thus, it creates conditions for the synthesis of various derivatives of the original compound. And the existence of compounds with a formyl group in various tautomeric forms (aldehyde, enol, amide, enamine) is of theoretical interest (Gordon A., Ford R., 1976; Nasrullaev A. O., Tillaev S. U., Tukhtaev D. B., Gaibullaev Sh. Sh., Kadyrov Kh. I., Zakhidov K. A., 2023; Elmuradov B. Zh., Yakubov U. M., Zhurayev B. B., Tadjimukhamedov K. S., Zakhidov K. A., 2017; Samarov Z. U., Urazov T. S., Urinov I. O., Ravshanov A. S., Zakhidov K. A., 2017; Samarov Z. U., Urinov I. O., Zhavkharov Zh. Zh., 2018; Gaibullaev Sh. Sh., Tukhsanov F. S., Asrorov D. A., Nasrullaev A. O., Tillaev S. U., Zakhidov K. A., 2022; Nasrullaev A. O., Til-

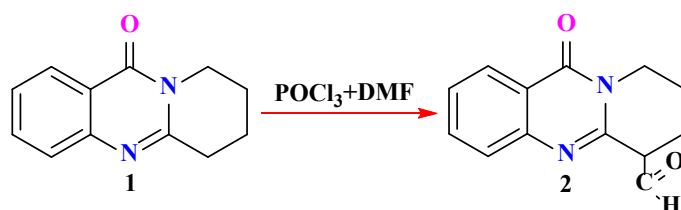
laev S. U., Tukhtaev D. B., Gaibullaev Sh. Sh., Zakhidov K. A., 2023).

Methods and results

The aim of this work is to study the formylation reaction of 2,3-tetramethylene-3,4-dihydroquinazolin-4-one and -thione using the Vilsmeier-Haack reagent (phosphorus oxychloride + dimethylformamide), and to study the reaction of the obtained products with nucleophilic reagents.

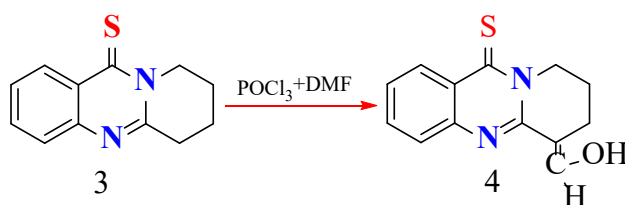
Continuing the research in this direction, we decided to study the formylation reactions of 2,3-tetramethylene-3,4-dihydroquinazolin-4-one and its thioanalogue, as well as to study the nucleophilic substitution reactions of the resulting formylation products.

When 2,3-tetramethylene-3,4-dihydroquinazolin-4-one is formylated with the Vilsmeier-Haack reagent (phosphorus oxychloride + dimethylformamide), α -formylmethylidene-2,3-tetramethylidene-3,4-dihydroquinazolin-4-one is formed.



The existence of the obtained product (2) in a stable aldehyde form was proven using chemical methods and physical methods of analysis. In particular, using X-ray structural analysis it was established that the obtained compound exists in the enamine aldehyde form. Unlike 2,3-tetramethylene-3,4-dihydroquinazolin-4-one,

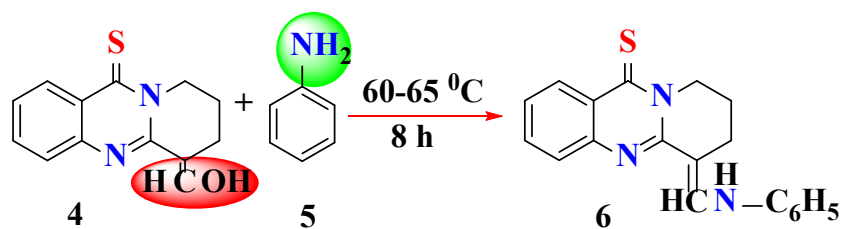
the formylation of its thioanalogue 2,3-tetramethylene-3,4-dihydroquinazolin-4-one with the Vilsmeier-Haack reagent proceeds with the formation of α -hydroxymethylidene-2,3-tetramethylidene-3,4-dihydroquinazolin-4-thione (3) instead of the expected α -formyl product.



According to physical analysis methods, it was established that the obtained compound (4) exists in the enol form.

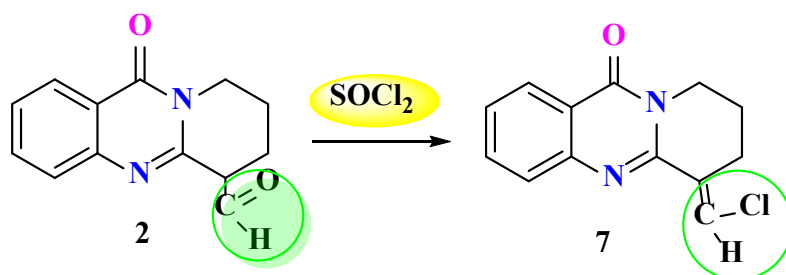
When the obtained α -hydroxymethylidene-2,3-tetramethylidene-3,4-dihydroquinazolin-4-thione interacted with aniline (5) in an amount of (1: 9) at a tem-

perature of 60–65 °C for 8 hours, α -anilinomethylidene-2,3-tetramethylidene-3,4-dihydroquinazolin-4-thione (6) was obtained with a good yield (73%).



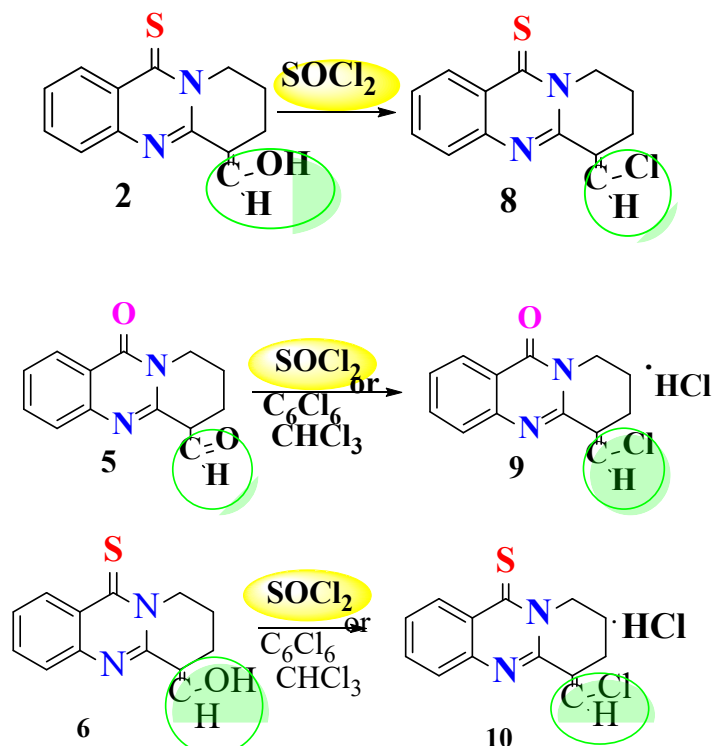
When α -formyl-2,3-tetramethylidene-3,4-dihydroquinazolin-4-one (5) reacts with an excess of thionyl chloride, nucleophilic substitution of the hydroxyl group by

a chlorine atom occurs to form α -chloromethylidene-2,3-tetramethylidene-3,4-dihydroquinazolin-4-one (7).



When α -hydroxymethylidene-2,3-tetramethylidene-3,4-dihydroquinazolin-4-one (6) reacts with an excess of thionyl chloride, nucleophilic substitution of the hydroxyl group by a chlorine atom also occurs,

resulting in the formation of α -chloromethylidene-2,3-tetramethylidene-3,4-dihydroquinazolin-4-thione (10):

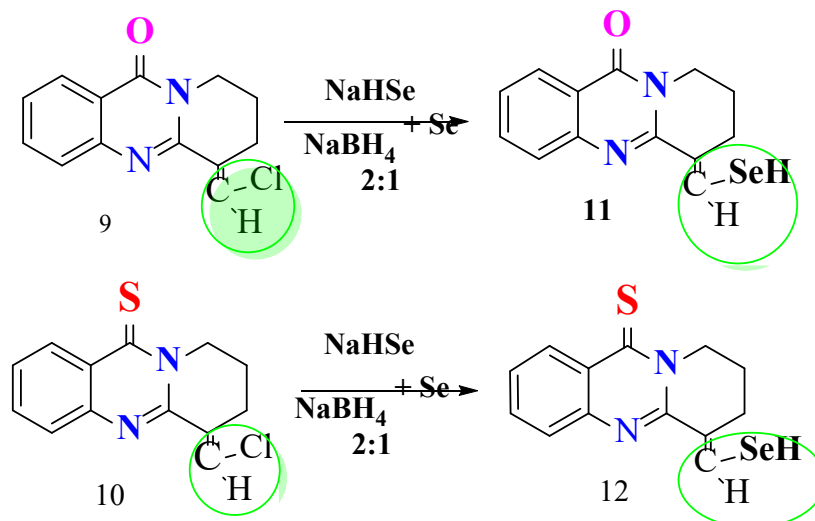


In this case, α -chloromethylidene is formed with good yields. Since the obtained compounds are unstable and can decompose during storage with the release of hydrogen chloride. Therefore, in order for the obtained compound

to be in a stable form, the reactions were carried out with substrate + thionyl chloride in equimolar quantities in absolute solutions of benzene or chloroform with the formation of the corresponding hydrochlorides (9, 10):

Since the chlorine atom in the obtained α -chloromethylidene-2,3-tetramethylidene-3,4-dihydroquinazolin-4-one and -thione (9,10) is very active and can interact with other nucleophilic reagents, we decided to study reactions with sodium hydroselenide. The reaction of α -chloromethylidene-2,3-tetramethylidene-3,4-dihydroquinazolin-4-one (8) and α -chloromethylidene-2,3-tetrame-

thylidene-3,4-dihydroquinazoline-4-thione (9) with sodium hydroselenide (at the time of isolation from sodium borohydride and selenium) gave the corresponding α -hydroselenylmethylidene-2,3-tetramethylidene-3,4-dihydroquinazolin-4-one (10) and α -hydroselenylmethylidene-2,3-tetramethylidene-3,4-dihydroquinazoline-4-thione (11) in good yield:



The obtained compounds (11, 12) are the first representatives of selenium-containing tricyclic and quinazolin-4-ones and thioanalogues with a hydrogenated pyridine ring.

Experimental part

To achieve the set goal, we carried out reactions of formylation of 2,3-tetramethylene-3,4-dihydroquinazolin-4-one and its thioanalogue with the Vilsmeier-Haack reagent. Then, the reactions of nucleophilic substitution of the obtained products with aniline, thionyl chloride and sodium hydroselenide were studied.

Synthesis of α -formyl-2,3-tetramethylene-3,4-dihydroquinazolin-4-one

0.68 ml (8.25 mmol) of dimethylformamide was placed in a 100 ml three-neck flask and cooled in an ice bath. The flask was stirred mechanically for 10–15 minutes. Then, 0.8 ml (8.25 mmol) of phosphorus oxychloride was added dropwise with stirring. Then, 0.5 g (2.5 mmol) of 2,3-tetramethylene-3,4-dihydroquinazolin-4-one was added with stirring for 15 minutes. The reaction mixture was stirred for 1 hour at room temperature and left overnight. On the second day, the reaction mixture was heated in a wa-

ter bath at 95–98 °C for 2 hours, then cooled to room temperature and POCl₃ was decomposed with water. The mixture was neutralized with a saturated sodium acetate solution to pH=7. The formed precipitate was filtered, washed with water and dried. Product yield 0.51 g (90%). IR spectrum (ν , cm⁻¹): 1630 (ν C=N), 1675 (ν C=C), 3300–3600 (ν OH). Molecular weight = 228 (mass spectrometric).

Synthesis of α -hydroxymethylidene-2,3-tetramethylene-3,4-dihydroquinazolin-4-thione

1.49 g (4.6 mmol) of dimethylformamide were placed in a 100 ml three-neck flask and the flask was cooled in an ice bath. The contents of the flask were stirred mechanically for 10–15 minutes. Then, 1.54 g (10 mmol) of phosphorus oxychloride were added dropwise with stirring. Then, 1 g (4.6 mmol) of 2,3-tetramethylene-3,4-dihydroquinazolin-4-thione was added with stirring for 10–15 minutes. The reaction mixture was stirred for 2 hours at room temperature and left overnight. The next day, the reaction mixture was heated in a water bath (95–98 °C) for 2 hours, then cooled to room temperature and decomposed into

5–10 g of ice, neutralized with an ammonia solution (10%) to a weak alkaline medium (pH=8). The yellow precipitate that formed was filtered off, washed with water (3–4 times) and dried. Product yield 0.88 g (78%). IR spectrum (ν , cm^{-1}): 3435 (νOH), 1563 ($\nu\text{C}=\text{N}$), 1488 ($\nu\text{C}-\text{N}$), 1283 ($\nu\text{C}=\text{S}$).

Synthesis of α -(Anilino)methylidene-2,3-tetramethylidene-3,4-dihydroquinazolin-4-thione

A solution of 0.2 g (0.82 mmol) of α -hydroxymethylidene-2,3-tetramethylidene-3,4-dihydroquinazolin-4-thione and 0.7 ml (7.7 mmol) of aniline was prepared in a 100 ml round-bottomed flask. The reaction mixture was heated in a water bath (60–65 °C) for 8 hours and left overnight while cooling. The reaction mixture was treated with ether, the precipitate that fell was filtered off and recrystallized from methanol. The yield of the product was 0.19 g (73%). Tm 152 °C (methanol) Rf=0.85 (A). ^1H NMR (400 MGs, CCl_4+DMSO , δ , ppt J/Gs): 12.3 (1H, c, $J = 7.5$, NH). 7.4–8.1 (4H, m, H-5,6,7,8), 7.35 (1H, d, $J = 7.5$, CH), 6.6–7.3 (5H, m, H-Ph),

Synthesis of α -chloromethylidene-2,3-tetramethylidene-3,4-dihydroquinazolin-4-one

450 mg (1.9 mmol) of α -formyl-2,3-tetramethylidene-3,4-dihydroquinazolin-4-one and 4 ml (56.2 mmol, $\rho = 1.66 \text{ g / cm}^3$) of freshly distilled thionyl chloride were placed in a 100 ml round-bottomed flask and the reaction mixture was heated in a water bath (70–75 °C) for 1.5–2 hours. Cooled, decomposed with distilled water (100 ml). The formed precipitate was filtered, washed 3–4 times with water and dried. Product yield 336 mg (70%). Tm 172 °C (benzene).

Synthesis of α -chloromethylidene-2,3-tetramethylidene-3,4-dihydroquinazolin-4-thione

595 mg (2.44 mol) of α -hydroxy-2,3-tetramethylidene-3,4-dihydroquinazolin-4-thione and 3.5 ml (48.8 mmol, $\rho = 1.66 \text{ g / ml}$) of freshly distilled thionyl chloride were placed in a 100 ml round-bottomed flask. After 5 minutes, a precipitate began to fall out. The reaction mixture was stirred for another 30 minutes at room temperature. The precipitate was filtered off with chloro-

form and dried. Yield 0.9 g (78.4%). IR spectrum (ν , cm^{-1}): 1567 ($\nu\text{C}=\text{N}$), 1484 ($\nu\text{C}-\text{N}$), 1284 ($\nu\text{C}=\text{S}$), 757 ($\nu\text{C}-\text{Cl}$).

Synthesis of α -hydroselenylmethylidene-2,3-tetramethylidene-3,4-dihydroquinazolin-4-one.

In a four-necked round-bottomed flask with a capacity of 250 ml, equipped with a mechanical stirrer, thermometer, reflux condenser, glass gas conductor were placed 25 ml of distilled water, 720 mg (9 mmol) of selenium and the suspension was stirred for 15–20 minutes by passing molecular nitrogen (N_2) through it. Then 430 mg (13.4 mmol) of sodium borohydride were added in portions and the reaction mixture was stirred for 15–20 minutes, after which it was heated in a water bath at 35–40 °C for 1 hour. During this process, the color of the solution changed from colorless to brown-burgundy. Then the reaction mixture was cooled and 1.66 g (7.3 mmol) of α -chloromethylidene-2,3-tetramethylidene-3,4-dihydroquinazolin-4-one were added. The reaction mixture was stirred for 1 hour at room temperature, then with heating in a water bath (90–95 °C) while passing molecular nitrogen (N_2) through it. The reaction mixture was cooled, the residue was filtered, the filtrate was neutralized with glacial acetic acid. The resulting red precipitate was filtered, washed with a sufficient amount of water, and dried. Product yield 882 mg (45%).

Synthesis of α -hydroselenylmethylidene-2,3-tetramethylidene-3,4-dihydroquinazolin-4-thione

In a 150 ml four-neck round-bottomed flask equipped with a mechanical stirrer, thermometer, reflux condenser, glass gas conductor were placed 15 ml of distilled water, 235 mg (3 mmol) of selenium and the suspension was stirred for 15–20 minutes by passing molecular nitrogen (N_2) through it. Then 160 mg (4.2 mmol) of sodium borohydride were added in portions and the reaction mixture was stirred for 15–20 minutes. Then it was heated in a water bath (35–40 °C) for 1 hour. During this time, the color of the solution changed from colorless to brown burgundy. Then the reaction mixture was cooled and 0.6 g (2.3 mmol) of α -chloromethylidene-2,3-tetramethylidene-3,4-dihydroquinazolin-4-thione was added. The reaction mixture was stirred for 1 hour at room tempera-

ture, then with heating in a water bath (90–95 °C) while passing molecular nitrogen (N₂) through it. The reaction mixture was cooled, the residue was filtered, the filtrate was neutralized with glacial acetic acid. The resulting red precipitate was filtered, washed with a sufficient amount of water, dried. The yield of the product is 288 mg (41%). IR spectrum (ν , cm⁻¹): 2795 (ν Se-H), 1563 (ν C=N), 1474 (ν C-N), 1283 (ν C=S).

Conclusion

The formylation reactions of 2,3-tetramethylene-3,4-dihydroquinazolin-4-one and its thioanalogue were studied, as well as the nucleophilic substitution reactions of the formed formylation products. The first synthesized compound 2,3-tetramethylene-3,4-dihydroquinazolin-4-one (3) was synthesized in high yield by condensation of anthranilic acid with valerolactam in the presence of chlorooxyphosphorus. For the first time, selenium-containing tricyclic heterocyclic compounds were synthesized.

References

- Gordon A., Ford R. Chemist's Companion. Physicochemical properties, methods, bibliography. Per. from English – M: Mir, 1976. – 541 p.
- Nasrullaev A. O., Tillaev S. U., Tukhtaev D. B., Gaibullaev Sh. Sh., Kadyrov Kh. I., Zakhidov K. A. Synthesis of some derivatives of 2,3-trimethylene-3,4-dihydroquinazolin-4-thione // *Universum: chemistry and biology*. – No. 10(112). October, 2023. – P. 20–26.
- Selective Bromination of Tricyclic Quinazolines // *World wide journal of multidisciplinary research and development*. 2017. – 3(10). – P. 1–5.
- Samarov Z. U., Urazov T. S., Urinov I. O., Ravshanov A. S., Zakhidov K. A. Amidomethylation of 2,3-polymethylene-1,2,3,4-tetrahydroquinazolin-4-ones with N-methylolpyrrolidine-2 // *Scientific Bulletin of SSU*. – 5(105). 2017. – P. 140–144.
- Samarov Z. U., Urinov I. O., Zhavkharov Zh. Zh. Interaction of 2,3-polymethylene-1,2,3,4-tetrahydroquinazolin-4-ones with o-, m-chlorophenylisocyanates // *Proceedings of the V international scientific and practical conference "Problems and Prospects of Chemistry of Goods and Traditional Medicine"*. (Andijan, 2018, September 4–5). – P. 104–105.
- Synthesis and nitration of 2,3-polymethylene-3,4-dihydroquinazolin-4-thiones // *Scientific Bulletin of SSU*. – 3(133). 2022. – P. 61–64.
- Nasrullaev A. O., Tillaev S. U., Tukhtaev D. B., Gaibullaev Sh. Sh., Zakhidov K. A. Synthesis and biological activity of α -arylidene(furfurylidene-2)-2,3-polymethylene-3,4-dihydroquinazolin-4-thiones // *Universum: Chemistry and biology*. – No. 6 (108). June, 2023. – P. 14–20.

submitted 22.09.2024;

accepted for publication 07.10.2024;

published 28.11.2024

© Nasrullaev A. O., Tukhtaev D. B., Samiev R. A., Kodirov Kh. I., Karimov I. M., Zakhidov K. A., Saitkulov F. E.

Contact: z.qosim2019@g.mail.com



DOI:10.29013/AJT-24-9.10-49-53



SYNTHESIS REACTIONS OF QUINAZOLIN-4-ONE IN THE PRESENCE OF IRON (III)-CHLORIDE CATALYSTS

*Oripov Oybek Bekboyevich*¹, *Saitkulov Foziljon Ergashevich*²,
*Mirvaliev Zoid Zoxidovich*²

¹ School №22, Nurobod District, Samarkand Region, Samarkand, Uzbekistan

² Tashkent State Agrarian Universitet, Tashkent, Uzbekistan

Cite: Oripov O.B., Saitkulov F.E., Mirvaliev Z.Z. (2024). *Synthesis Reactions of Quinazolin-4-One in the Presence of Iron (Iii)-Chloride Catalysts. Austrian Journal of Technical and Natural Sciences 2024, No 9 – 10.* <https://doi.org/10.29013/AJT-24-9.10-49-53>

Abstract

Quinazolin-4-one is a significant ring-shaped compound with various biological and pharmacological effects. Iron trichloride (FeCl_3) is being used as a catalyst in making quinazolin-4-one because it works well and is also eco-friendly. FeCl_3 , functioning as a Lewis acid, speeds up the closing of the ring by activating centers that attract electrons and helping with the attack of molecules that donate electrons, resulting in faster reactions, better amounts of product, and increased specificity. This paper examines how FeCl_3 helps with creating reactions, particularly by finding the best conditions for the reaction like temperature, solvent, and concentration. The research shows that FeCl_3 can be a useful and environmentally-friendly catalyst for making quinazolin-4-one derivatives, which can be very beneficial for industries and pharmaceutical purposes.

Keywords: *Quinazolin-4-one, iron (III)-chloride, FeCl_3 , Lewis acid, catalysis, heterocyclic compounds, synthesis reactions, nucleophilic attack, ring closure, sustainable chemistry*

Introduction

Quinazolin-4-one is an important compound with a diverse range of biological and pharmacological effects, which has attracted a lot of interest. The substances that come from it have many health benefits, such as fighting cancer, reducing inflammation, and killing germs. This makes it an important structure for creating medicines. Therefore, the effective production of quinazolin-4-one

and its variations is currently a primary area of study in the field of organic chemistry.

Catalysts are important for making quinazolin-4-one by helping the reaction happen faster, produce more, and be more selective. Out of the various catalysts researched, iron (III) chloride (FeCl_3) has become a popular choice because of its Lewis acid characteristics, affordable price, easy accessibility, and environmentally friendly

qualities. FeCl_3 is recognized for speeding up reactions by activating positively charged centers in the substances and encouraging attacks from negatively charged particles, which are necessary for the closing of a ring and the creation of the quinazoline structure (Saitkulov F. E., Elmuradov B. Zh., Sapaev B., 2024; Saitkulov F. E., Elmuradov B. Zh., Giyasov K., 2023; Saitkulov, F., Sapaev, B., Nasimov, K., Kurbanova, D., & Tursunova, N., 2023; Murodillayevich, K. M., Shoyimovich, K. G., & Ergashevich, S. F., 2022; Sapaev, B., Saitkulov, F. E., Normurodov, O. U., Haydarov, G., & Ergashyev, B., 2023).

Utilizing FeCl_3 as a catalyst has various benefits compared to other metal-based catalysts, like being more eco-friendly and economical. It has been demonstrated to efficiently speed up a variety of reactions, making it a flexible tool for creating quinazolin-4-one derivatives. Furthermore, improving the reaction conditions such as temperature, type of solvent, and the amount of catalyst can greatly improve the effectiveness of the process.

This paper investigates how iron (III) chloride speeds up the creation of quinazolin-4-one and its related compounds. The study seeks to explore how FeCl_3 affects these reactions in order to better understand how this catalyst can be used to improve the production of quinazolin-4-one for different industrial and pharmaceutical purposes (Saitkulov, F., Ibragimov, B. R., Allaqulova, M., Umarov, S., & Xolmatova, M., 2022; Saitkulov, F., Azimov, I., Ergasheva, M., & Jo'raqulov, H., 2022; . Sapaev, B., Sapaev, I. B., Saitkulov, F. E., Tashniyazov, A. A., & Nazaraliev, D., June, 2022; Sapaev, B., Saitkulov, F. E., Tashniyazov, A. A., & Normurodov, O. U., 2021; Saitkulov, F., Qilichyeva, N., Abdullayev, B., Anvarov, A., & Ergasheva, M., 2022; Khatamov, K., Saitqulov, F., Ashurov, J., & Shakhidoyatov, K., 2012; Baymuratova, G., Nasimov, K., & Saitkulov, F., 2023).

Method and results

The synthesis of quinazolin-4-one in the presence of iron (III) chloride (FeCl_3) as a catalyst was carried out using ortho-substituted anilines and ortho-carbonyl compounds as starting materials. FeCl_3 was added in an anhydrous form in specific molar ratios (5–10 mol%) to the reaction mixture. The mix-

ture was dissolved in various solvents, including ethanol, methanol, and dimethylformamide (DMF), to evaluate their impact on the reaction efficiency.

The reaction was conducted under reflux at a temperature range of 100–150 °C, depending on the solvent. Thin-layer chromatography (TLC) and gas chromatography-mass spectrometry (GC-MS) were used to monitor the progress of the reaction. After completion, the mixture was cooled, quenched with water, and the product was extracted using ethyl acetate. The crude product was dried over magnesium sulfate and concentrated under reduced pressure.

The resulting product was purified through column chromatography or recrystallization. The structure of the synthesized quinazolin-4-one derivatives was confirmed using nuclear magnetic resonance (NMR) spectroscopy, infrared (IR) spectroscopy, and mass spectrometry (MS).

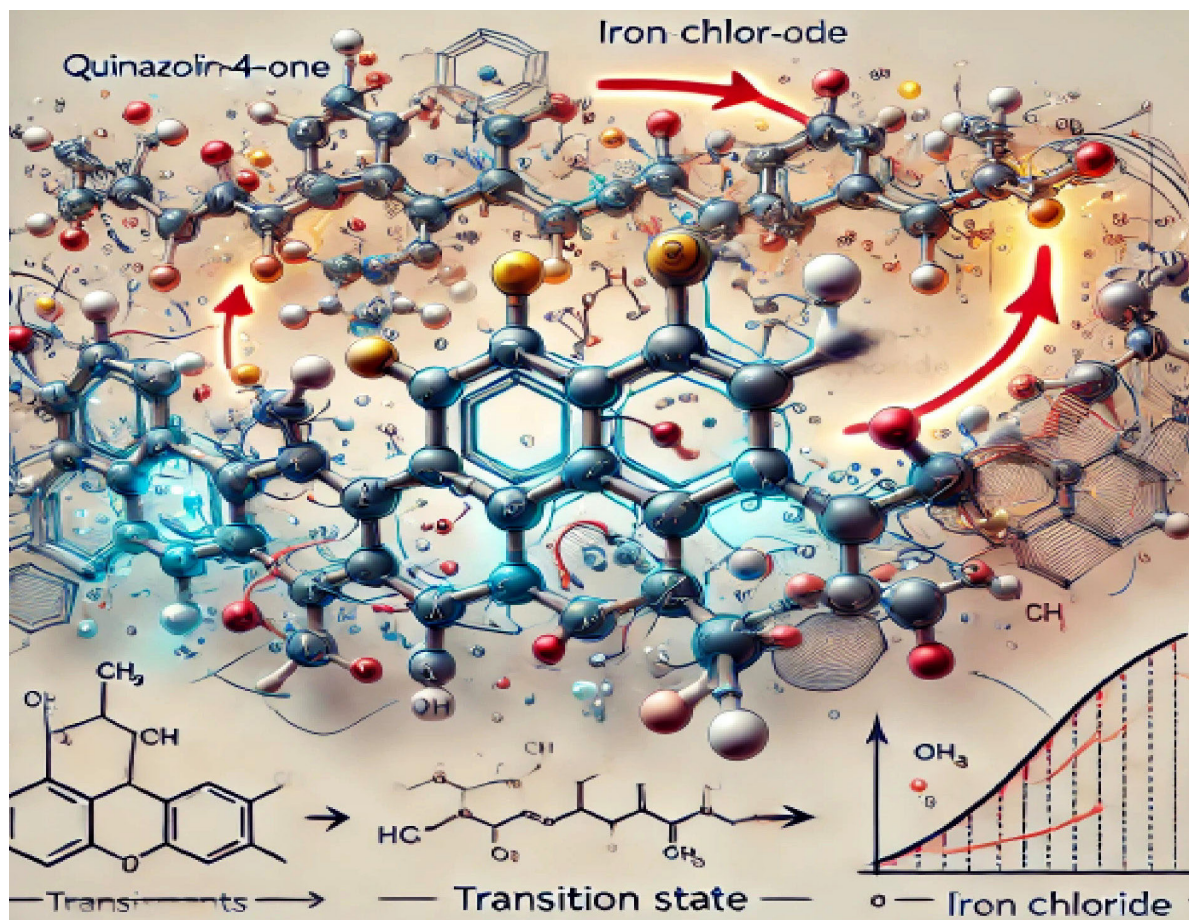
Iron (III) chloride concentrations of 5–10 mol % were found to be optimal, with higher concentrations not significantly improving yield but increasing by-product formation. Lower catalyst concentrations led to slower reaction rates.

Dimethylformamide (DMF) was identified as the most effective solvent, providing the highest yield (85%) of quinazolin-4-one. Ethanol and methanol produced lower yields (60–70%). The optimal reaction temperature was found to be between 120–140 °C, with lower temperatures resulting in slower reactions and higher temperatures leading to side reactions.

Under optimized conditions (5 mol% FeCl_3 , DMF as solvent, 130 °C, and 6-hour reaction time), quinazolin-4-one was obtained with a yield of 85% and high selectivity. Characterization of the product through NMR and IR spectroscopy confirmed the quinazolin-4-one structure, with mass spectrometry verifying the molecular weight of the synthesized compound.

Here is the 3D illustration showing the synthesis reactions of quinazolin-4-one in the presence of iron (III) chloride catalysts, with the key molecular structures and boundaries defined as requested. If you'd like to make any adjustments or need further details (Fig. 1).

Figure 1. The 3D illustration showing the synthesis reactions of quinazolin-4-one in the presence of iron (III) chloride catalysts



Experimental part

In this experiment, **o-aminobenzoic acid** was used as the starting material for the synthesis of quinazolin-4-one in the presence of iron (III) chloride (FeCl_3) as a catalyst.

The key starting material, *o*-aminobenzoic acid (1 mmol), was used without further purification. Other reagents included formamide (1 mmol), iron (III) chloride (FeCl_3), and dimethylformamide (DMF) as the solvent. All chemicals were of analytical grade.

Synthesis Procedure: In a 100 mL round-bottom flask, 1 mmol of *o*-aminobenzoic acid and 1 mmol of formamide were dissolved in 10 mL of DMF. Anhydrous iron (III) chloride (5 mol%) was added to the solution. The reaction mixture was stirred continuously and heated under reflux conditions at 130 °C for 6 hours.

Monitoring the Reaction: The progress of the reaction was monitored by thin-layer chromatography (TLC) at regular intervals. The disappearance of the starting material

and the formation of the product were observed using a suitable solvent system.

Work-Up Procedure: After the reaction was complete, the reaction mixture was cooled to room temperature. Water (20 mL) was added to the mixture to quench the reaction, and the product was extracted with ethyl acetate (3×20 mL). The organic layers were combined, dried over anhydrous magnesium sulfate, filtered, and concentrated under reduced pressure using a rotary evaporator to obtain the crude product.

Purification: The crude quinazolin-4-one product was purified by recrystallization from ethanol or by column chromatography using silica gel and a mixture of hexane and ethyl acetate (1:1) as the eluent.

Characterization: The purified product was characterized using nuclear magnetic resonance (NMR) spectroscopy to confirm the structure. The NMR spectrum showed characteristic peaks corresponding to the quinazoline ring structure. Infrared (IR)

spectroscopy was also performed, confirming the presence of C = O and C = N functional groups. Finally, mass spectrometry (MS) was used to determine the molecular weight of the synthesized quinazolin-4-one.

Yield Determination: The yield of quinazolin-4-one was calculated by comparing the mass of the purified product with the theoretical yield based on the starting materials. Under the optimized reaction conditions (5 mol% FeCl₃, DMF solvent, 130°C, and 6-hour reaction time), quinazolin-4-one was obtained with a high yield of 80–85%. The product was found to be of high purity, as confirmed by NMR, IR, and MS analyses.

This experimental setup demonstrated that o-aminobenzoic acid can be efficient-

ly converted to quinazolin-4-one using iron (III) chloride as a catalyst under mild reaction conditions.

Conclusion

The use of iron (III)-chloride as a catalyst in the synthesis of quinazolin-4-one presents a highly efficient, economical, and environmentally friendly method. The process can be optimized through careful control of reaction parameters such as temperature, solvent, and catalyst loading. This approach holds great promise for large-scale industrial applications and pharmaceutical development, given the bioactivity of quinazolin-4-one derivatives.

References

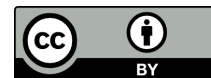
- Saitkulov F. E., Elmuradov B. Zh., Sapaev B. Syntheses and biological activity of quinazolin-4-one hydrochloride // *Austrian Journal of Technical and Natural Sciences*. 2024. — № 1–2. — P. 28–35.
- Сайткулов Ф. Э., Элмурадов Б. Ж., Гиясов К. Алкилирования хиназолин-4-она “мягким” и “жестким” алкилирующими агентами // *Universum: Химия и биология*: — Москва. 2023. — № 1. — С. 53–57.
- Saitkulov, F., Sapaev, B., Nasimov, K., Kurbanova, D., & Tursunova, N. (2023). Structure, aromatic properties and preparation of the quinazolin-4-one molecule. In *E3S Web of Conferences* (Vol. 389, p. 03075). EDP Sciences.
- Murodilayevich, K. M., Shoyimovich, K. G., & Ergashevich, S. F. (2022). Chromato-Mass Methods for Detecting Simple Esters in Chromatography-Mass Spectrometry Method. *International journal of biological engineering and agriculture*, — 1(6). — P. 53–56.
- Sapaev, B., Saitkulov, F. E., Normurodov, O. U., Haydarov, G., & Ergashyev, B. (2023). Studying Complex Compounds of Cobalt (II)-Chloride Geccacrystolohydrate with Acetamide and Making Refractory Fabrics from Them.
- Saitkulov, F., Ibragimov, B. R., Allaqulova, M., Umarov, S., & Xolmatova, M. (2022). The role in the plant and the functions of nutrients. *Инновационные исследования в науке*, — 1(16). — P. 29–31.
- Saitkulov, F., Azimov, I., Ergasheva, M., & Jo'raqulov, H. (2022). Carbohydrates are the main source of energy in the body. *Solution of social problems in management and economy*, — 1(7). — P. 68–71.
- Sapaev, B., Sapaev, I. B., Saitkulov, F. E., Tashniyazov, A. A., & Nazaraliev, D. (2022, June). Synthesis of 2-methylquinazoline-4-thione with the purpose of alkylation of 3-propyl 2-methylquinazoline-4-thione with alkylating agents. In *AIP Conference Proceedings* (Vol. 2432, No. 1). AIP Publishing.
- Sapaev, B., Saitkulov, F. E., Tashniyazov, A. A., & Normurodov, O. U. (2021). Study of methylation reactions of 2-phenylquinazoline-4-tion with “soft” and “hard” methylation agents and determination of its biological activity. In *E3S Web of Conferences* (Vol. 258, p. 04023). EDP Sciences.
- Saitkulov, F., Qilichyeva, N., Abdullayev, B., Anvarov, A., & Ergasheva, M. (2022). Titrimetric analysis of calcium cation in “megaton” variety of cabbage. *International Bulletin of Applied Science and Technology*, 2(10), 134–135.

- Khatamov, K., Saitkulov, F., Ashurov, J., & Shakhidoyatov, K. (2012). 3, 5, 6-Trimethylthieno [2, 3-d] pyrimidin-4 (3H)-one. *Acta Crystallographica Section E: Structure Reports Online*, – 68(9). — o2740-o2740.
- Baymuratova, G., Nasimov, K., & Saitkulov, F. (2023). Synthesis of 6-benzylaminopurine and the study of biological active properties of cotton C-6424 plants. In *E3S Web of Conferences* (Vol. 389, p. 03032). EDP Sciences.

submitted 12.11.2024;
accepted for publication 27.10.2024;
published 29.11.2024
© Oripov O. B., Saitkulov F. E., Mirvaliev Z. Z.
Contact: fsaitkulov@bk.ru



DOI:10.29013/AJT-24-9.10-54-57



INVESTIGATION OF AROMATIC PROPERTIES OF XINAZOLIN-4-ONE

Oripov Oybek Bekboyevich¹, **Saitkulov Foziljon Ergashevich**²,
Mirvaliev Zoid Zoxidovich², **Baymuratova Gulbaxar Orinaevna**²

¹ School № 22, Nurobod District, Samarkand Region, Samarkand, Uzbekistan

² Tashkent State Agrarian Universitet, Tashkent, Uzbekistan

Cite: Oripov O.B., Saitkulov F.E., Mirvaliev Z.Z., Baymuratova G.O. (2024). *Investigation of Aromatic Properties of Xinazolin-4-one. Austrian Journal of Technical and Natural Sciences 2024, No 9–10.* <https://doi.org/10.29013/AJT-24-9.10-54-57>

Abstract

The investigation of the aromatic properties of Xinazolin-4-one aims to comprehend the compound's aromatic nature. Aromaticity is a critical characteristic that impacts the stability and reactivity of organic molecules. This study utilizes computational and experimental methods, including infrared spectroscopy, Raman spectroscopy, and nuclear magnetic resonance (NMR), to assess electron delocalization in the quinazoline ring. The influence of various substituents on the aromaticity of xinazolin-4-one is also investigated. The findings enhance our knowledge of the compound's behavior, helping its use in drug design and material science.

Keywords: *Xinazolin-4-on, Aromaticity, Electron Delocalization, Infrared Spectroscopy, Raman Spectroscopy, NMR, Substituent Effects, Heterocyclic Compounds, Organic Chemistry*

Introduction

Aromaticity is a key concept in organic chemistry that significantly influences the stability, reactivity, and chemical properties of compounds. Aromatic compounds have increased stability compared to non-aromatic compounds due to the delocalization of π -electrons within conjugated ring systems. Heterocyclic compounds, especially, provide a valuable opportunity to examine aromaticity because they contain both carbon and heteroatoms in the ring, resulting in distinctive electronic characteristics. One compound of interest is xinazolin-4-one, which is a heterocycle with nitrogen atoms in its quinazoline

core structure. Xinazolin-4-one and its derivatives have various biological activities, such as antimicrobial, anti-inflammatory, and anticancer properties. The aromaticity of the quinazoline ring in xinazolin-4-one can strongly impact its biological and chemical properties. Detailed studies on the aromatic properties of this compound are limited, despite its importance (Saitkulov F. E., Elmuradov B. Zh., Sapaev B. 2024; Saitkulov F. E., Elmuradov B. Zh., Giyasov K., 2023; Saitkulov, F., Sapaev, B., Nasimov, K., Kurbanova, D., & Tursunova, N., 2023; Murodillayevich, K.M., Shoyimovich, K.G., & Ergashevich, S.F., 2022; Sapayev, B., Saitku-

lov, F.E., Normurodov, O.U., Haydarov, G., & Ergashyev, B., 2023). Understanding the aromatic character of a substance can offer valuable insights into its reactivity and stability. This knowledge is essential for its use in drug development, materials science, and catalysis. This study is focused on examining the aromatic properties of xinazolin-4-one through a combination of experimental and computational methods. Techniques such as infrared spectroscopy (IR), Raman spectroscopy, and nuclear magnetic resonance (NMR) will be used to assess electron delocalization in the molecule. The impact of different substituents on the aromaticity of the core structure will be examined to understand how these changes influence the compound's behavior. This investigation will offer useful information about the chemical properties of xinazolin-4-one, which can be beneficial for its potential use in different scientific and industrial applications (Saitkulov, F., Ibragimov, B.R., Allaqulova, M., Umarov, S., & Xolmatova, M., 2022; Saitkulov, F., Azimov, I., Ergasheva, M., & Jo'raqulov, H., 2022; Sapaev, B., Sapaev, I.B., Saitkulov, F.E., Tashniyazov, A.A., & Nazaraliev, D., June, 2022; Sapaev, B., Saitkulov, F.E., Tashniyazov, A.A., & Normurodov, O.U., 2021; Saitkulov, F., Qilichyeva, N., Abdullayev, B., Anvarov, A., & Ergasheva, M., 2022; Khatamov, K., Saitqulov, F., Ashurov, J., & Shakhidoyatov, K., 2012; Baymuratova, G., Nasimov, K., & Saitkulov, F., 2023).

Method and results

The aromatic properties of xinazolin-4-one were investigated using experimental and computational methods to evaluate electron delocalization and ring stability, which are important indicators of aromaticity. The methods used were:

IR spectroscopy was utilized to analyze the vibrational frequencies of the bonds in the xinazolin-4-one molecule. The distinct C-H stretching modes and their shifts offer insights into the aromatic nature of the compound. Aromatic C-H bending vibrations peaks were analyzed to confirm delocalization patterns.

Raman spectroscopy was used to supplement the IR findings by studying molecular vibrations. The Raman-active modes of

xinazolin-4-one, particularly in the low-frequency range, confirmed the existence of conjugation and electron delocalization within the quinazoline ring. Comparison of the spectra with known aromatic and non-aromatic systems helped to establish aromaticity.

Proton and carbon NMR spectra were recorded to explore the electronic environment of the atoms in the xinazolin-4-one framework. The chemical shifts in the aromatic region (δ 7.0–8.5 ppm for protons) helped assess the level of electron delocalization. Downfield shifts in proton signals indicated an aromatic system's presence. Coupling constants and integration patterns further confirmed the aromatic characteristics.

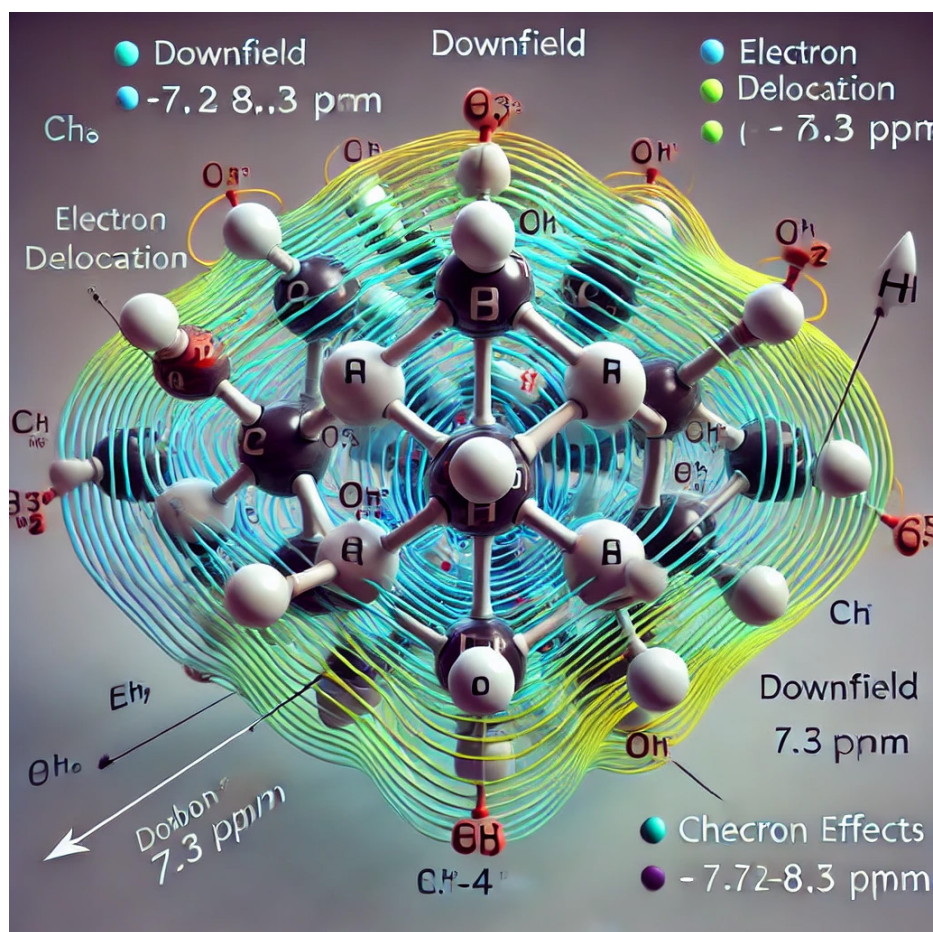
Density Functional Theory (DFT) calculations were utilized to model the distribution of electron density within the xinazolin-4-one ring. The optimized molecular geometry and electron density maps were employed to illustrate the extent of delocalization. Aromatic stabilization energy (ASE) and harm.

The IR spectra displayed characteristic peaks within the range of 3050–3100 cm^{-1} , which correspond to aromatic C-H stretching vibrations. Furthermore, C = N stretching vibrations detected at approximately 1650 cm^{-1} suggest electron delocalization in the heterocyclic ring. Raman spectra showed strong signals between 1000–1600 cm^{-1} , indicating vibrational modes related to aromatic ring systems. The results collectively confirmed the presence of aromatic characteristics in xinazolin-4-one.

Proton NMR analysis showed downfield shifts for the protons attached to the aromatic ring, with chemical shifts observed between δ 7.2–8.3 ppm. The behavior of aromatic compounds involves electron delocalization causing protons to be deshielded. Carbon NMR data also confirmed this finding, showing aromatic carbons with chemical shifts between δ 120–140 ppm. The coupling constants aligned with those commonly observed in aromatic systems, showing substantial π -electron delocalization (Fig. 1).

The 3D visualization showing the protons in the structure of xinazolin-4-one, with their boundaries and chemical shift regions clearly marked. If you need further adjustments or additional details.

Figure 1. The 3D visualization showing the protons in the structure of xinzazolin-4-one



DFT calculations revealed even distribution of electron density across the quinazolin-4-one ring, indicating a significant level of conjugation. The HOMA index was calculated to be 0.85, indicating significant aromaticity. A HOMA value near 1 signifies strong aromatic character. Aromatic stabilization energy (ASE) values confirmed the observed aromaticity, further supporting experimental findings. The electron density maps indicate delocalization in the quinazolinone core of xinzazolin-4-one, revealing aromatic properties akin to other known aromatic heterocycles.

Discussion

The density functional theory (DFT) calculations supported the experimental results by offering a comprehensive view of the electron distribution in the quinazolinone ring. The electron density maps showed substantial π -electron delocalization throughout the ring, indicating the presence of an aromatic system. The calculated Harmonic Oscilla-

tor Model of Aromaticity (HOMA) index, which was approximately 1, quantitatively confirmed the high degree of aromaticity in xinzazolin-4-one. Aromatic stabilization energy (ASE) values confirm resonance stabilization in the molecule, supporting its classification as an aromatic compound. The nitrogen atoms in the heterocyclic ring of xinzazolin-4-one enhance overall aromaticity by aiding in the delocalization of electron density across the ring. This is consistent with observed behavior in other heterocyclic aromatic compounds, in which heteroatoms (such as nitrogen) are crucial for stabilizing the electronic structure.

Conclusion

Both experimental and computational analyses support the assertion that xinzazolin-4-one displays notable aromatic properties. The IR, Raman, and NMR data support the results of computational modeling, confirming electron delocalization within the quinazolinone ring. This aromatic character

is essential for the stability and reactivity of the compound, making it a promising option for future research in pharmaceutical and materials science.

References

- Saitkulov F. E., Elmuradov B. Zh., Sapaev B. Syntheses and biological activity of quinazolin-4-one hydrochloride // *Austrian Journal of Technical and Natural Sciences*. 2024. — № 1–2. — P. 28–35.
- Сайткулов Ф. Э., Элмурадов Б. Ж., Гиясов К. Алкилирования хиназолин-4-она “мягким” и “жестким” алкилирующими агентами // *Universum: Химия и биология*: — Москва. 2023. — № 1. — С. 53–57.
- Saitkulov, F., Sapaev, B., Nasimov, K., Kurbanova, D., & Tursunova, N. (2023). Structure, aromatic properties and preparation of the quinazolin-4-one molecule. In *E3S Web of Conferences* (Vol. 389, p. 03075). EDP Sciences.
- Murodillayevich, K. M., Shoyimovich, K. G., & Ergashevich, S. F. (2022). Chromato-Mass Methods for Detecting Simple Esters in Chromatography-Mass Spectrometry Method. *International journal of biological engineering and agriculture*, — 1(6). — P. 53–56.
- Sapayev, B., Saitkulov, F. E., Normurodov, O. U., Haydarov, G., & Ergashyev, B. (2023). Studying Complex Compounds of Cobalt (II)-Chloride Gecsacrystolohydrate with Acetamide and Making Refractory Fabrics from Them.
- Saitkulov, F., Ibragimov, B. R., Allaqulova, M., Umarov, S., & Xolmatova, M. (2022). The role in the plant and the functions of nutrients. *Инновационные исследования в науке*, — 1(16). — P. 29–31.
- Saitkulov, F., Azimov, I., Ergasheva, M., & Jo'raqulov, H. (2022). Carbohydrates are the main source of energy in the body. *Solution of social problems in management and economy*, — 1(7). — P. 68–71.
- Sapaev, B., Sapaev, I. B., Saitkulov, F. E., Tashniyazov, A. A., & Nazaraliev, D. (2022, June). Synthesis of 2-methylquinazoline-4-thione with the purpose of alkylation of 3-propyl 2-methylquinazoline-4-thione with alkylating agents. In *AIP Conference Proceedings* (Vol. 2432, No. 1). AIP Publishing.
- Sapaev, B., Saitkulov, F. E., Tashniyazov, A. A., & Normurodov, O. U. (2021). Study of methylation reactions of 2-phenylquinazoline-4-tion with “soft” and “hard” methylation agents and determination of its biological activity. In *E3S Web of Conferences* (Vol. 258, p. 04023). EDP Sciences.
- Saitkulov, F., Qilichyeva, N., Abdullayev, B., Anvarov, A., & Ergasheva, M. (2022). Titrimetric analysis of calcium cation in “megaton” variety of cabbage. *International Bulletin of Applied Science and Technology*, 2(10), 134–135.
- Khatamov, K., Saitqulov, F., Ashurov, J., & Shakhidoyatov, K. (2012). 3, 5, 6-Trimethylthieno [2, 3-d] pyrimidin-4 (3H)-one. *Acta Crystallographica Section E: Structure Reports Online*, — 68(9). — o2740-o2740.
- Baymuratova, G., Nasimov, K., & Saitkulov, F. (2023). Synthesis of 6-benzylaminopurine and the study of biological active properties of cotton C-6424 plants. In *E3S Web of Conferences* (Vol. 389, p. 03032). EDP Sciences.

submitted 12.11.2024;

accepted for publication 27.10.2024;

published 28.11.2024

© Oripov O. B., Saitkulov F. E., Mirvaliev Z. Z., Baymuratova G. O.

Contact: fsaitkulov@bk.ru



Section 2. Earth sciences

DOI:10.29013/AJT-24-9.10-58-82



THEORY OF THE EXPANDING EARTH ON THE SOLUTION TO THE PROBLEM OF ENERGY AND MATTER SOURCES

*Murad Zinaliyev*¹

¹ SAS Mecalac-France, France

Cite: Zinaliyev M. (2024). *Theory of The Expanding Earth on the Solution to the Problem of Energy and Matter Sources. Austrian Journal of Technical and Natural Sciences 2024, No 9–10.* <https://doi.org/10.29013/AJT-24-9.10-58-82>

Abstract

Mathematical models and estimates of the Earth's size and mass, intended to discredit the theory of a planet growing in both diameter and mass, prove untenable when faced with geological experimental data. However, the main reason why the theory of plate tectonics continues to dominate in geology is the challenge of identifying a mechanism that would enable planetary growth.

The idea of the existence of an ether, the flow of which is pushing matter toward the planet's center, while aimed at addressing the generation of matter and energy at the Earth's core, falls short in several respects. It fails to answer simple questions such as, 'What force attracts ether to the center of celestial bodies?', 'Where is the source of ether?', 'Why has the ether flow not been exhausted after 14 billion years of the Universe's existence?', 'What is the mechanism of ether transformation into baryonic matter with energy release?', 'What energy source sustains the continuous excited state of ether particles?', 'What constitutes ether matter in its unexcited state?' Furthermore, this concept lacks experimental support, as demonstrated by direct measurements of space 'graininess' (quantization) (ESA, 2011).

Proponents of the idea that a fragment of a neutron star exists at the Earth's core should understand that a neutron star is a hypothetical object, which exists in astrophysicists' imagination due to a mathematical model that corresponds to the properties of certain celestial bodies. According to this same model, a separate fragment of neutron matter is unstable, disintegrating explosively within 10 minutes of separation from the main mass.

Nevertheless, the principle of conservation of matter and energy, while experimentally validated through the laws of conservation of energy, momentum, angular momentum, electric charge, etc., is not absolute. This circumstance, combined with astrophysical observational data, points to the existence of sources of energy and matter within the interiors of celestial bodies that are unknown to current science.

Keywords: *plate tectonics, expanding Earth theory, cosmic matter accretion, primordial*

hydride Earth theory, paleontological paradox, internal activity of celestial bodies, Earth's magnetic field, vacuum energy, variation in gravitational field intensity, gravitational-meteorological paradox

Myth or Reality?

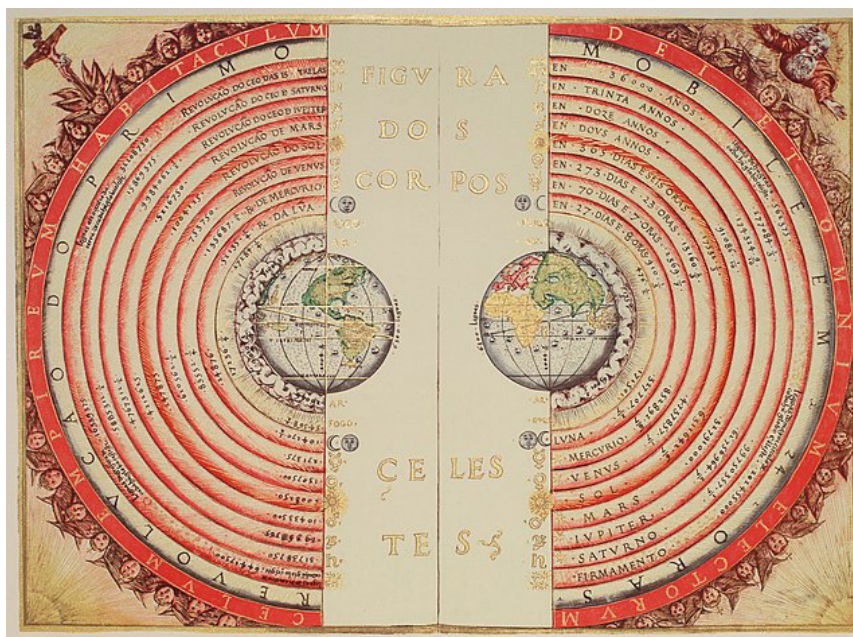
Science and Established Truths

Remarkable scientific discoveries over the past two decades have changed scientists' understanding of the Earth's interior. However, due to the inherent conservatism of science, it takes decades for new experimental data to reach a broad audience.

In ancient times, practical knowledge based on everyday activities was highly valued. For example, sailors knew from experience

about the convex shape of the water's surface and the change in the position of the Pole Star as they moved from south to north. The hypothesis of a spherical planet was able to explain the round shadow of the Earth on the Moon's surface. As a result, Eratosthenes (4th century BCE) was able to calculate the diameter and surface area of our planet by conducting an experiment to determine the proportions of the shadow cast by objects at noon at different latitudes.

Figure 1. Illustration of celestial bodies in the geocentric system. A colored illustration of the Ptolemaic geocentric concept of the universe, presented by Portuguese cosmographer and cartographer Bartolomeu Velho in his work *Cosmography*, published in France in 1568 (National Library of France, Paris). Note the distances of the celestial bodies from the Earth's center (left) and the revolution periods in years (right). The outermost text reads: "The Celestial Empire, the abode of God and all the chosen"



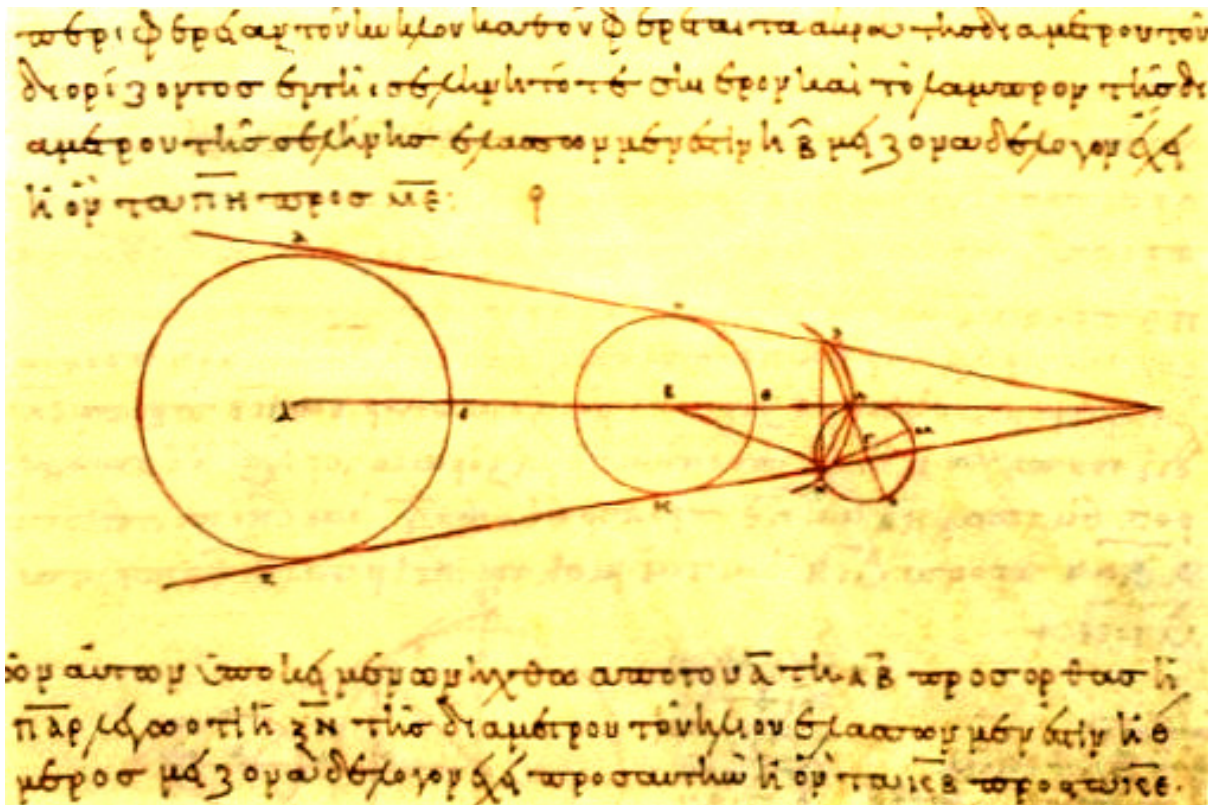
Source: Wikipedia

Other knowledge, such as the rotation of planets around the Sun, was obtained by the philosopher Aristarchus of Samos through mathematical calculations as early as the 3rd century BCE, but was far removed from the everyday world and had no practical application (Veselovsky, I.N., 1961).

Aristarchus was an authoritative astronomer of his time, living and working in Alexandria. One of his works, *On the Sizes and*

Distances of the Sun and Moon, was later included in the collection *Minor Astronomers*. Those who wished to devote themselves to astronomy had to study it after completing Euclid's geometry course but before starting Ptolemy's *Almagest*. However, Aristarchus himself was accused of blasphemy during a period of increased religious persecution and was expelled from Alexandria (Veselovsky, I.N., 1961).

Figure 2. Illustrations from Aristarchus of Samos's book on the Sizes and Distances of the Sun and Moon. ΓΑ Greek copy from the 10th century CE (Vat. gr. 204 fol. 116 recto math 06 NS. 02)



Source: Wikipedia

If we assume that the Earth revolves around the Sun, its trajectory, which is almost circular, has a radius of more than 23,000 Earth radii, i.e., more than 150 million kilometers. Thus, the Earth moves 300 million kilometers over six months in relation to the Sun – a gigantic distance! However, the starry sky appears the same to an observer on Earth. The Earth moves closer to and farther from the stars by 300 million kilometers, but neither the apparent distances between the stars (e.g., the shape of constellations) nor their brightness changes. This means that the distances to the stars must be thousands of times greater, implying that the celestial sphere must have unimaginably large dimensions! (Protasov, V. Yu., 2010).

Aristarchus himself realized this, writing in his book: “The volume of the sphere of fixed stars is as many times larger than the volume of the sphere with the radius Earth-Sun as the volume of the latter is larger than the volume of the Earth,” meaning that, ac-

ording to Aristarchus, the distance to the stars was $(23.455)^2$ times greater than R , or over 3.5 trillion kilometers. In reality, the distance from the Sun to the nearest star is about 11 times greater. Instead of a compact and cozy world centered on the Earth and enclosed within a relatively small celestial sphere, Aristarchus painted an abyss. And this abyss terrified everyone (Protasov, V. Yu., 2010).

Simple ideas are easier to understand and are preserved for millennia. One such idea is that Aristarchus of Samos's teachings are absurd since there is practically no room for the celestial sphere. Where, then, do the souls of people go after death?

The crystalline sphere still appears in Nicolaus Copernicus's book *On the Revolutions of the Celestial Spheres* 1.700 years after Aristarchus. In his heliocentric system, the planets were still compactly arranged and moved in circular orbits, introducing even greater errors in calculations than the geocentric system.

Figure 3. The celestial spheres in Nicolaus Copernicus’s manuscript: 1) Stationary sphere of fixed stars; 2) Saturn. 30-year revolution; 3) Jupiter. 12-year revolution; 4) Mars. 2-year revolution; 5) Earth. Annual revolution with the Moon in orbit; 6) Venus. 9-month revolution; 7) Mercury. 80-day revolution; 8) The Sun is at the center of the system



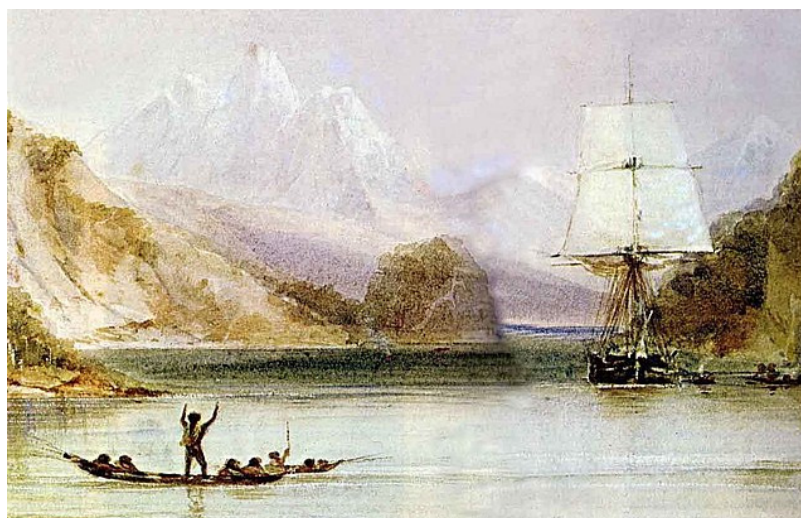
Source: Wikipedia

Continental Drift or Expanding Earth?

The Expanding Earth hypothesis, which Charles Darwin arrived at in the 1830s while studying the coast of South America, and the

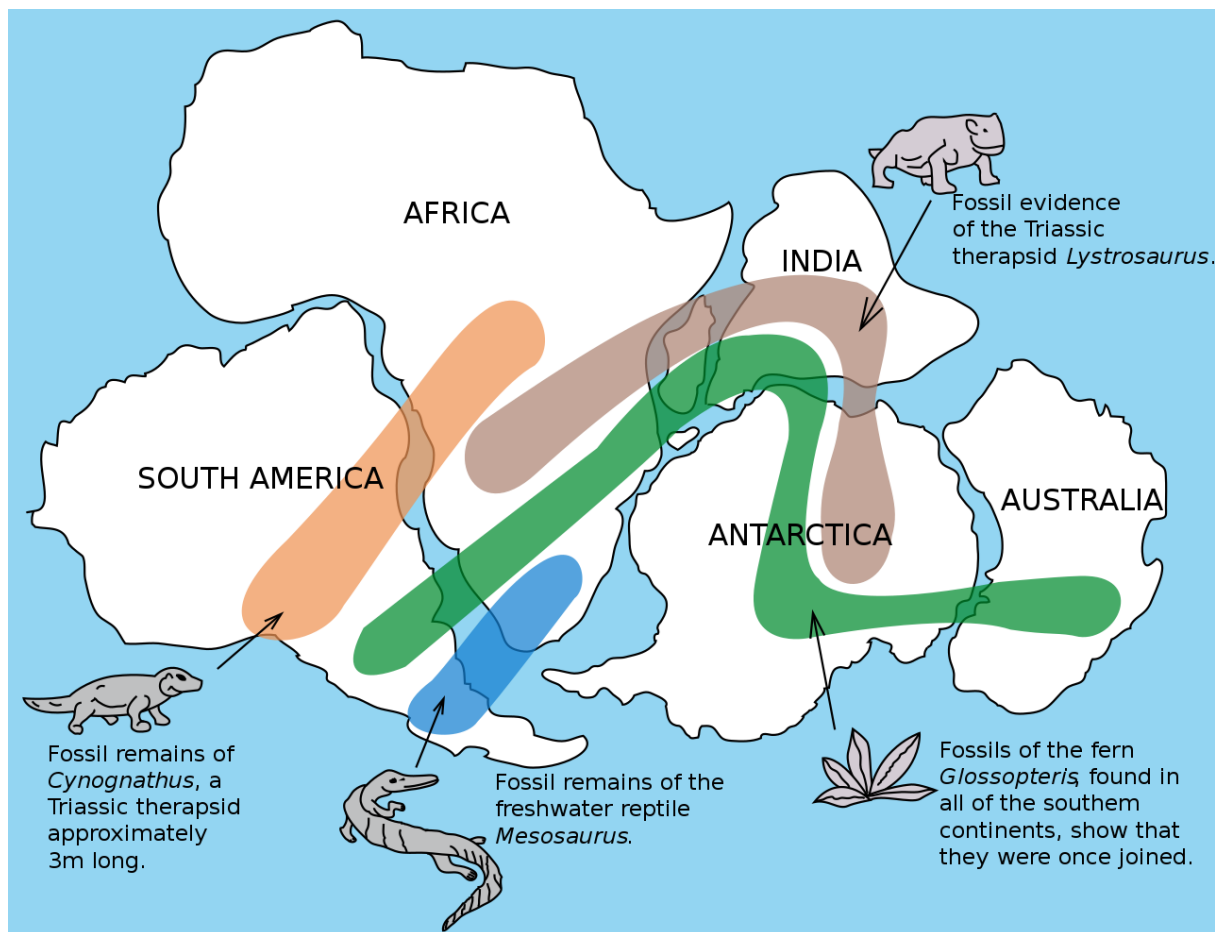
Continental Drift hypothesis, formulated and proposed in 1912 by Alfred Wegener, both fell outside the dominant scientific worldview of their times.

Figure 4. The HMS Beagle surveys the coast of South America. While on this expedition, Darwin proposed the theory of an expanding Earth and the extinction of less evolved life forms. A watercolor by ship’s artist Conrad Martens in Tierra del Fuego



Source: Wikipedia

Figure 5. The location of certain fossil plants and animals on present-day continents, far apart from each other, would form specific patterns (shown by colored bands) if the continents were rejoined



Source: United States Geological Survey (USGS)

Both hypotheses were based on the striking similarity of coastlines and geological data, including identical structures and compositions of sedimentary rocks, and the presence of flora and fauna from the geological past on opposite continents, now separated by vast ocean distances.

Plate Tectonics

Initially, the primary obstacle to the acceptance of these hypotheses was the lack of an explanation for the source of energy and matter needed to implement these grand planetary processes.

However, the discovery of mid-ocean ridges and strip-like magnetic anomalies on the ocean floor (indicating irregular reversals of Earth's magnetic field) elevated the hypothesis of continental drift to a widely accepted theory. This new science became known as the theory of plate tectonics.

However, several unresolved issues with this theory persist for example:

At the same time, there are a number of unresolved problems of this theory, such as:

1) To explain the universal similarity in the structure and composition of sedimentary rocks, as well as the similarity of flora and fauna from past geological eras along the edges of opposite continents, one must assume that in the Earth's geological past, there was a recurring process of disassembly and reassembly of supercontinents in different regions of the globe, opening and closing entire oceans (Blinov, V.F., 2010; Carey, S.W., 1991).

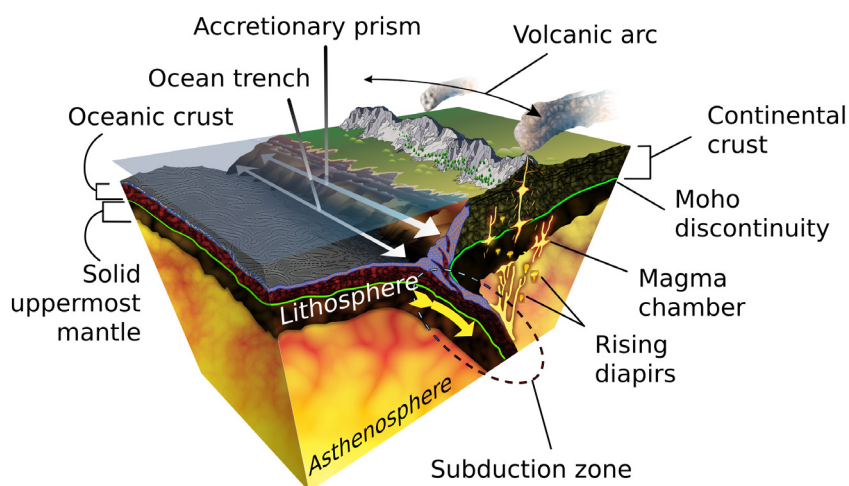
2) Processes of cracking in oceanic and continental plates are observed on the Earth's crust's surface and have been well-studied, as have the measured rates of Earth's surface expansion due to spreading, (Blinov, V.F., 2010; Carey, S.W., 1991);

Figure 6. Formation of continents within the framework of plate tectonics. As the supercontinent Gondwana broke apart (approximately 175 million years ago), modern continents emerged. However, to explain, for example, the unified range of titanosaurs across present-day China and Argentina, the reassembly of another supercontinent on the opposite side of the globe would be required



Source: Wikipedia

Figure 7. Outdated conceptions of a subduction zone. Studies have shown that the accretionary prism of a continental slope is actually composed of island arc or continental deposits, rather than sedimentary and hard oceanic rocks as suggested by the subduction hypothesis. Additionally, the higher density of the asthenosphere material should push the less dense solid oceanic crust to the surface, preventing it from sinking into the Earth's mantle



Source: Wikipedia

3) The expansion of the ocean floor over the past 250 million years has accelerated. (Blinov, V.F., 2010);

4) There is no empirical confirmation of the existence of the subduction process – where oceanic lithospheric plates submerge beneath continental plates – because:

- the mantle has a layered structure (Pushcharovsky, Yu.M., Pushcharovsky, D.Yu., 2010), a property indicating the absence of mantle material circulation and the absence of a mechanism capable of driving the drift of lithospheric plates;

- the density of the mantle is higher than that of the oceanic crust, and thus the idea of subduction contradicts the physical phenomenon known as “Archimedes’ principle” (Blinov, V.F., 2003; Koronovsky, N.V., 2001; Burundukov, A.S., Drozdov, A.L.);
- drilling of continental slopes near trenches revealed that they are composed of series of island arc or continental deposits, whereas subduction zones (where oceanic crust is supposedly sinking under continental crust) should contain accretionary prisms formed by the scraping off of soft sedi-

ments and irregularities in hard rocks that inevitably occur when one plate slides beneath another (Blinov, V.F., 2003; Koronovsky, N.V., 2001; Burundukov, A.S., Drozdov, A.L., 2015);

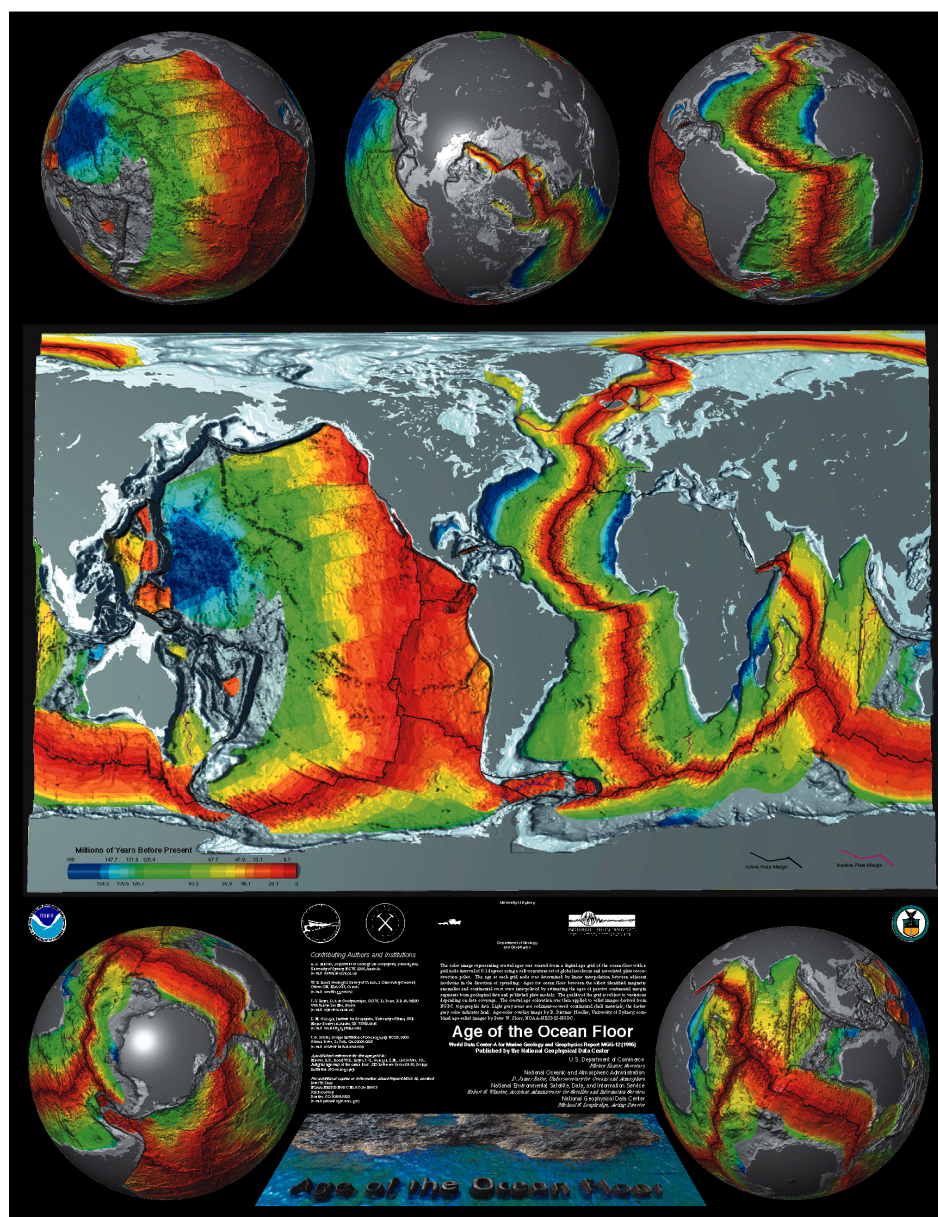
- there is a lack of experimental data regarding subduction rates, such as the speed at which the distance between the shoreline and nearby islands in the ocean decreases. (Blinov, V.F., 2003; Koronovsky, N.V., 2001; Burundukov, A.S., Drozdov, A.L., 2015).

5) There is a multitude of other experimental data that refutes the hypothesis of the existence of subduction zones.

Expanding Earth Theory

There are several works by geologists and biologists who have proposed various hypotheses to explain the mechanism behind the increase in the Earth's volume (Blinov, V.F., 2003; Burundukov, A.S., Drozdov, A.L., 2015; Carey, S.W., 1991; Larin, V.N., 2005).

Figure 8. Deep ocean ridges on the globe and the age of the bedrock of the oceanic crust. Red indicates the youngest seafloor sections. Older ones are shown in yellow and green. The oldest are marked in blue



Source: NOAA

The answer lies in an interdisciplinary area of knowledge, leading to a shift in the scientific paradigm, which not only affects our understanding of the processes occurring within our planet but also necessitates the revision of some fundamental scientific concepts.

To properly address the issue, let us consider two possible scenarios for the Earth's size increase:

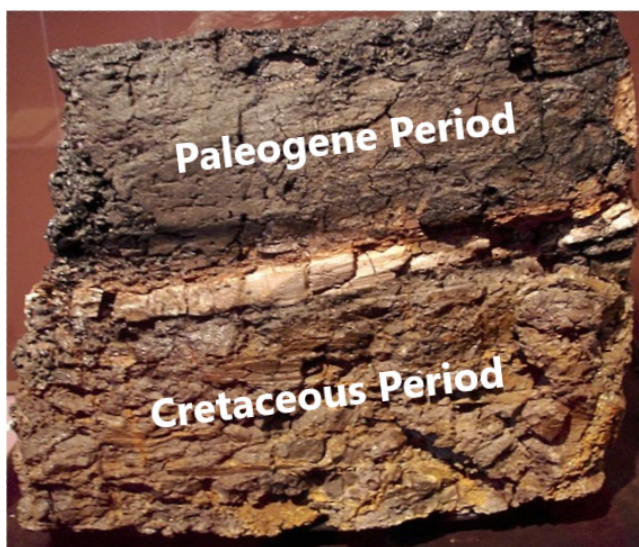
1) accretion of material from space, (Burundukov, A.S., Drozdov, A.L., 2015);

2) expansion of the Earth's metal hydride core due to the emission of dissolved hydrogen (Larin, V.N., 2005).

Accretion of Material from Space

The accretion of material from space suggests that cosmic material settling on the Earth's surface from space could be a mechanism capable of increasing the planet's volume along with its mass.

Figure 9. A fragment of a sedimentary rock section, showing a thin light layer of argillite (containing 1.000 times more iridium than the upper and lower layers). The sharp increase in iridium concentration in this layer indicates a sudden increase in the amount of cosmic material within it. Many overlook that Cretaceous deposits continue just above the iridium anomaly



Source: Wikipedia

Cosmic material falling onto the planet's surface consists of water-insoluble solid dust particles and meteorites:

1) cometary dust: a mixture of crystalline and amorphous silicates, refractory organic materials, and a small amount of oxides;

2) meteorites and asteroid dust: various rocks (mainly chondrites), minerals, and metals;

3) interstellar dust: composed of larger refractory minerals that condensed from matter left after star formation.

Today, about 100 tons of cosmic dust and meteorites fall on our planet daily. (Zook, H.A., 2001) But if this amount is multiplied by 365 days, and then by the entire existence of our planet (4.5 billion years), the total amount of fallen material would account for

an insignificant fraction of 1% of its current mass.

According to supporters of the expanding Earth theory, the acceleration due to gravity on the planet's surface has doubled (Burundukov, A.S., Drozdov, A.L., 2015) over the past 150 million years, implying an increase in the Earth's radius by 1,950 km, requiring an average sediment accumulation rate of about 13 mm/year (including today). For comparison, the soil formation process (which does not increase the Earth's mass) is roughly 10,000 times slower than the rate required for the hypothetical cosmic sediment accumulation (Gennadiev, A.N., Gerasimova, M.I., Patsukevich, Z.V., 1987).

If cosmic material accretion had been intense, the entire surface of our planet would primarily consist of cosmic material, with all

the resulting consequences for the biosphere (plant and animal life).

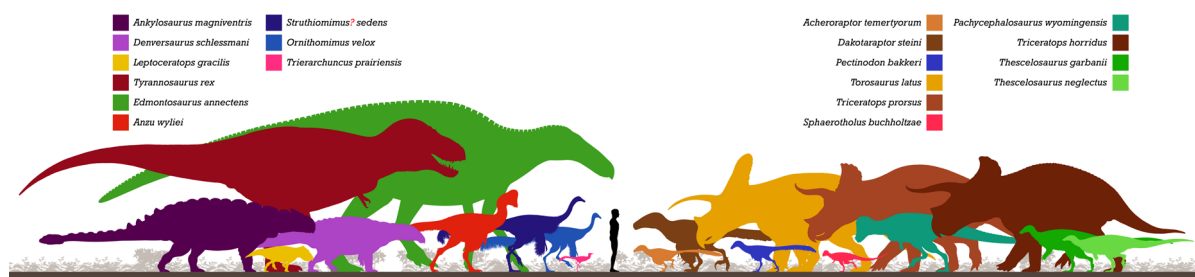
Some researchers explain the absence of cosmic material traces in the sediments on continental surfaces and ocean floors by processes of weathering, erosion, chemical, and mechanical impacts followed by washing this material into the oceans and absorption into the Earth's interior at subduction zones.

If we assume that, alongside the abundant deposition of cosmic dust on Earth, there were atmospheric precipitation and various natural impacts, why did these factors selectively fragment and wash away only cosmic dust and meteorites but did not affect

the iridium layer, soil, or fragments of Earth's rocks?

For example, the Hell Creek Formation's sedimentary rocks formed over 1.3 million years between the late Cretaceous and early Paleocene (Maastrichtian epoch). The most recent deposits are estimated to be 66.043 million years old. The formation is primarily known for the large number of dinosaur fossils found there. Its depth is about 2.5 km (not the expected 858 km according to the cosmic accretion hypothesis). Naturally, these sedimentary rocks are not composed of cosmic dust and meteorites. (Lamanna, M.C. et al., 2014; Husson, D., et al., 2011).

Figure 10. *Hell Creek Fauna*



Source: Wikipedia

Considering these facts, it is easy to conclude that the hypothesis of cosmic material deposition on Earth's surface cannot explain the increase in the planet's size and mass.

Expansion of the Earth's Metal Hydride Core

This theory was born from the discovery by geologist, Doctor of Geological and Mineralogical Sciences Vladimir Nikolaevich Larin of the effect of melting at room temperatures, as well as the expansion of metal hydrides during hydrogen release. (Larin, V.N., 2005)

However, applying this effect as a cause for the planet's size increase encounters several unresolved contradictions with paleontological data. The well-known Tyrannosaurus rex (T. rex) is well-studied, as initially incomplete and then complete skeletons were found.

The well-known Tyrannosaurus rex (T. rex) is well-studied because initially, several incomplete skeletons were discovered, followed later by the discovery of complete skeletons.

The weight of T. rex, according to various estimates, ranges from 7.8 to 9.9 tons (Erickson, G.M., et al., 2004; Farlow, J.O. et al, 1995; Seebacher, F., 2001; Farlow, J.O. et al., 1995), exceeding the average weight of Indian elephants, which is between 3 and 5 tons (Shoshani, J.; Eisenberg, J. F., 1982; Pillai, N.G., 1941; Furaha ten Velde, P., 1997).

Why is the comparison made with Indian elephants and not with the larger African elephants? Indian elephants are smaller than African elephants and, therefore, have practical value: they can carry or push-pull additional loads.

However, even Indian elephants, moving on four legs, cannot run or jump (and even sleep standing, although they can lie down and wallow in mud, sand, or water, then get up)(Hutchinson, J. R. at al., 2006). T. rex, on the other hand, hunted, moving on two hind legs, ran, and was fast enough to catch its prey (Hone, D., 2017; Sellers, W.I., and Manning, P.L., 2007; Hutchinson, J. R, Garcia M., 2002; Hutchinson, J. R., 2004).

Figure 11. *Reconstruction of Tyrannosaurus (CM 9380)
at the Carnegie Museum of Natural History*



Source: Wikipedia

The methods that successfully calculate the weight of modern megafauna based on the thickness of their supporting bones under current gravitational conditions, when applied to T. rex (Anderson, J.F., Hall-Martin A., Russell D.A., 1985), predict approximately half the mass compared to what is determined by volumetric models (McNeill, A.R., 1985). This suggests that the leg bones of T. rex would have fractured under its own weight in today's gravitational force on Earth.

There is also a geophysical reason for the inconsistency of Larin's theory.

It is generally accepted that the Earth's core is metallic, which, in turn, is the source of the Earth's magnetic field. To justify his theory, Larin only needed to replace the iron-nickel core concept with the idea of a metal hydride core and prove that hydrogen is continuously and ubiquitously emitted from the Earth's interior to the surface and atmosphere.

V. N. Larin's doctrine of the originally hydride Earth is a theory, not a hypothesis, as it is a structured and substantiated system of views, judgments, and propositions that adequately explains facts, analyzes processes, predicts, and regulates their development, and has experimental confirmation:

1) the volume of material indeed increases during hydrogen emission from the crystal lattice of metal hydrides;

2) gas emissions (hydrogen, carbon dioxide, hydrogen sulfide, methane, etc.) and water from the Earth's interior to the surface are observed;

3) the possibility of synthesizing inorganic hydrocarbons in the Earth's crust is confirmed (Deep Carbon Observatory, 2019; Kutcherov, V.G., 2013).

Meanwhile, the generally accepted concept of an iron-nickel core arose from the understanding that the density of surface-accessible rocks on Earth is insufficient to justify existing gravity and that the metallic core could serve as the generator of our planet's magnetic field.

However, the impressive edifice of the dominant worldview collapses like a house of cards upon careful analysis of geophysical research results from the past two decades.

This issue is further explored in sections 3.7 "The Geometry of Earth's Magnetic Field Lines," 3.8 "The Non-Dipole Nature of Earth's Magnetic Field," 3.9 "The Geoid", and 3.10 "Variation in the Earth's Gravitational Field Intensity."

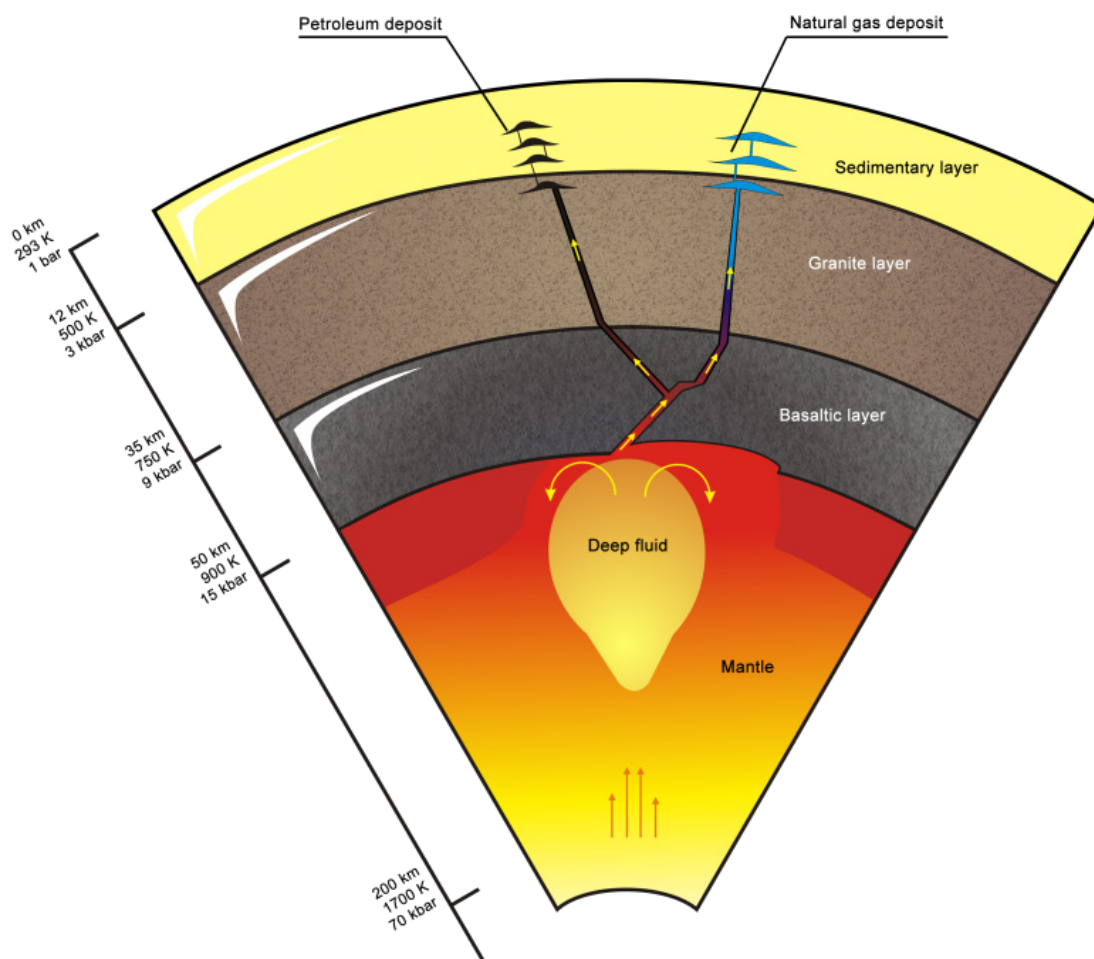
In this article, we will not discuss other hypotheses proposed to explain the mechanism of the Earth's size increase, as they either fall outside the scope of the scientific method or contradict experimental data.

As we can see, the fundamental truth regarding the expanding Earth theory is the

following statement: “The expanding Earth theory is absurd, as its hypothetical implementation violates the principle of conser-

vation of matter and energy. This theory belongs to the realm of magical arts!”

Figure 12. *The scheme of hydrocarbon genesis and oil field formation*



Source: V.G. Kucherov

A New Paradigm

Vacuum Energy as a Source of Matter-Energy in the Earth's Core

The results of research within the framework of the Standard Model of elementary particles and quantum field theory are gradually bringing fundamental science out of a crisis that has lasted for a century. The problem lies in the disregard for the violation of the conservation of matter-energy when evaluating quantum mechanical processes.

Experimental data indicate the reality of an enormous vacuum energy density (Weinberg, S., 1989), which, for unknown reasons, does not interact with material bodies within the space of the Universe. However, quantum mechanical tunneling effects allow this

energy to penetrate into the Universe in the form of weak thermal radiation (mistakenly called relic radiation) as well as through the spontaneous emission of electron-positron pairs by the vacuum (CERN, 2013).

These newly discovered realities are key to solving the issues of fulfilling the conservation of matter-energy principle at the microscopic level and the problem of generating matter-energy at the center of our planet.

Quantum Field Theory

It is not widely known that the idea of creating quantum field theory was debunked more than ten years ago (ESA, 2011; Smolin, L.; 2006, Susskind, L.; 2015, Zinaliev, M., 2017). Grand theoretical and experi-

mental research spanning about fifty years concluded:

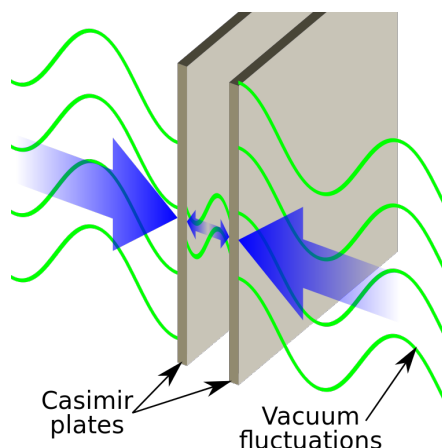
1) with the realization that the fundamental principles of quantum field theory are flawed, leading to various insurmountable theoretical contradictions and depriving numerical simulations of certainty;

2) that the hypothesis of the possibility of quantizing the space of the Universe

was experimentally disproven in 2011 during a cosmic mission aimed at detecting the “graininess” (degree of quantization) of space, revealing that space granularity does not manifest down to a scale of 10–48 meters, which is 10¹⁴ times smaller than the Planck length. (ESA, 2011; Smolin, L., 2006; Susskind, L., 2015; Zinaliev, M., 2017).

Figure 13. Casimir forces on parallel grounded neutral metal plates.

Vacuum energy contains contributions from all wavelengths except those excluded by the distance between the plates. As the plates move closer, more wavelengths are excluded, and vacuum energy decreases. A decrease in energy means a force must act on the plates, doing work as they move closer together



Source: Wikipedia

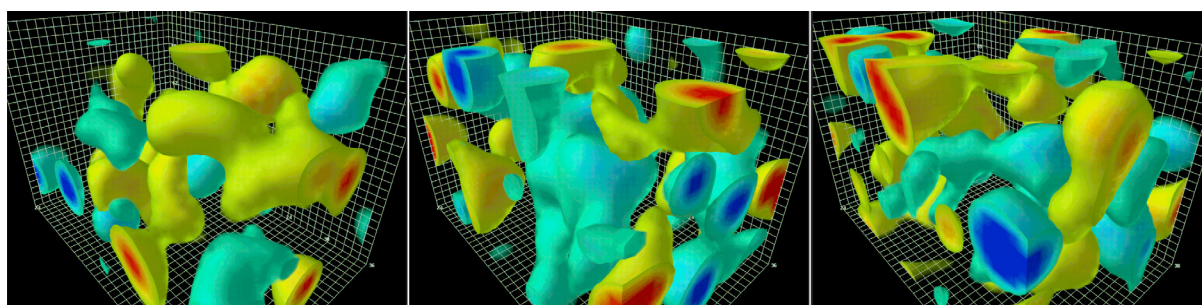
At the same time, quantum mechanical phenomena such as spontaneous emission, the Casimir effect, the Lamb shift, and vacuum polarization (spontaneous generation and annihilation of electron-positron pairs in a vacuum) point to the reality that the vacuum energy density is about 120 orders of magnitude higher than the vacuum energy measured using macroscopic instruments. (Weinberg, S., 1989)

This colossal energy density is comparable to the energy density of the Big Bang singularity.

Quantum Mechanics

It is known that all elementary particles are perpetual motion machines of the first kind (drawing energy from nowhere) – they are in a continuous process of energy fluctuation (Ponomarev, L.I., 1989).

Figure 14. Illustration of the typical four-dimensional structure of gluon field fluctuations



Source: Wikipedia

In 1913, Niels Bohr became the founder of quantum mechanics by formulating the first laws of this new science.

The first postulate – about stationary states: “In an atom, there are orbits where the electron does not emit energy while revolving (this assertion contradicts the behavior of electrically charged particles in conductors)” (Ponomarev, L. I., 1989).

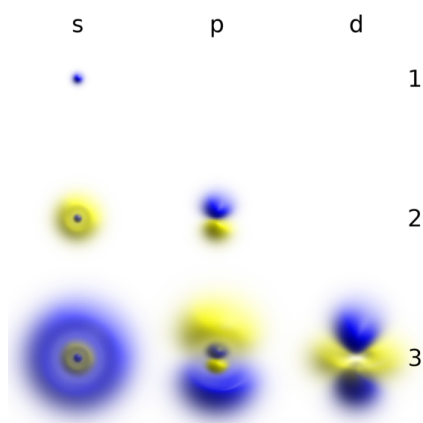
The second postulate – about quantum jumps: “Radiation occurs only when an electron jumps from one stationary orbit to another” (Ponomarev, L. I., 1989).

Modern formulations of these laws consist exclusively of quantum mechanical terms, and the idea of electron rotation has been replaced by a description of the mathematical probability of its location at a certain point in space (quantum fluctuations). However, the essence of these laws has not changed since Niels Bohr’s time (Ponomarev, L. I., 1989).

It is essential to understand that the magnetic field is generated both by the electron and by the atom, whose magnetic properties are determined by the magnetic moments of the electrons within them (Ponomarev, L. I., 1989).

If anyone doubts that a magnetic field exerts force, recommend that they repeatedly open and close the door of a cabinet with a latch using a permanent magnet, which requires no energy input, and then recall the existence of industrial magnets capable of lifting hundreds of kilograms of iron objects, albeit with the expenditure of electrical energy.

Figure 15. Electron atomic orbitals at different energy levels. The more opaque areas are where the electron is most likely to be found at any given moment



Source: Wikipedia

Now, if we know that a certain system generates a force field, what is the source of the energy that produces it?

The answer to this question is forbidden by the informal humorous principle of quantum mechanics: “Shut up and calculate!” (Smolin, L., 2006; Susskind, L., 2015). By default, the violation of the conservation of energy principle is enshrined in the first law of quantum physics.

Dark Energy and Dark Matter

How are the concepts of dark energy and dark matter related to the principle of conservation of matter-energy?

In essence, when researchers encounter the influx of energy from nowhere (a perpetual motion machine of the first kind) on a cosmic scale, particularly with the accelerated expansion of the Universe, they refer to this phenomenon as “dark energy” (Verkhovanov, O. V., 2020).

If a natural phenomenon associated with excess gravity is discovered, along with the amount of matter necessary for this being absent, then the solution to this kind of problem is the presence of dark matter (Verkhovanov, O. V., 2020).

In the last two decades, dark matter has been attributed with yet another ability – to decay into electron-positron pairs (vacuum polarization) (CERN, 2013).

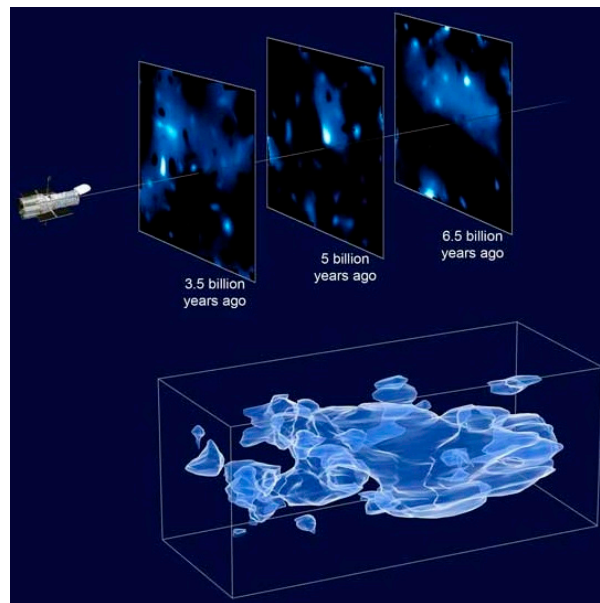
Attempts to detect elementary particles of dark matter, as predicted by some theorists, have been unsuccessful (Verkhovanov, O. V., 2020). Therefore, it is unclear what scheme or components this “something” decays into, leading to the observed real physical phenomenon of vacuum polarization.

In modern science, a contradictory situation has arisen where the hypotheses of dark energy and dark matter, on the one hand, emerge from astrophysical observations, and on the other hand, the astrophysical observations themselves serve as proof of the reality of these two entities!

However, using conclusions as evidence for a hypothesis is a logical error. This error is known as “affirming the consequent”.

All of these accumulating facts illustrate how the principle of energy conservation is violated at the level of the large-scale structure of the universe.

Figure 16. *Dark matter map from 2007, compiled by the Cosmic Evolution Survey using the Hubble telescope*



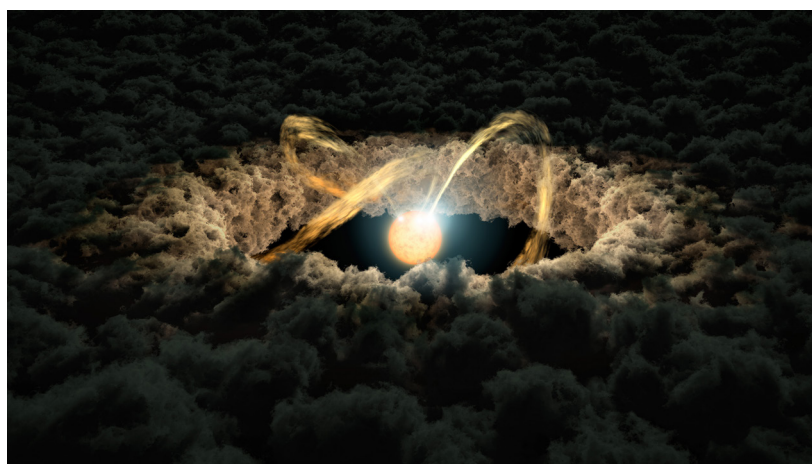
Source: NASA

The Problem of Celestial Body Formation from Gas-Dust Clouds

It is generally accepted that the process of the formation of celestial bodies in the solar system occurred through the formation of an accretion disk, the collapse of the protostellar

nebula into a central star, and the formation of planetesimals. A planetesimal is a celestial body orbiting a protostar, formed by the gradual accumulation of smaller bodies composed of particles from the protoplanetary disk.

Figure 17. *Artist's depiction of a protoplanetary disk*



Source: NASA/JPL–Caltech

Numerical modeling has shown that both the initiation of accretion disk formation and the birth of planetesimals require a seed in the form of a celestial body (Verkhovanyov, O. V., 2020).

The asteroid belt and the Oort cloud have existed for about 4 billion years, and yet, for some reason, the numerous celestial bodies have not coalesced into a single object.

The absurdity of the situation is obvious: for the Sun and planets to form, an accretion process is necessary, involving a protoplanetary disk and planetesimals, but to initiate this process, small planets are required.

Theorists have slipped out of this situation with a serious face: the dominant viewpoint now is that dark matter serves as the seed for the protosun and planets of the solar system! (Verkhovanov, O. V., 2020).

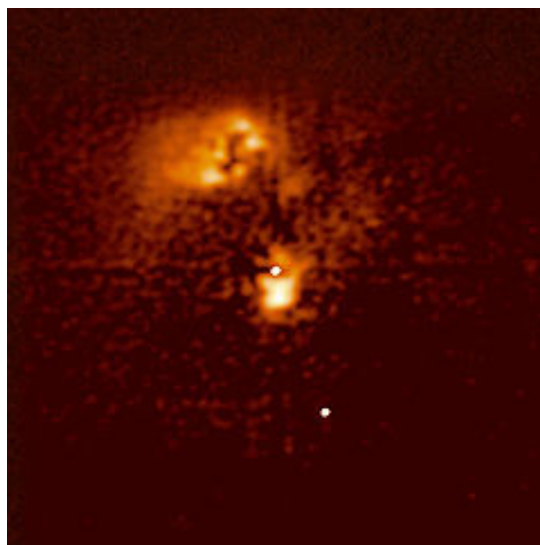
Quasars

In the distant cosmos, there are various exotic celestial bodies. Among them, quasars hold a special place as a class of astronomical objects that are among the brightest (in absolute terms) in the visible Universe (Wikipedia, 2024).

It is commonly accepted that quasars represent the active nuclei of galaxies in their early stages of development, where a supermassive black hole absorbs surrounding matter, forming an accretion disk. A quasar is a source of extremely powerful radiation (sometimes tens or hundreds of times greater than the combined power of all the stars in galaxies like ours) and exhibits, in addition to the cosmological redshift, a gravitational redshift predicted by A. Einstein in the general theory of relativity (Wikipedia, 2024).

The official explanation of the nature of quasars is nullified by the unusual object HE0450–2958. This object is called a “naked quasar” or “homeless quasar” because no host galaxy has been detected (Wikipedia, 2024).

Figure 18. *Quasar HE0450–2958, image by HST. The quasar is located near the center of the image; no apparent host galaxy is visible. At the top of the image is a highly disturbed star-forming galaxy. Next to the quasar is a gas clump that appears to be ionized by the quasar’s radiation. The point object in the lower right corner is a foreground star that accidentally entered the field of view*



Source: ESA/Hubble Images and Videos

Astrophysicists attempted to attribute the energy of this celestial object to processes associated with nearby galaxies. They are not deterred by the vast cosmic distances between galaxies or by the fact that the supermassive black hole (SMBH) in our galaxy, situated amid stars, gas, and dust, bears little resemblance to a quasar! (ESA, 2005).

As we see from observational astrophysical data, there are colossal energy sources in deep space whose nature is infinitely far from

the unconditional and universal observance of the conservation of matter-energy principle.

Comets

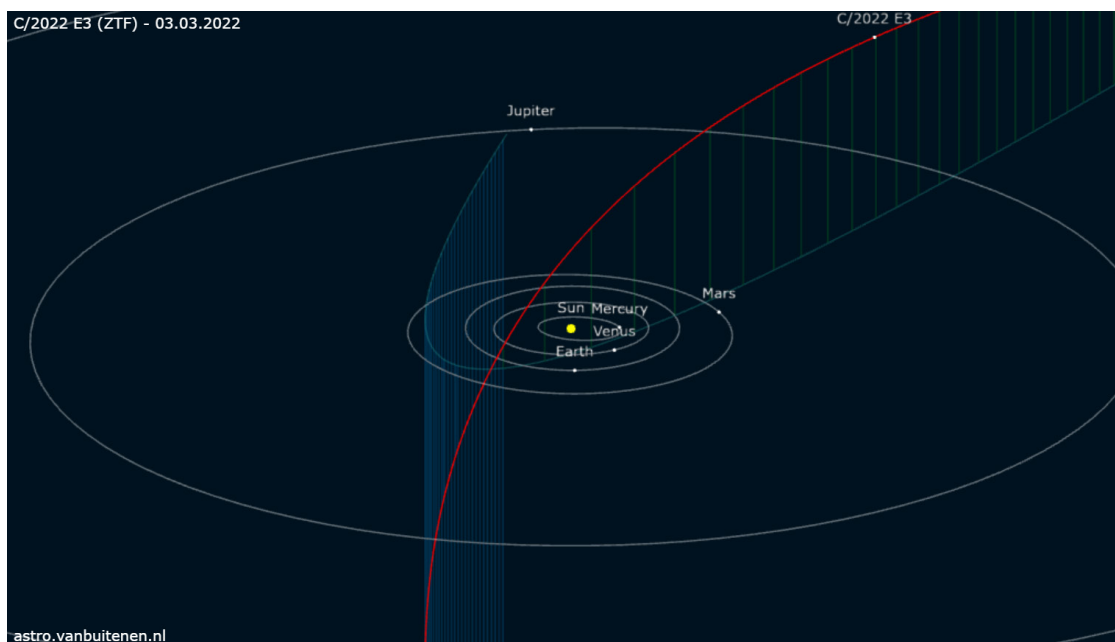
On February 1, 2023, comet C/2022 E3 (ZTF) was especially visible in the sky. It is no different from other comets, whose sizes range from about 1 km to 45 km (Guido, E., 2022).

Comet C/2022 was discovered by astronomers Bryce Bolin and Frank Masci using the Zwicky Transient Facility (ZTF) survey

on March 2, 2022. At the time of its discovery, the comet had an apparent magnitude of

17.3m and was about 4.3 AU from the Sun. (Guido, E., 2022).

Figure 19. Position of comet C/2022 E3 (ZTF) on March 3, 2022



Source: Gideon van Buitenen

The distance at which the comet was discovered exceeds the distance from the Sun to the astronomical snow line, which ranges between 2.7–3.1 AU (Wikipedia, 2023).

Let's recall that the snow line in astronomy and planetology is the distance from a star at which the temperature becomes low enough for simple volatile compounds (such as water, ammonia, methane, molecular nitrogen, and chlorine) to transition into a solid state (Wikipedia, 2023).

Depending on the theoretical model applied, various temperature values are used to define these conditions. For example, in the case of water, at temperatures of 140–170 K and under the current luminosity of the Sun, the water snow line corresponds to a distance of 2.7–3.1 AU, approximately midway between the current orbits of Mars and Jupiter, within the asteroid belt. Following this are the snow lines for carbon dioxide, methane, and, finally, carbon monoxide. The carbon monoxide snow line is located roughly at Neptune's orbit (Wikipedia, 2023).

It is worth noting that in astronomy and planetology, the snow line is the distance from a star at which the temperature becomes low enough for simple volatile compounds (such

as water, ammonia, methane, molecular nitrogen, and chlorine) to condense into solid ice.

However, there is a significant detail: the diameter of comet C/2022 E3 (ZTF) is about 1 km (Guido, E., 2022), and it can only be detected at such a distance using the most powerful telescopes from Earth's orbit.

What Bolin and Masci observed was the coma, a gas-dust cloud surrounding the comet. Through a telescope, this cloud appears as a round spot with blurry edges, resembling a galaxy. However, unlike galaxies, cometary comas move against the backdrop of stationary stars.

On March 3, 2023, the iTelescope observatory (H06) captured ten 60-second sequential images, confirming cometary activity. The angular size was 6" (six arcseconds), which corresponds to a body size one and a half times the diameter of Earth (Guido, E., 2022).

This raises a natural question: "How can comets, arriving from beyond the Solar System, form a coma of planetary size?" After all, a comet's gravitational force is weak. To sustain a coma of this size, it must be continuously replenished with gas and dust, as the coma's material constantly dissipates into space!

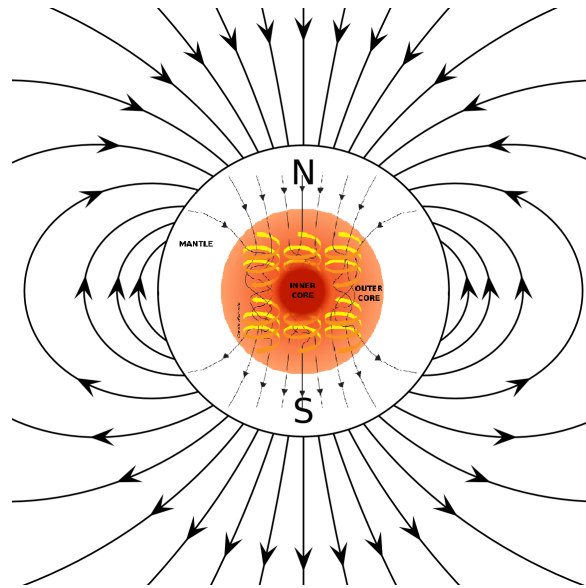
As we can see, the ability of comets to form a massive coma beyond the snow line suggests a violation of the conservation of energy-matter within the core of comets.

our planet. However, if we examine all possible hypotheses for the formation of planetary magnetic fields, we find an insurmountable flaw in the very idea of generating a magnetic field in this way.

The Geometry of Earth's Magnetic Field Lines

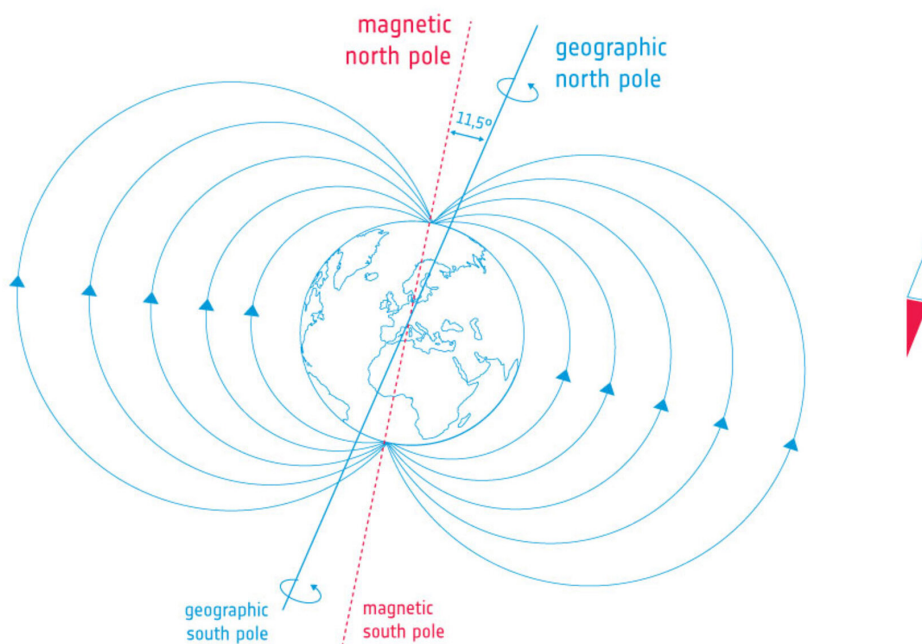
It is widely accepted that Earth's magnetic field is generated in the outer liquid core of

Figure 20. Common model of magnetic field generation in the liquid core



Source: Wikipedia

Figure 21. Geometry of Earth's magnetic field lines according to the European Space Agency.

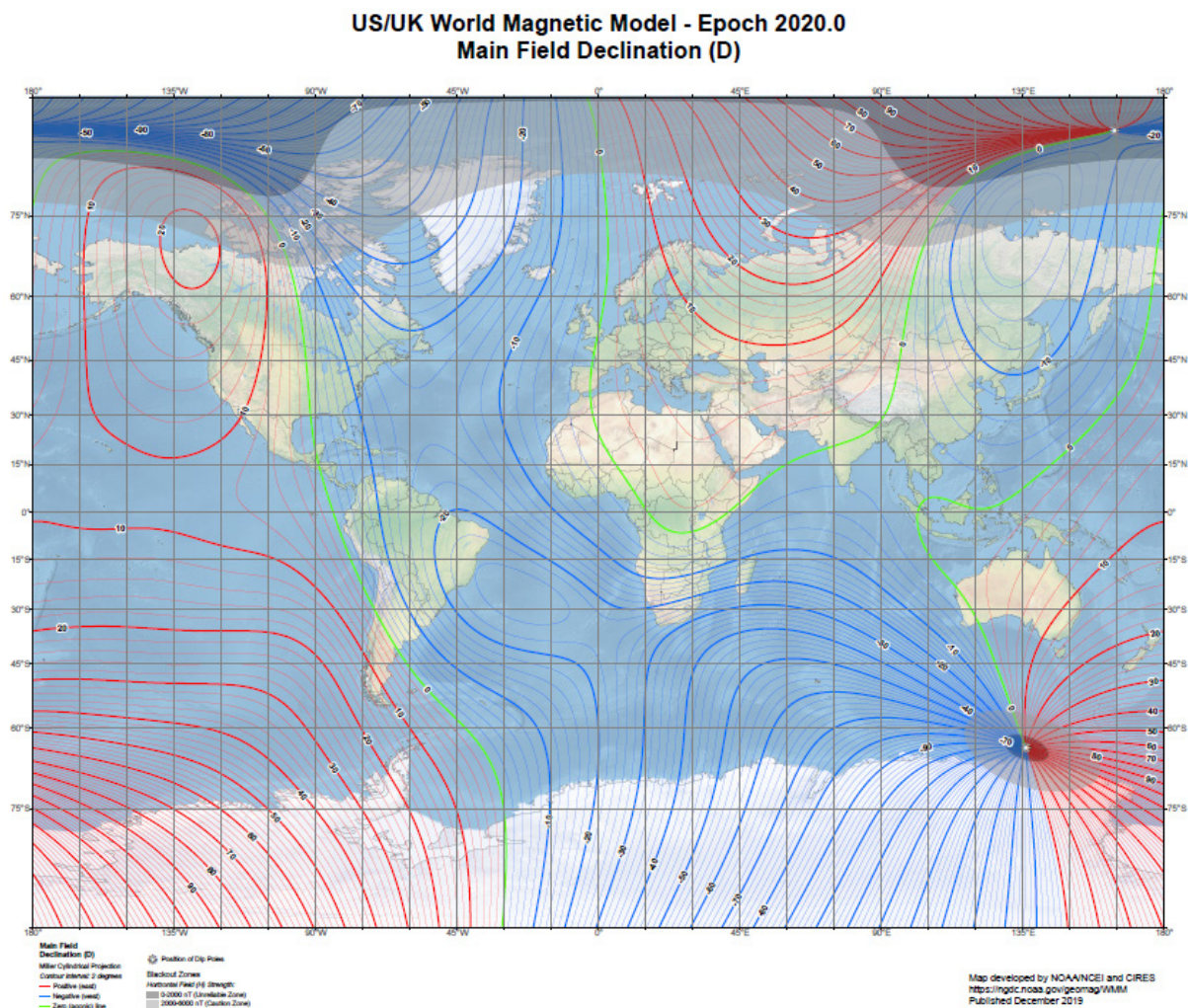


Source: ESA

To grasp the futility of attempting to explain Earth’s magnetic field formation within the framework of this 250-year-old geophysical paradigm, it is enough to compare:

- the common scheme for generating a magnetic field in a liquid core (see Fig. 20), which allows for the placement of magnetic field line exits and entries on Earth’s surface outside the magnetic poles (Pourovskii, L.V. et al., 2017; Wikipedia, 2023);
- the geometry of Earth’s magnetic field lines (see Fig. 21), where the exits and entries of the magnetic field lines are located at the points of the South and North magnetic poles (ESA, 2016);
- the actual geometry of Earth’s magnetic field lines (see Fig. 22), where the exits of the magnetic field lines are at the South Pole and the entries at the North Pole. Additionally, besides the main magnetic poles, there are Global Magnetic Anomalies with a similar nature and comparable intensity (NCEI, 2023).

Figure 22. Map of the actual geometry of Earth’s magnetic field lines (2019)



Source: NGA and DGC

The inconsistency of the dominant scientific worldview regarding the global magnetic field is confirmed by the contradiction between the results of the refined model of our planet’s core, which indicates that the solid core – one of the elements of the geo-

dynamo mechanism– in the Earth’s centre formed no earlier than 1 billion years ago (NCEI, 2023), and radiometrically measured geological data on the oldest rocks on the planet’s surface, which suggest the existence of a global magnetic field for as

long as 4.2 billion years (Tarduno, J. et al., 2015).

The Non-dipolar Nature of Earth's Magnetic Field

Earth's magnetic field consists of magnetic monopoles (see Fig. 22). This conclusion is based on the following observations:

1) the magnetic field lines of both the magnetic poles and the WMA (World Magnetic Anomalies) originate from specific points (southern poles) and converge at other points (northern poles) (NCEI, 2023);

2) the positioning of magnetic poles and WMAs does not depend on the structure of the Earth's crust, and their intensity does not correlate with the magnetic properties of the lithosphere and mantle rocks (Pechersky, D.M., 1985);

3) the intensity of the magnetic poles and WMAs decreases with altitude (with increased distance of magnetic measurements from the Earth's surface) only slightly, and they extend vertically towards the planet's center, indicating a deep location for the sources of these anomalies (Pechersky, D.M., 1985);

4) a drift has been observed both in the North Pole toward Siberia and in the overall "westward drift" of the WMAs, i.e., a shift of the WMA isolines to the west, suggesting variability in the properties of its source located at the Earth's center; (Pechersky, D.M., 1985);

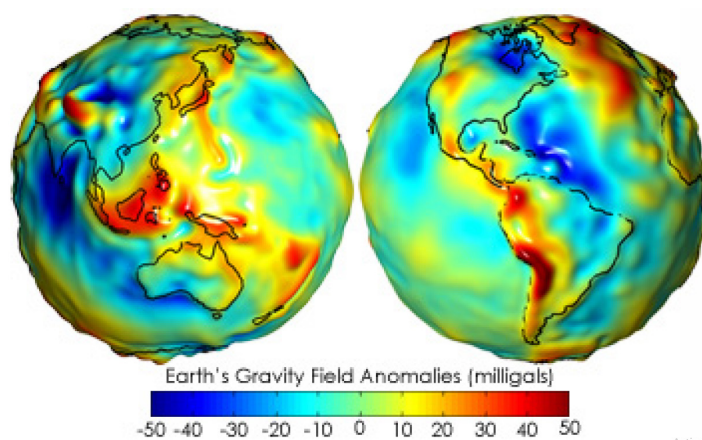
5) the cumulative amplitude of secular variations in the direction of the geomagnetic field consistently increases as it approaches the epicenters of positive WMAs over the past 0–10 thousand years; this dependence "weakens" for the earlier interval of 10–100 thousand years ago and disappears entirely in the interval of 0.1–0.7 million years ago (Pechersky, D.M., 1985).

It is evident that the exotic nature of the magnetic poles and world magnetic anomalies does not fit within the hypothesis of a magnetic field generated in the Earth's liquid outer core. It calls for a change in the geophysical paradigm regarding the object at the Earth's center, whose diameter is at least three orders of magnitude smaller than the inner solid core of the Earth and which forms a magnetic field geometry unexplained by traditional perspectives.

The Geoid

Earth's shape closely resembles an oblate spheroid. More precise measurements of our planet's shape have led to the conclusion that its surface is slightly deformed on a planetary scale, forming a geoid (Earth Observatory, 2004). These deformations are minor, with an amplitude of about 100 meters. On the planetary scale, these anomalies are almost imperceptible.

Figure 23. The geoid with exaggerated distortions and color corresponding to gravitational anomalies (the same weight measured on the same spring scale will be heavier in the «red areas» and lighter in the «blue areas»)



Source: NASA.

For example, the sea level of the Pacific Ocean near the Panama Canal is about 12

centimeters higher than that of the Atlantic Ocean. However, water does not flow through

the Panama Canal from the Pacific Ocean to the Atlantic, as this part of the transport artery is fed by rivers located on the Isthmus of Panama, whose levels are significantly higher than those of both oceans.

But there is a scientific consensus that Earth's interior has undergone gravitational differentiation (material is evenly distributed according to its physical and chemical properties), and that the process of isostasy exists, implying that the buoyant force of Earth's mantle is equal to the weight of the continental crust.

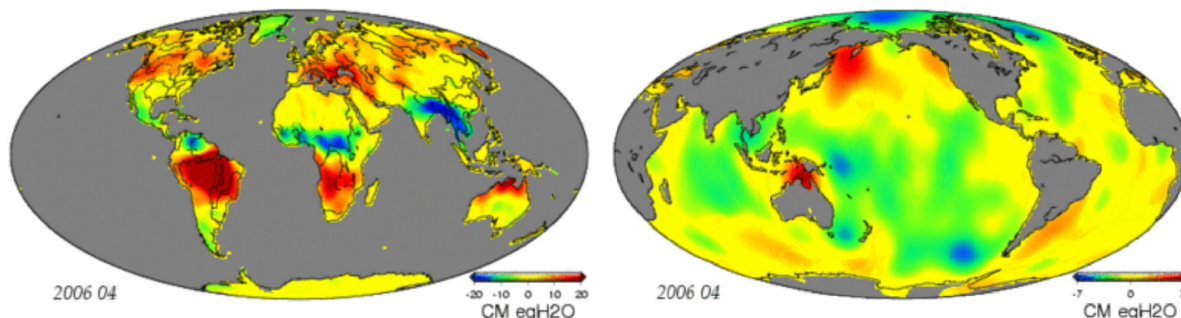
This raises a very natural question: «What energy powers the forces that hold Earth's shape in a constant deformed state?»

Variation in Gravitational Field Intensity

Among the natural phenomena that are difficult to believe in, the most important is the variation in gravitational field intensity on the geoid's surface (Wikipedia, 2024).

What does this mean? The point is that Earth's gravitational field is not constant.

Figure 24. Variation in gravitational field intensity on the geoid's surface



Source: Wikipedia

Moreover, the process of changing the gravitational field intensity can occur within the first dozen hours in different areas of Earth's surface.

What kind of energy could drive the rocks of the Earth's interior at such speed that, by altering gravity, it could synchronously move billions of tons of water on the planet's surface *and underground*? After all, the natural process of rock differentiation during the planet's formation and over the subsequent 4 billion years of its existence inevitably leads to the material in the Earth's interior having the minimal level of internal mechanical stress in the present epoch. As a result, any local volume of rock has the smallest possible pressure gradient on its external side.

From the perspective of the dominant scientific worldview, phenomena of this kind cannot be explained by processes within our planet, as the immense heat generated inside the Earth at its formation has continuously dissipated, facilitating the physical and chemical differentiation of its interior. In the present epoch, the fluidity of Earth's rock material becomes noticeable only on geological timescales (thousands to millions of

years), even under the influence of external factors. Furthermore, observations indicate that tidal forces are not related to variations in the gravitational field of the geoid, as there is no correlation between them.

Meanwhile, a distinctive feature of this phenomenon is the inverse correlation between gravity and atmospheric pressure, which contradicts the laws of physics and is termed the Gravitational-Meteorological Paradox. Specifically:

- 1) in areas of low atmospheric pressure, spacecraft detect increased gravitational field intensity;
- 2) in areas of high atmospheric pressure, spacecraft detect decreased gravitational field intensity;
- 3) the geoid – the average value of gravitational field variation – corresponds to normal atmospheric pressure (Zinaliev, M., 2017).

The most widespread yet erroneous views on the factors shaping atmospheric conditions are based on the idea that vertical air circulation is the cause of atmospheric pressure changes. According to these views, warm air rises and creates a low-pressure zone, while cold air descends, creating a high-pressure

zone. Thus, air currents circulate across the globe. These currents are considered responsible for weather patterns such as hurricanes, tornadoes, and thunderstorms.

As a counterargument, it is sufficient to recall that Earth's atmosphere has year-round zones of high and low pressure that persist regardless of the succession of days and nights or even seasons. For example, one of these – the Azores High – is located in the middle of the Atlantic Ocean near the equator. During the era of sailed navigation, crews caught in this zone would perish from thirst and hunger, as high-pressure zones are characterized by calm weather, no rainfall, and no fish in the water.

An even more striking example is the summer heat and drought periods on the Peloponnese (Greece) and the Apennine Peninsula (Italy). According to conventional views, the hotter air over the peninsula should be displaced by cooler air over the surrounding seas. This convection would supposedly create a low-pressure zone over Greece and Italy, leading to cloud formation and precipitation. Yet, this does not occur, sometimes for as long as two months!

During this season, temperatures rise so high that vegetation rich in essential oils can spontaneously ignite. Forest fires should further enhance the upward movement of hot air over land and the inflow of moist, cool air from the surrounding seas. Fine ash particles rising into the atmosphere should act as centers of moisture condensation in the upper layers, inevitably leading to immediate cloud formation and rainfall. But this is not observed during the drought season, which can last up to two months! The hypothesis of atmospheric circulation as a cloud formation mechanism is nothing more than an urban myth.

The real factor determining atmospheric pressure is the variation in gravitational strength. A decrease in gravitational intensity leads to a drop in atmospheric pressure in a given area of the Earth, resulting in cloud formation and precipitation (Zinaliev, M., 2017).

Conversely, a decrease in atmospheric pressure, cloud formation, and precipitation cannot coincide with an increase in gravitational force over that segment of the surface. Higher gravity would lead to an increase in atmospheric thickness and thus the

pressure of the atmospheric column, which, in turn, would alter the atmospheric conditions – promptly resulting in clear, precipitation-free weather.

However, the GRACE space mission, dedicated to studying Earth's gravitational field over several decades, has observed the gravitational-meteorological paradox – over zones of low atmospheric pressure, for example, during the winter rainy season over the Amazon, a zone of increased gravity forms (Zinaliev, M., 2017).

This contradiction can be resolved by assuming that the source of gravitational field variation on the planet is the same unknown object that generates the Earth's magnetic field (see section 3.8. Non-dipolar Nature of Earth's Magnetic Field) (Zinaliev, M., 2017).

The GRACE space mission records an additional gravitational influence arising from the rise in oceanic and subterranean water levels, as well as an increase in atmospheric density due to cloud formation. This influence is 100 times more intense than that of the source at Earth's center, as the distance from the spacecraft to the excess water masses on the planet's surface is ten times smaller than its distance from the source of gravitational field variation at the planet's center (Zinaliev, M., 2017).

Conclusions

The variety, quality, and scientific value of the above-listed studies, along with many others not mentioned in this article, combined with the reluctance of scientific and educational authorities to incorporate these insights into school and popular science programs, point to serious issues within scientific, educational, and outreach fields. This obstruction, present worldwide without regard for national boundaries, is euphemistically called «scientific conservatism».

Isn't it strange that, for example, the primary properties of our planet's gravitational and magnetic fields are labeled as anomalies, while the theories unable to account for them are called the dominant scientific worldview?

Experimental data from geology, space missions, and observational astronomy, particularly from the past two decades, suggest a different nature of the interiors of celestial bodies with internal activity, different from

the conventional view. Specifically, they indicate the presence of an unknown energy-matter source at the center of both our planet and other celestial bodies. The intensity of such a source varies from barely detectable, as in comets with minimal gas and dust production, to the tremendous power of quasars.

Considering the inability to explain the configuration of the planetary magnetic field, as well as the phenomena of the «geoid» and the “planetary gravitational field intensity variation” through properties of Earth’s outer liquid core, it is easy to conclude about:

1) the futility of the idea that the Earth’s core is metallic;

2) the existence of a source of the Earth’s magnetic and gravitational properties that has a diameter at least three orders of magnitude smaller than that of the supposed solid inner core and that is unknown to modern science.

The collective experimental data from the past two decades point to physical vacuum as the source that provides the internal activity of those celestial bodies in whose depths processes occur in violation of the principle of conservation of energy and matter.

The study of the interior of comets near Earth’s orbit will not only finally resolve the

issue of the growth of the Earth with the increase in its mass, but will also open a new chapter in the history of humanity’s scientific and technological progress.

Acknowledgements

I express my gratitude to PhD Anatoly Cherepovsky for the idea of writing this article based on my comments on his lectures regarding the problem of Earth’s expansion. His scientific potential, combined with his talent as a lecturer, has provided new momentum for advancing the concept of the growth of our planet along with its increasing mass.

Anatoly also participated in the preparation of this article for publication and made several valuable remarks that helped improve its content.

I am grateful to my family – my wife Rilana, my daughter Dinara, and my son Timur – for their supportive attitude towards my scientific research at home and for the opportunity to discuss scientific issues within the family circle. I extend special thanks to my daughter Dinara, who conducted the final review of the article’s translation into English.

References

- Anderson, J. F., Hall-Martin A., Russell D. A. (1985) Long Bone Circumference and Weight in mammals, birds, and dinosaurs. *Zoological Journal of the Linnean Society*, – 207 (1). – P. 53–61. Retrieved from: URL: <https://zslpublications.onlinelibrary.wiley.com/doi/10.1111/j.1469-7998.1985.tb04915.x>
- Blinov, V. F. (2003) *Growing Earth: From Planets to Stars* (In Russ.). – Moscow: Editorial URSS.
- Burundukov, A. S., Drozdov, A. L. (2015). Giant reptiles – a paleontological challenge to interdisciplinary synthesis. *Biota and Environment of the Far Eastern Reserves* (In Russ.), – 5. – P. 93–112. Retrieved from: URL: https://drive.google.com/file/d/11ShkTsRQZEc-99MeqdgB9SOYpXf1v_hGY/view
- Carey, S. W. (1991). *In Search of Patterns in the Development of Earth and the Universe: A History of Earth Science Doctrines* (In Russ.). Moscow: Mir.
- CERN. (2013, April 3). *AMS Experiment Measures Antimatter Excess in Space*. Retrieved from: URL: <https://home.cern/news/press-release/cern/ams-experiment-measures-antimatter-excess-space>
- Cherepovsky, A. V. (2020, July 9) Earth Expansion or the Russian View on the Geological History of the Planet (In Russ.). Retrieved from: URL: https://www.youtube.com/watch?v=U_TRixMg49k&t=572s
- Christiansen, P., Farina, R., (2004). Mass Prediction in Theropod Dinosaurs. *Historical Biology*, – 16(2–4). – P. 85–92. Retrieved from: URL: <https://www.tandfonline.com/doi/abs/10.1080/08912960412331284313>

- Deep Carbon Observatory. (2019). Rewriting the Textbook on Fossil Fuels: New Technologies Help Unravel Nature's Methane Recipes. *Phys.org*. Retrieved from: URL: <https://phys.org/news/2019-04-rewriting-textbook-fossil-fuels-technologies.html>
- Earth Observatory. (2004, March 30). *Gravity Anomaly Maps and The Geoid*. Retrieved from: URL: <https://earthobservatory.nasa.gov/features/GRACE/page3.php>
- ESA. (2016 June 03). Illustration showing Earth's magnetic field. Retrieved from: URL: https://www.esa.int/ESA_Multimedia/Images/2016/06/Illustration_showing_Earth_s_magnetic_field
- ESA (2011, June 30). *Integral Challenges Physics Beyond Einstein*. Retrieved from: URL: https://www.esa.int/Science_Exploration/Space_Science/Integral_challenges_physics_beyond_Einstein
- ESA. (2005, September 14). Looking “underneath” the quasar HE0450–2958. Retrieved from: URL: <https://esahubble.org/images/heic0511b>
- Erickson, G.M., Makovicky, P.J., Currie, P.J., Norell, M.A., Yerby, S.A., Brochu, C.A. (2004). Gigantism and Comparative Life-History Parameters of Tyrannosaurid Dinosaurs. *Nature*, – 430(7001). – P. 772–775. Retrieved from: URL: <https://pubmed.ncbi.nlm.nih.gov/15306807>
- Farlow, J. O., Smith, M. B., Robinson, J. M. (1995). Body mass, bone “strength indicator,” and cursorial potential of *Tyrannosaurus rex*, *Journal of Vertebrate Paleontology*, – 15(4). – P. 713–725. Retrieved from: URL: <https://www.tandfonline.com/doi/abs/10.1080/02724634.1995.10011257>
- Furaha tenVelde, P. (1997). The Wild Elephants of the Royal Bardia National Park, Nepal. Gajah: *Journal of the IUCN/SSC Asian Elephant Specialist Group*, – 17. – P. 41–44. Retrieved from: URL: <https://www.asesg.org/PDFfiles/Gajah/17-41-tenVelde.pdf>
- Gennadiev, A. N., Gerasimova, M. I., Patsukevich, Z. V. (1987). Soil formation rate and permissible soil erosion rates (In Russ.). *Bulletin of Moscow University*. – 3. – P. 31–36. Retrieved from: URL: <https://ru-ecology.info/term/52632/?ysclid=m2xcrvme89396219476>
- Hone, D. (2017). *Chronicles of the Tyrannosaur. Biology and Evolution of the World's Most Famous Predator* (In Russ.). – Moscow: Alpina Non-Fiction.
- Husson, D., Galbrun, B., Laskar, J., Hinnov, L. A., Thibault, N., Gardin, S., & Locklair, R. E. (2011). Astronomical Calibration of the Maastrichtian (Late Cretaceous). *Earth and Planetary Science Letters*, – 305(3). – P. 328–340. Retrieved from: URL: <https://www.sciencedirect.com/science/article/abs/pii/S0012821X1100152X>
- Hutchinson, J.R., Schwerda, D., Famini, D.J., Dale, R.H., Fischer, M.S., Kram, R. (2006). The locomotor kinematics of Asian and African elephants: changes with speed and size. *Journal of Experimental Biology*, – 209(19). – P. 3812–3827. Retrieved from: URL: <https://journals.biologists.com/jeb/article/209/19/3812/16362/The-locomotor-kinematics-of-Asian-and-African>
- Hutchinson, J.R, Garcia M. (2002). *Tyrannosaurus Was Not a Fast Runner*. *Nature*, – 415(6875). – P. 1018–1021. Retrieved from: URL: <https://www.nature.com/articles/4151018a>
- Hutchinson, J.R. (2004). Biomechanical Modeling and Sensitivity Analysis of Bipedal Running Ability. II. Extinct Taxa. *Journal of Morphology*, – 262(1). – P. 441–461. Retrieved from: URL: <https://onlinelibrary.wiley.com/doi/10.1002/jmor.10240>
- Koronovsky, N. V. (2001). Isostasy (In Russ.). *Soros Educational Journal*, – 7(11). – P. 73–78. Retrieved from: URL: https://web.archive.org/web/20050817034058/http://journal.issep.rssi.ru/articles/pdf/0111_073.pdf
- Kutcherov, V.G. (2013). *Abiogenic Deep Origin of Hydrocarbons and Oil and Gas Deposits Formation*. EBOOK. Retrieved from: URL: <https://www.intechopen.com/chapters/41889>
- Lamanna, M.C. et al. (2014). A New Large-Bodied Oviraptorosaurian Theropod Dinosaur from the Latest Cretaceous of Western North America. *PLoS ONE*, – 9(3). – e92022. Retrieved from: URL: <https://journals.plos.org/plosone/article?id=10.1371/journal.pone.0092022>

- Larin, V.N. (2005). *Our Earth (origin, composition, structure and development of the originally hydride Earth)* (In Russ.). – M. «Agar».
- McNeill, A.R. (1985). Mechanics of Posture and Gait of Some Large Dinosaurs. *Zoological Journal of the Linnean Society*. – 83. – P. 1–25. Retrieved from: URL: <https://scite.ai/reports/mechanics-of-posture-and-gait-WY50xO>
- Guido, E. (2022, March 22). *New Comet C/2022 E3 (ZTF) may reach mag. +6 in Feb. 2023*. Retrieved from: URL: <https://www.cobs.si/news/archive/new-comet-c2022-e3-ztf-may-reach-mag-6-in-feb-2023>
- Pechersky, D.M. (1985). *Petromagnetism and Paleomagnetism: A Reference Guide for Specialists from Related Fields of Science* (In Russ.). – Moscow: Nauka.
- Pillai, N.G. (1941). On the Height and Age of an Elephant. *Journal of the Bombay Natural History Society*. – 42. – P. 927–928. Retrieved from: URL: – <https://zenodo.org/records/13658398>
- Ponomarev, L.I. (1989). *Under the Sign of Quantum* (In Russ.). – Moscow: Nauka.
- Pourovskii, L.V. et al. (2017). Electron–Electron Scattering and Thermal Conductivity of Epsilon-Iron at Earth’s Core Conditions. *New Journal of Physics*, – 19. – 073022 p. Retrieved from: URL: <https://iopscience.iop.org/article/10.1088/1367-2630/aa76c9>
- Protasov, V.Yu. (2023). Geometry of the Starry Sky (In Russ.). *Kvant*, 2. Retrieved from: URL: https://elementy.ru/nauchno-populyarnaya_biblioteka/431102/Geometriya_zvezdno-go_neba
- Pushcharovsky, Yu.M., Pushcharovsky, D.Yu. (2010). *Geology of the Earth’s Mantle* (In Russ.). – Moscow: GEOS
- Seebacher, F. (2001) A New Method to Calculate Allometric Length-Mass Relationships of Dinosaurs. *Journal of Vertebrate Paleontology*, – 21(1). – P. 51–60. Retrieved from: URL: <https://www.tandfonline.com/doi/abs/10.1080/02724634.1995.10011257>
- Sellers, W.I., and Manning, P.L. (2007). Estimating Dinosaur Maximum Running Speeds Using Evolutionary Robotics. *Proc. of The Royal Society B*, – 274(1626). – P. 2711–2716. Retrieved from: URL: <https://royalsocietypublishing.org/doi/10.1098/rspb.2007.0846>
- Shoshani, J.; Eisenberg, J.F. (1982). “*Elephas maximus*.” *Mammalian Species*, – 182. – P. 1–8. Retrieved from: URL: <https://academic.oup.com/mspecies/article/doi/10.2307/3504045/2600564>
- Smolin, L. (2006). *The Trouble with Physics: The Rise of String Theory, the Fall of a Science, and What Comes Next*. Houghton Mifflin Harcourt.
- Susskind, L. (2015). *The Cosmic Landscape: String Theory and the Illusion of Intelligent Design* (In Russ.). – St. Petersburg: Piter.
- Tarduno, J. et al. (2015). Ancient Roots of Earth’s Magnetism. *Nature*, – 524(9). – P. 521–524. Retrieved from: URL: <https://www.nature.com/articles/524009c>
- Verkhovyanov, O.V. (2020). *Approaching the Unknown in Cosmology* (In Russ.). Retrieved from: URL: <https://www.youtube.com/watch?v=IXsXDdbNcAI&list=PL1R6z4Sx8h-Qov7RFJVSzkcBQbqaQyG0x&index=4>
- Veselovsky, I.N. (1961). *Aristarchus of Samos – Copernicus of the Ancient World* (In Russ.). HAJ.
- NCEI. (2023, December 31). *World Magnetic Model (WMM)*, Retrieved from: URL: <https://www.ncei.noaa.gov/products/world-magnetic-model>
- Weinberg, S. (1989). *The Cosmological Constant Problem* (In Russ.). *Physics-Uspekhi, Series: Physics of Our Days*, – 158(4). – P. 639–678. Retrieved from: URL: <https://ufn.ru/ru/articles/1989/8/d/?ysclid=m2xiw34w7s176133368>
- Wikipedia (2023, April 24). *Dynamo Theory*. Retrieved from: URL: https://en.wikipedia.org/wiki/Dynamo_theory
- Wikipedia (2024 September 17). *Galactic Center*. Retrieved from: URL: https://en.wikipedia.org/wiki/Galactic_Center
- Wikipedia (2024 April 24). *GRACE and GRACE-FO*. Retrieved from: URL: https://en.wikipedia.org/wiki/GRACE_and_GRACE-FO

- Wikipedia (2024, October 21). *Quasar*. Retrieved from: URL: <https://en.wikipedia.org/wiki/Quasar>
- Wikipedia (2023, April 24). *Snow Line (Astronomy)* (In Russ.). Retrieved from: URL: https://ru.wikipedia.org/wiki/%D0%A1%D0%BD%D0%B5%D0%B3%D0%BE%D0%B2%D0%B0%D1%8F_%D0%BB%D0%B8%D0%BD%D0%B8%D1%8F
- Zinaliev, M. (2021, September 18) *Why Quantum Field Theory Is Inconsistent?* (In Russ.). Retrieved from: URL: <https://sites.google.com/view/fizikavremeni/%D0%BF%D0%BE%D1%87%D0%B5%D0%BC%D1%83-%D0%BA%D0%B2%D0%B0%D0%BD%D1%82%D0%BE%D0%B2%D0%B0%D1%8F-%D1%82%D0%B5%D0%BE%D1%80%D0%B8%D1%8F-%D0%BF%D0%BE%D0%BB%D1%8F-%D0%BD%D0%B5%D1%81%D0%BE%D1%81%D1%82%D0%BE%D1%8F%D1%82%D0%B5%D0%BB%D1%8C%D0%BD%D0%B0?authuser=0>
- Zinaliev, M. (2017). On Solving the Paleontological Paradox. *The European Journal of Technical and Natural Sciences*. – 5. – P. 15–37. Retrieved from: URL: https://ppublishing.org/media/uploads/journals/journal/EJT_5_2017.pdf
- Zook, H. A. (2001). *Spacecraft Measurements of the Cosmic Dust Flux*. New York: *Kluwer Academic/Plenum Publishers*. Retrieved from: URL: https://link.springer.com/chapter/10.1007/978-1-4419-8694-8_5
mouradzinaliyev@gmail.com

submitted 10.10.2024;
accepted for publication 25.10.2024;
published 28.11.2024
© Zinaliyev M.
Contact: mouradzinaliyev@gmail.com



Section 3. Food processing

DOI:10.29013/AJT-24-9.10-83-85



FEATURES OF PROCESSING OF OILS OBTAINED FROM LOW GRADE COTTON SEEDS

*Akhmedov Azimjon Normuminovich*¹, *Irnazarov Shukhrat
Ismatullaevich*¹, *Niyazov Mamurjon Bobonazarovich*²

¹ Department of Food Technology of Products of the Karshi
engineering-economics institute, Karshi, Uzbekistan

² Department of Scientific Research, Innovation and Training of Scientific Pedagogical
Personnel of the Karshi engineering-economics institute, Karshi, Uzbekistan

Cite: *Akhmedov A.N., Irnazarov Sh.I., Niyazov M.B. (2024). Features of Processing of Oils
Obtained From Low Grade Cotton Seeds. Austrian Journal of Technical and Natural Sciences
2024, No 9 – 10. <https://doi.org/10.29013/AJT-24-9.10-83-85>*

Abstract

This paper presents a technology for refining low-grade cottonseed oil, in which refined high-grade cottonseed oil has a yield of 85% and 12 colors and 35 yellow units in a 13.5 cm layer of Lovibond with 35 yellow units. k units, and the yield of refined oil obtained from low-grade cottonseed is 81.5%, the color is 18 red and 4 blue units, 35 yellow, the refined oil obtained from non-standard cottonseed has a yield of 78.3% and 13 It was found that 35 yellow, 19 red and 5 blue units were found in the 5 cm layer.

Keywords: *Low-grade cotton seeds, cottonseed oil, urea, gossypol, acid value, alkali, refining, pre-clarification, pressing*

Introduction

Along with high-grade cotton seeds, oil and fat enterprises in Uzbekistan annually receive low-grade ones, the amount of which varies between 25–35% (depending on the climatic conditions of the year, etc.) (Akhmedov A. N., Ishankulova G. N., 2024. 44; Akhmedov A. N., Ishankulova G. N., 2023. 44).

When processing such seeds at enterprises, oils with a high content of free fatty acids, gossypol, chlorophyll and their derivatives are ob-

tained, which negatively affects the quantity of refined oils obtained and their quality. Known technological schemes (Beloborodov V. V., 1960. 164; Abdullaev N. Sh., 1989. 7). Refining of oils obtained from low-grade cotton seeds is not effective enough and requires improvement. To develop new technological methods, first of all, it is necessary to study the distinctive features of the qualitative composition of oils obtained from low-grade and non-standard cotton seeds (Akhmedov A. N., 2019. 23).

We conducted a comparative study of the qualitative composition of black oils obtained from high-grade, low-grade and non-standard cotton seeds under the production conditions of Limited liability company “Asiangolden”. Sampling of black oil was carried out after the filter presses during the normal functioning of the pre-press shop, established in the technological regulations (Zaremba G. V., 1967. 471).

Materials and methods

The acid number of oils was determined by potentiometric and indicator methods using a 1% alcohol solution of thymolphthalein as an indicator.

– the color of cottonseed oil was determined using a Lovibond color meter.

Results

The analysis of black (crude) cottonseed oils obtained by prepressing was carried out according to the methods described in the “Guide to Research Methods...” (Zaremba G.V. et al. 1967. 502). The results of the analyzes are presented in table 1.

From Table 1. It can be seen that oils obtained from low-grade and non-standard cotton seeds contain significantly more free fatty acids, phosphatides, gossypol and its derivatives. These oils also contain more Lovibond red and blue coloring components. Very low quality oil is obtained from non-standard cotton seeds, which should also be taken into account when refining it.

Table 1. Indicators of crude forex oils obtained from high-grade, low-grade and non-standard cotton seeds

Oil sample	Indicators of crude cottonseed oils				
	Acid number, mg KOH/g	Color in 1 cm layer		Phosphatides, %	Gossypol and its derivatives, %
		red units	blue units		
High grade seed oil (I–II grades)	4.35	63.8	4	1.12	0.18
Low grade seed oil (III–IV varieties)	7.19	74.5	6	1.38	0.28
Non-standard seed oil	8.44	82.7	9	1.55	0.31

It is known that increasing the content of phosphatides in crude cottonseed oil increases its emulsifying properties during alkaline

refining. This increases the loss of neutral oil in the soap stock, which negatively affects the yield of refined oil.

Table 2. Indicators of alkaline refining of oils obtained from various cotton seeds

Oil sample	Alkali consumption (NaOH)			Refined cottonseed oil		
	Concentration g/l	kg/t	Excess alkali, %	Color in 13.5 cm layer		Exit, %
				red units	blue units	
High grade seed oil (I–II grades)*	250	8.6	50	12	3	85.0
Low grade seed oil (III–IV varieties)	250	8.6	100	18	4	81.5
Non-standard seed oil	310	13	200	19	5	78.3

Note: * Corresponds to the samples in Table 1

An increase in the color of oils obtained from low-grade and non-standard cotton

seeds is associated with an increase in the content of gossypol and its derivatives. For ex-

ample, if in oil obtained from I–II varieties of cotton seeds, the content of gossypol and its derivatives is 0.18%, then in oil obtained from III–IV varieties of seeds it is 0.28%, and in oil obtained from non-standard seeds – 0.31%. Consequently, when selecting alkaline refining modes, it is necessary to take into account these features in the composition of such oils. We studied the refinability of selected oils in laboratory conditions using a standard method (Sergeev, A. G., 1973. 163). The results of alkaline refining of crude oils obtained from various cotton seeds are presented in Table 2.

From Table 2 it is clear that during alkaline refining of oil obtained from high-grade seeds, an excess of alkali of 50% is used, for oils obtained from low-grade seeds – 100%, for non-standard seeds – 200%.

Discussion and Conclusion

At the same time, refined oil obtained from high-grade seeds has a yield of 85% and a color of 12 color. 3 blue units with 35 yellow units in a 13.5 cm layer according to Lovibond. Refined oil obtained from low-grade cotton seeds has a yield of 81.5% and a color of 18 red and 4 blue units with 35 yellow. Refined oil obtained from non-standard cotton seeds has a yield of 78.3% and a color

of 19 red and 5 blue units with 35 yellow in a 13.5 cm layer.

Analysis of these indicators confirms that with a decrease in the grade of cotton seeds, the quality of the resulting black oil deteriorates, and the consumption (concentration and excess quantity) of alkali (NaOH) increases. All this negatively affects the yield of refined oil and its quality indicators. For example, an increase in excess alkali by 50% leads to a decrease in the yield of refined cottonseed oil by 3.5%, and at 150% – by 6.5%. Of course, such oil losses negatively affect the technical and economic indicators of the refining shop and oil and fat production in general.

Thus, the conducted research allows us to draw the following conclusions: – to increase the yield and improve the quality indicators of crude oils obtained from low-grade and non-standard cotton seeds, it is advisable to partially remove from them phosphatides, gossypol, chlorophyll and their derivatives, as well as other components associated with triacylglycerols, which reduce the efficiency of their alkaline refining process. At the same time, the selectivity of the process of preliminary removal of these components determines the increase in the yield and quality of the resulting refined cottonseed oils.

References

- Akhmedov A. N., Ishankulova G. N. Analysis Of Oils Obtained By The Pressing Method From Fruit Grains. *Austrian Journal of Technical and Natural Sciences*, 2024. – P. 44–47.
- Akhmedov A. N., Ishankulova G. N. Technology of preliminary clarification of oils from low-quality cotton seeds. *Austrian Journal of Technical and Natural Sciences*, 2023. – P. 23–28.
- Guide to the technology of production and processing of vegetable oils and fats / [ed. V. V. Beloborodov et al.] – L.: VNIIZH, 1960-I–II. – 348 p.
- Abdullaev N. Sh. Development of a combined process of oil extraction and oil refining as applied to the processing of low-grade cotton seeds. Abstract of Candidate of Technical Sciences, Leningrad: VNIIZH, 1989. – 19 p.
- Akhmedov A. N. Investigation of indicators of cottonseed oil obtained by pre-pressing from low-grade cotton seeds // *Universum: Technical Science*. Issue: 4(61). April, 2019. – Moscow, 2019. – P. 23–26.
- Guide to research methods, technical and chemical control and production accounting in the oil and fat industry / [edited by G. V. Zarembo et al.] – L.: VNIIZH, 1967. – 1042 p.
- Guide to the technology of production and processing of vegetable oils and fats / [ed. A. G. Sergeev and others] – L.: VNIIZH, 1973-I–II, – 846 p.

submitted 16.10.2024;

accepted for publication 31.10.2024;

published 28.11.2024

© Akhmedov A. N., Irnazarov Sh. I., Niyazov M. B.

Contact: a.ahmedov80@mail.ru

Contents

Section 1. Chemistry

- Gulmira Azimova, Mukhabbat Yuldasheva, Khabibullo Tadjimuhamedov*
INFLUENCE OF A NANOSTRUCTURAL CATALYST
IN THE ALLYLATION REACTIONS OF ANISOLE AND NEROLIN 3
- Alieva Mushtari Zaylobidin qizi, Nuraliyeva Guzal Abdulhamidovna*
STUDY OF THE STRUCTURE OF COMPLEX COMPOUNDS
BASED ON 2-AMINO-1,3,4-THIADIZOLE AND ADIPIC ACID OF
SALTS OF CO(LL), NI(LL), CU(LL), ZN(LL) USING PHYSICAL MEANS..... 8
- Boydadaev Azizbek Anvarjon ugli, Mukhitdinov Bakhtiyor*
Ikromovich, Amonova Dilnoza Mukhtarovna, Normakhamatov
Nodirali Sakhobataliyevich, Turaev Abbaskhan Sabirkhanovich
POLYSACCHARIDE-BASED CROSSLINKED GEL MATERIALS
AND THEIR PROPERTIES..... 14
- Guzal Khamraeva, Yunusjon Valiev, Abdugani Berdiev,*
Foziljon Saitkulov, Burkhon Elmuradov
TARGETED MODIFICATIONS OF 5,6-DISUBSTITUTED-4-
CHLOROTHIENO[2,3-d]PYRIMIDINES WITH BENZYLAMINE 20
- Yunusova Maftuna Valijon qizi, Babasadikov Shukrullo*
Sayfulloyevich, Erkaev Aktam Ulashevich, Kucharov Bakhrom
Khayrievich, Yulbarsova Mashkhura Vakhobovna,
Zakirov Bakhtiyor Sabirjanovich
ISOTHERMAL SOLUBILITY DIAGRAM OF THE SODIUM
HYDROXIDE – HUMIC ACID – WATER SYSTEM AT 25 °C 27
- Nurmatov Doston Urolovich, Abdushukurov Anvar Kabirovich,*
Xoliqov Tursunali Suyunovich, Yusufov Muxriddin Saidovich,
Yodgorov Chinmurot G'ulomovich
AMIDE REACTIONS OF IZONICOTINE ACID WITH SOME
AROMATIC AMINES 34
- Nasrullaev Azizbek Ozodovich, Tukhtaev Davlat, Samiev Rajab*
Akbarovich, Kodirov Khakim Iskandarzoda, Karimov Ilyasbek,
Zohidov Kasim Akilovich, Saitkulov Foziljon Ergashevich
SYNTHESIS AND METHYLATION OF SOME DERIVATIVES OF
2,3-TETRAMETHYLENE-3,4-DIHYDROQUINAZOLIN-4-ONE
AND –THIONE 39

Nasrullaev Azizbek Ozodovich, Tukhtaev Davlat, Samiev Rajab Akbarovich, Kodirov Khakim Iskandarzoda, Karimov Ilyasbek, Zohidov Kasim Akilovich, Saitkulov Foziljon Ergashevich
SYNTHESIS OF SOME DERIVATIVES OF
2,3-TETRAMETHYLENE-3,4-DIHYDROQUINAZOLIN-4-ONE
AND –THIONE 43

Oripov Oybek Bekboyevich, Saitkulov Foziljon Ergashevich, Mirvaliev Zoid Zoxidovich
SYNTHESIS REACTIONS OF QUINAZOLIN-4-ONE IN THE
PRESENCE OF IRON (III)-CHLORIDE CATALYSTS. 49

Oripov Oybek Bekboyevich, Saitkulov Foziljon Ergashevich, Mirvaliev Zoid Zoxidovich, Baymuratova Gulbaxar Orinaevna
INVESTIGATION OF AROMATIC PROPERTIES
OF XINAZOLIN-4-ONE 54

Section 2. Earth sciences

Murad Zinaliyev
THEORY OF THE EXPANDING EARTH ON THE SOLUTION TO
THE PROBLEM OF ENERGY AND MATTER SOURCES. 58

Section 3. Food processing

Akhmedov Azimjon Normuminovich, Irnazarov Shukhrat Ismatullaevich, Niyazov Mamurjon Bobonazarovich
FEATURES OF PROCESSING OF OILS OBTAINED FROM LOW
GRADE COTTON SEEDS 83